

Ab initio nuclear structure with SRG-transformed chiral NN plus NNN interactions

Master-Thesis

Angelo Calci

Advisor Robert Roth

Second advisor Sven Binder



TECHNISCHE
UNIVERSITÄT
DARMSTADT

Institut für Kernphysik

September 2010

Contents

1	Introduction	5
2	The Significance of three-body interactions	9
3	Basics of chiral effective field theory (χEFT)	11
3.1	Chiral symmetry	11
3.2	Principle of chiral perturbation theory (χ PT)	14
3.3	LECs, power counting and matrix element production	15
4	Transformation: Jacobi coordinates to m-scheme	21
4.1	Jacobi coordinates	21
4.2	The m-scheme	23
4.3	Coupling and coordinate-transformation formulas	24
4.3.1	6-j symbols	24
4.3.2	9-j symbols	25
4.3.3	Harmonic-oscillator brackets (HOBs)	26
4.4	Two-body Jacobi basis to m-scheme transformation	28
4.5	Three-body Jacobi basis to m-scheme transformation	38
4.5.1	Simplifying the matrix element	38
4.5.2	Calculating the T-coefficient	46
4.6	Implementation of the three-body basis transformation	57
4.6.1	Implementation of the J -coupling	62
4.6.2	Problems and limits of the implementation	66
5	Similarity renormalization group (SRG)	69
5.1	Basic concepts	69
5.2	Application to the NN+NNN interaction and subtraction procedure	71
5.3	Implementation of the SRG evolution	76
5.3.1	SRG transformation of $V_{NN}^{[2]}$	76
5.3.2	SRG transformation of $V_{NN+NNN}^{[2,3]}$	77
5.4	Diagonalization of the interaction matrix	78
6	Many-body methods	83
6.1	Exact ab initio approaches	83
6.1.1	No-core shell model (NCSM)	83

6.1.2	Importance truncated no-core shell model (IT-NCSM)	85
6.2	Hartree-Fock method	88
7	Many-body calculation results	93
7.1	(IT-)NCSM calculations for ${}^4\text{He}$	93
7.2	IT-NCSM calculations for ${}^6\text{Li}$	101
7.3	Closed-shell nuclei with the Hartree-Fock method	104
8	Summary and outlook	109
A	Appendix	113
A.1	Antisymmetrization in Jacobi basis	113
A.2	Conversion of two-body to three-body m-scheme matrix elements	117
A.3	NN+NNN interactions in four-body basis	119

1 Introduction

Nuclear structure theory plays an important role in the understanding of the atomic nucleus, e.g., by predicting the relevant experimental observables based on the fundamental theory of the strong interaction. These calculations can be of huge impact especially for the nuclear astrophysics, because a lot of nuclear data, e.g., for neutron-rich nuclei, are not reachable by experiments at the moment. Therefore, one has to use theoretical predictions to get this data for the astrophysical simulations.

For the theoretical description of an atomic nucleus one has to deal with two demanding problems. The first one is the construction of the proper nuclear interaction. The second one is the solution of the many-body eigenvalue problem $\hat{H}|\psi_n\rangle = E_n|\psi_n\rangle$, where the Hamiltonian \hat{H} contains the nuclear interaction. There is a wide range of nuclear interactions from phenomenological approaches over interactions based on meson exchange theory (like the CD Bonn interaction), to interactions derived in a QCD motivated effective field theory. We will focus on the latter.

Due to the non-perturbative character of QCD in the low-energy regime it becomes very complicated to use the quarks and gluons as the underlying degrees of freedom for the nucleons, which would be the correct choice from a fundamental point of view. Therefore, the nucleons are used as effective degrees of freedom. This assumption is justified for excitation energies below the delta resonance $\Delta(1232)$ of about 300 MeV. For higher energies the nucleons have inner excitations and cannot be described as inert particles anymore.

As a consequence, the effects of the quark- and gluon-substructure of the nucleon must be subsumed in the interaction between the nucleons. To achieve this with some fundamental justification one operates in the framework of chiral effective field theory (χ EFT). The chiral symmetry, a symmetry of QCD in the limit of vanishing quark masses, is spontaneously broken. The consequence is the existence of the pion as a so-called pseudo-Goldstone boson. These pions are added to the nucleons in the χ EFT as fundamental degrees of freedom.

Generally, nucleon-nucleon (NN) interactions are not sufficient to describe even the low-energy states in light nuclei, although the two-body phase shifts can be reproduced exactly. Because of this one has to consider higher-order interactions, like three-body (NNN) interactions and possibly also four-body interactions. According to Weinberg, the importance of the many-nucleon force decreases with the number m of involved nucleons [1, 2]. Due to this and to the fact that the computational cost rises dramatically with increasing m , we use NN+NNN interactions obtained from chiral effective field theory,

which provides the Hamiltonian $\hat{H}_{NN+NNN}^{\chi EFT}$. The NN+NNN interaction is constructed by using chiral perturbation theory, where one expands the nuclear potential in powers of the pion mass or momentum. In this expansion the three-body interaction appears naturally at next-to-next-to leading order (N²LO). Therefore, the χ EFT determines the NN and NNN interaction in a consistent manner, which is a crucial advantage of this theory. For the construction of the Hamiltonian, a two-body interaction from the N³LO was used, while the three-body interaction was extracted from the N²LO.

To solve the many-body eigenvalue problem we will choose a basis space which usually consists of an infinite number of many-body basis states. Since the numerical solution in such an infinite Hilbert space is impossible, one has to restrict the model space to a finite number of basis states generally by discarding high-lying basis states. Because of this truncation, effects involving basis states with high energy or momentum, like short-range correlations, are not described adequately. An improvement of the description of these effects will be achieved by the similarity renormalization group (SRG) transformation of the Hamiltonian.

The untransformed Hamiltonian including NN+NNN interactions from χ EFT is provided through two- and three-body matrix elements in the harmonic oscillator basis, depending on Jacobi coordinates. For nuclear many-body calculations we need the Hamilton matrix elements in a Slater determinant basis composed of harmonic oscillator states depending on Cartesian coordinates. This basis is called the m-scheme basis. The first step will be to perform a basis transformation of the matrix elements using the techniques discussed in [3]. The implementation of this transformation is not trivial, because of the computational complexity careful optimization is necessary.

Two applications of this interaction will be discussed in this thesis. The first application of the SRG-transformed NN+NNN interaction from χ EFT is in the framework of the importance truncated no-core shell model (IT-NCSM). This exact ab initio method provides an extension of the classical NCSM and expands the coverage of the NCSM into the sd-shell. The IT-NCSM method will be applied for ⁴He and ⁶Li to investigate the properties of the NN+NNN interaction from χ EFT and of the SRG transformation. The second application of the SRG-transformed interaction will take place at the Hartree-Fock level. We will present the results of Hartree-Fock calculations for the ground-state energies and charge radii for a sequence of closed-shell nuclei.

This work is organized as follows. In Chapter 2 the necessity of a three-body interaction is motivated, in Chapter 3 the χ EFT is discussed and the interaction we use in

this thesis is introduced. Theoretical aspects and practical implementation of the basis transformation leading to m-scheme matrix elements of the interaction are reviewed in Chapter 4. In Chapter 5 we focus on the SRG transformation and their application in three-body space. In Chapter 6 the many-body methods are introduced and in Chapter 7 the results for the SRG-transformed NN+NNN interaction from χ EFT are presented. Finally, in Chapter 8 a summary and an outlook is provided.

2 The Significance of three-body interactions

We start with a brief motivation of the three-body (NNN) interaction, explaining its relevance and the problems occurring with its determination and application. High precision two-body interactions, e.g., the Argonne V_{18} or the charge-dependent Bonn (CD-Bonn) potential, are able to describe the scattering process of two nucleons as well as the bound-state properties of the deuteron with high precision. However, in nuclear structure physics one deals with many-particle systems, which can be much larger than a two-particle system. Thus, in principle all m -body interactions with $2 \leq m \leq A$ might be relevant for the description of the whole of nuclear physics of an A -particle system. Fortunately, the strong interaction among nucleons is very short ranged, therefore, the contribution of m -body interactions are expected to decrease with m . This expectation is also confirmed by χ EFT [1, 2]. We are restricted to m -body interactions with small m and have to neglect the remaining interaction contributions, because the complexity of the physical problem increases dramatically with m .

Generally, this circumstance does not inhibit an adequate prediction of nuclear structure properties based on two-body (NN) interactions in a phenomenological or approximative scheme. In the past 15 years the tremendous improvement of exact ab initio methods for solving the nuclear many-body problem, such as the Green's function Monte Carlo (GFMC) and the no-core shell model (NCSM) approaches, enable to verify the quality of a certain interaction. Figure 1 illustrates such an ab initio calculation with the GFMC approach. Obviously, even the low-energy states of light nuclei cannot be described in an adequate way with the NN interaction. The energy spectra show a sizable underbinding and the order of the states is not always reproduced correctly. The ground state of ^{10}B is predicted as an 1^+ -state instead of a 3^+ -state. With the inclusion of the Illinois-2 three-body interaction the results improve significantly. The energies are reproduced quite well and also the order of the states conform with experiment. There are several cases of few-body scattering and nuclear structure observables that clearly require three-nucleon forces for their microscopic explanation. Famous examples are the A_y puzzle of $N - d$ scattering [4] and the ground state of ^{10}B [5]. The results presented in Fig. 1 indicate the need of a NNN interaction.

But there are two problems arising with this approach. First, it is crucial to find a consistent way to obtain the NNN interaction with the same fundamental justification as for the NN interaction, instead of using an interaction which has no direct relation to the NN interaction and must be fitted to nuclear data. In χ EFT the interaction contributions for larger particle number m appear naturally from the power expansion (see Sec.

3), therefore, this theory provides the possibility to construct the NNN interaction in a consistent way to the NN interaction. The second problem occurring from the consideration of the NNN interaction is that the complexity of the matrix-element treatment increases. In this thesis we provide a solution of these two problems by using an interaction of χ EFT and presenting the techniques to handle the NNN interaction contributions.

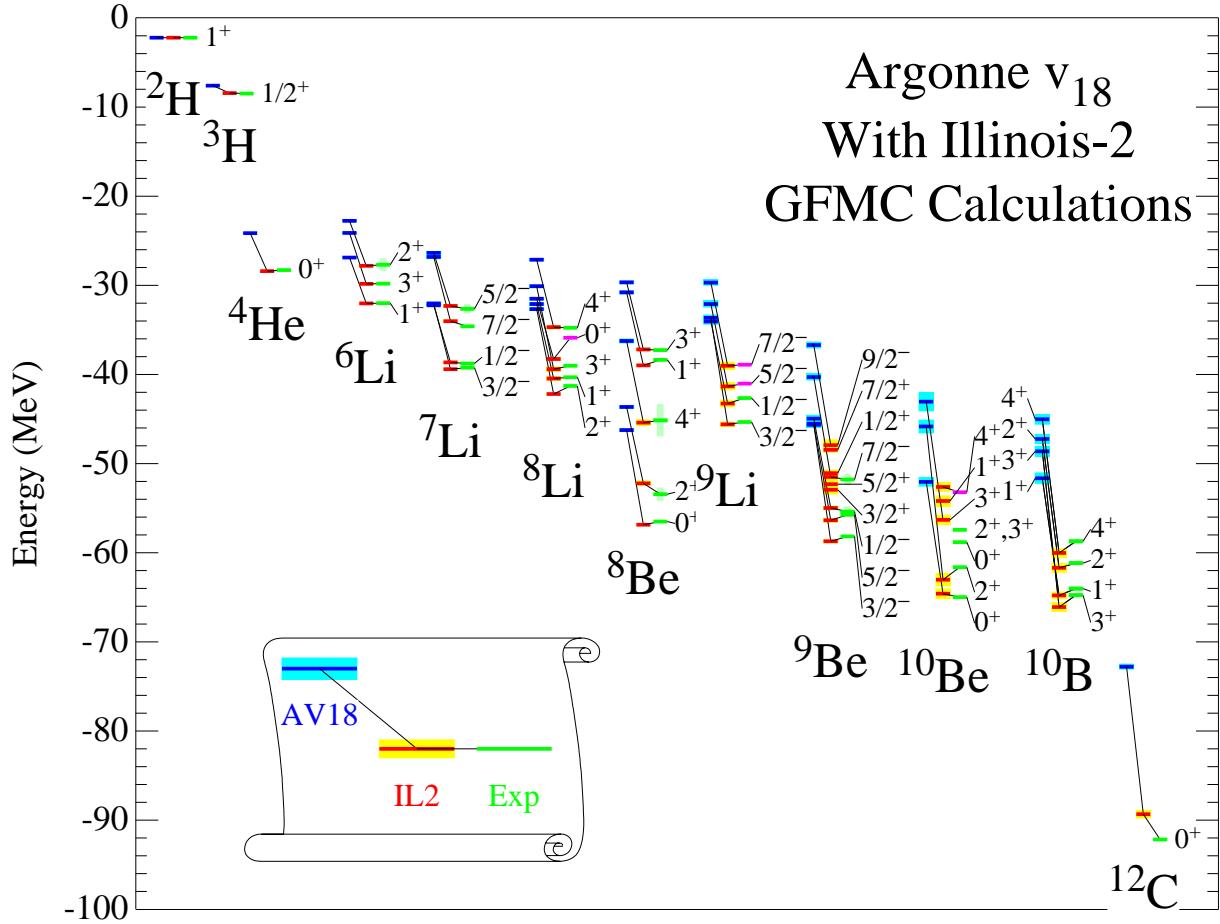


Figure 1: **Energy calculation with two- and three-body forces [6]:** The figure shows the low-energy states for light nuclei obtained with the two-body (blue) and two- plus three-body (yellow) Green's function Monte Carlo (GFMC) calculations. The experimental energies are indicated by the green bars. The two-body interaction is the Argonne V_{18} potential and the three-body part is the Illinois-2 interaction.

3 Basics of chiral effective field theory (χ EFT)

In the 1950s there were many attempts to derive the nuclear interaction within the pion-exchange theories, but these attempts failed because the chiral symmetry was not taken into account [7]. The χ EFT uses the pions and nucleons as internal degree of freedom and no heavy mesons and nucleon resonances. Besides, it considers chiral symmetry and establishes a connection to QCD, providing an interaction with a comparable explanatory power as phenomenological high-precision potentials like Argonne V18 and CD-Bonn. First, we discuss chiral symmetry. Second, we briefly describe the idea of the chiral perturbation theory and finally, we describe the procedure to obtain the matrix elements from χ EFT having a closer look at the power counting and parameter dependency.

3.1 Chiral symmetry

We start by investigating symmetries in general. One big advantage of the Lagrangian formulation is that symmetries lead to conserved quantities, so called currents. For example let us consider a transformation $\Phi \rightarrow \Phi + \delta\Phi$ which conserves the Lagrangian

$$\mathcal{L}(\Phi + \delta\Phi) = \mathcal{L}(\Phi), \quad (1)$$

$$\Rightarrow 0 = \mathcal{L}(\Phi + \delta\Phi) - \mathcal{L}(\Phi) = \delta\mathcal{L} = \frac{\partial\mathcal{L}}{\partial\Phi}\delta\Phi + \frac{\partial\mathcal{L}}{\partial(\partial_\mu\Phi)}(\partial_\mu\delta\Phi), \quad (2)$$

Using the equation of motion $\frac{\partial\mathcal{L}}{\partial\Phi} = \partial_\mu\frac{\partial\mathcal{L}}{\partial(\partial_\mu\Phi)}$ one obtains

$$0 = \partial_\mu \left(\frac{\partial\mathcal{L}}{\partial(\partial_\mu\Phi)}\delta\Phi \right),$$

so that the current $J^\mu = \frac{\partial\mathcal{L}}{\partial(\partial_\mu\Phi)}\delta\Phi$ is conserved. If the symmetry is explicitly broken in the Lagrangian, we can divide it into two parts $\mathcal{L} = \mathcal{L}_0 + \mathcal{L}_1$, where \mathcal{L}_0 is the symmetric part of the Lagrangian with respect to the symmetry transformation and \mathcal{L}_1 is the symmetry breaking part. Performing the above calculation again one gets

$$\delta\mathcal{L} = \delta\mathcal{L}_1 = \partial_\mu J^\mu \neq 0. \quad (3)$$

This means the current J^μ is not conserved anymore. After these general remarks we now concentrate on the idea of chiral symmetry [8] in QCD.

First of all, we consider the Lagrangian of free massless fermions

$$\mathcal{L} = i \sum_j \bar{\psi}_j \not{\partial} \psi_j, \quad (4)$$

where the index j refers to the different flavors, in our case of the up- and the down-quark. Therefore, we can reformulate our Lagrangian

$$\mathcal{L} = i\bar{\psi}_u \not{\partial} \psi_u + i\bar{\psi}_d \not{\partial} \psi_d = i\bar{\psi} \not{\partial} \psi. \quad (5)$$

In the last step we switched to an isospinor notation for the fermions, with $\psi = \begin{pmatrix} \psi_u \\ \psi_d \end{pmatrix}$. Let us have a look at the transformations of the chiral symmetry, also called $SU(2)_V \times SU(2)_A$ symmetry:

- **The vector transformation $\Lambda_V(\vec{\Theta})$**

$$\begin{aligned} \psi &\rightarrow e^{-i\frac{\vec{\tau}}{2}\vec{\Theta}}\psi \simeq \left(1 - i\frac{\vec{\tau}}{2}\vec{\Theta}\right)\psi \\ \Rightarrow \bar{\psi} &\rightarrow \bar{\psi}e^{i\frac{\vec{\tau}}{2}\vec{\Theta}} \simeq \bar{\psi}\left(1 + i\frac{\vec{\tau}}{2}\vec{\Theta}\right), \end{aligned} \quad (6)$$

where the absolute value of the rotation angles $\vec{\Theta}$ is infinitesimally small and $\vec{\tau}$ refers to the Pauli isospin matrices. Under this transformation the Lagrangian (5) is invariant and one obtains the vector-current

$$V_\mu^a = \bar{\psi}\gamma_\mu \frac{\tau^a}{2}\psi,$$

which is a conserved Noether current.

- **The axial transformation $\Lambda_A(\vec{\Theta})$**

$$\begin{aligned} \psi &\rightarrow e^{-i\gamma_5\frac{\vec{\tau}}{2}\vec{\Theta}}\psi \simeq \left(1 - i\gamma_5\frac{\vec{\tau}}{2}\vec{\Theta}\right)\psi \\ \Rightarrow \bar{\psi} &\rightarrow \bar{\psi}e^{-i\gamma_5\frac{\vec{\tau}}{2}\vec{\Theta}} \simeq \bar{\psi}\left(1 + i\gamma_5\frac{\vec{\tau}}{2}\vec{\Theta}\right). \end{aligned} \quad (7)$$

The Lagrangian (5) is also invariant under the axial transformation Λ_A and one

obtains the conserved axial current

$$A_\mu^a = \bar{\psi} \gamma_\mu \gamma_5 \frac{\tau^a}{2} \psi. \quad (8)$$

Now we introduce a mass term $\mathcal{L}_1 = -m(\bar{\psi}\psi)$ in the Lagrangian (5), i.e.

$$\mathcal{L} = i\bar{\psi}_u \not{\partial} \psi_u + i\bar{\psi}_d \not{\partial} \psi_d = i\bar{\psi} \not{\partial} \psi - m(\bar{\psi}\psi). \quad (9)$$

\mathcal{L}_1 is invariant under vector transformations Λ_V , but not under axial transformations Λ_A . Therefore, Λ_A is not a good symmetry if the fermions (quarks) have a finite mass. But one can regard Λ_A as an approximate symmetry, because the quark masses (5 – 10 MeV) are small in comparison to the relevant energy scale of QCD ($\Lambda_{QCD} \simeq 200$ MeV). This is the basis of the so-called partially conserved axial current hypothesis (PCAC).

An interesting point is the application of the upper transformation to meson states

$$\begin{aligned} \text{pion-like states: } \vec{\pi} &= i\bar{\psi} \vec{\tau} \gamma_5 \psi, & \sigma\text{-like states: } \sigma &= \bar{\psi} \psi, \\ \rho\text{-like states: } \vec{\varrho}_\mu &= \bar{\psi} \vec{\tau} \gamma_\mu \psi, & a_1\text{-like states: } \vec{a}_{1\mu} &= \bar{\psi} \vec{\tau} \gamma_\mu \gamma_5 \psi, \end{aligned} \quad (10)$$

where the meson states are given as quark fields, which carry the quantum numbers of the corresponding meson. The vectors again indicate the iso-vector nature of the meson states, this means the states transform like vectors under isospin rotations. The index μ indicates that the states transform like vectors under Lorentz transformation.

Performing the vector transformations for the pion-like state in (11), e.g., one can identify Λ_V with the isospin rotation

$$\vec{\pi} \xrightarrow{\Lambda_V} \vec{\pi} + \vec{\Theta} \times \vec{\pi}. \quad (11)$$

The axial transformation rotates the pion and σ -meson into each other

$$\begin{aligned} \vec{\pi} &\xrightarrow{\Lambda_A} \vec{\pi} + \vec{\Theta} \sigma, \\ \sigma &\xrightarrow{\Lambda_A} \sigma + \vec{\Theta} \vec{\pi}. \end{aligned}$$

Similarly Λ_A mixes ρ -meson and a_1 -meson states

$$\vec{\varrho}_\mu \xrightarrow{\Lambda_A} \vec{\varrho}_\mu + \vec{\Theta} \times \vec{a}_{1\mu}.$$

If Λ_A is considered as approximate symmetry of the QCD Hamiltonian, states which are rotated into each other by this transformation must have approximately the same eigenvalue, i.e. the same mass. However, for the ρ -meson $m_\rho = 770$ MeV and the a_1 -meson $m_{a_1} = 1260$ MeV this is obviously not the case. Therefore, it seems as if chiral symmetry is not a symmetry of QCD. On the other hand one can show that the weak pion decay is approximately consistent with a (partially) conserved axial-vector current in the case of small pion mass compared to the nucleon mass. Furthermore, chiral symmetry predicts the pion-nucleon coupling constant, deduced from the so called Goldberger-Treiman relation, in good agreement with the experimental coupling constant from pion-nucleon scattering.

The solution to these contradictions is the spontaneous breaking of the axial symmetry. One speaks of a spontaneous symmetry breaking if the Hamiltonian exhibits a symmetry, which is not realized by the ground state. A consequence of this spontaneous symmetry breaking is the existence of so-called massless Goldstone bosons, which are represented by the pion in the two flavor sector. The pions are not exactly massless as it would be the case for massless up- and down-quarks, but they are light in comparison to other hadrons. Due to this the pions are sometimes called pseudo-Goldstone bosons. Low-energy or -temperature hadronic processes¹ are dominated by pions. This property is exploited in chiral perturbation theory (χ PT) [1].

3.2 Principle of chiral perturbation theory (χ PT)

QCD is the established theory of the strong nuclear interaction, providing precise predictions for the high-energy regime. This is due to the asymptotic freedom of QCD, allowing the application of perturbation theory for this regime. But in the low-energy domain the growing of the coupling constant and the corresponding confinement of quarks and gluons destroy the convergence of the perturbation series. Therefore, a new concept is needed to describe low-energy nuclear interactions.

The main idea of chiral perturbation theory (χ PT) (see also [9]) is that at low energies the dynamics is controlled by the lightest particles, the pions, and the chiral symmetry of the QCD. S -matrix elements, i.e. scattering amplitudes, are expanded in Taylor-series of pion-momenta or masses, which is consistent with chiral symmetry. Such an expansion

¹At high temperature or densities, one expects a chiral restored phase, that means chiral symmetry is not spontaneously broken anymore and the pion loses its identity as a Goldstone boson, i.e. the pion will become massive if it exists [8]. One of the major goals of the ultra-relativistic heavy ion program is to create and identify such a phase in the laboratory.

is valid until one encounters a resonance, like the one of the ρ -meson. In χ PT one takes the Lagrangian containing the terms which exhibit chiral symmetry and constructs an effective Lagrangian from chiral perturbation theory by expanding in a Taylor-series of pion-momenta or masses up to a certain order. The details of the QCD dynamics, which are not fixed by the symmetry are defined by low-energy constants (LECs) contained in the expansion coefficients. At some future time these LECs will need to be determined from Lattice Gauge calculations, but for now they must be obtained by fitting to experimental data. To the considered order the resulting effective Lagrangian should be equivalent to the full QCD Lagrangian. But χ PT is not a perturbation theory in usual sense, because it does not perform an expansion in powers of the QCD-coupling constant. To generate a pion, infinite orders of QCD-coupling constants are needed. Therefore, it is a non-perturbative method. χ PT represents a power expansion of scattering amplitudes.

3.3 LECs, power counting and matrix element production

Weinberg showed in the chiral perturbation scheme [1], that one can expand the nuclear potential in terms of $\left(\frac{Q}{\Lambda_\chi}\right)^\nu$, where Q denotes the momentum or mass of the pion, $\Lambda_\chi \approx 1$ GeV is the chiral symmetry breaking scale and ν is the order. The number of contributing terms for a given order is finite and calculable. The terms with $\nu = 0$ are called the leading order (LO), the terms with $\nu = 1$ vanish, the terms with $\nu = 2$ the next-to-leading order (NLO), $\nu = 3$ are the next-to-next-to-leading order (N²LO) and so on. In Fig. 2 the terms up to (N³LO) are listed. One can see that with increasing order ν , also the particle number of the interaction increases. Due to the fact that the terms with higher ν become less important, one can reason that also the importance of the interaction decreases with the increased irreducible particle number.

Before we discuss the three-body (NNN) interaction matrix elements from χ EFT we first have a look at the two-body (NN) interaction. As shown in [7] the NLO or N²LO two-body interaction is not sufficient to describe the nucleon-nucleon scattering data below 290 MeV. Therefore, we will use the N³LO potential for the two-body interaction from [7] with 29 LECs fitted to np data. With this potential one obtains a high precision description of the np data with an accuracy comparable to the Argonne V18 potential. Since there are expressions in the terms of the χ EFT interaction, which are only meaningful for momenta below a certain scale, the expressions have to be regularized. There

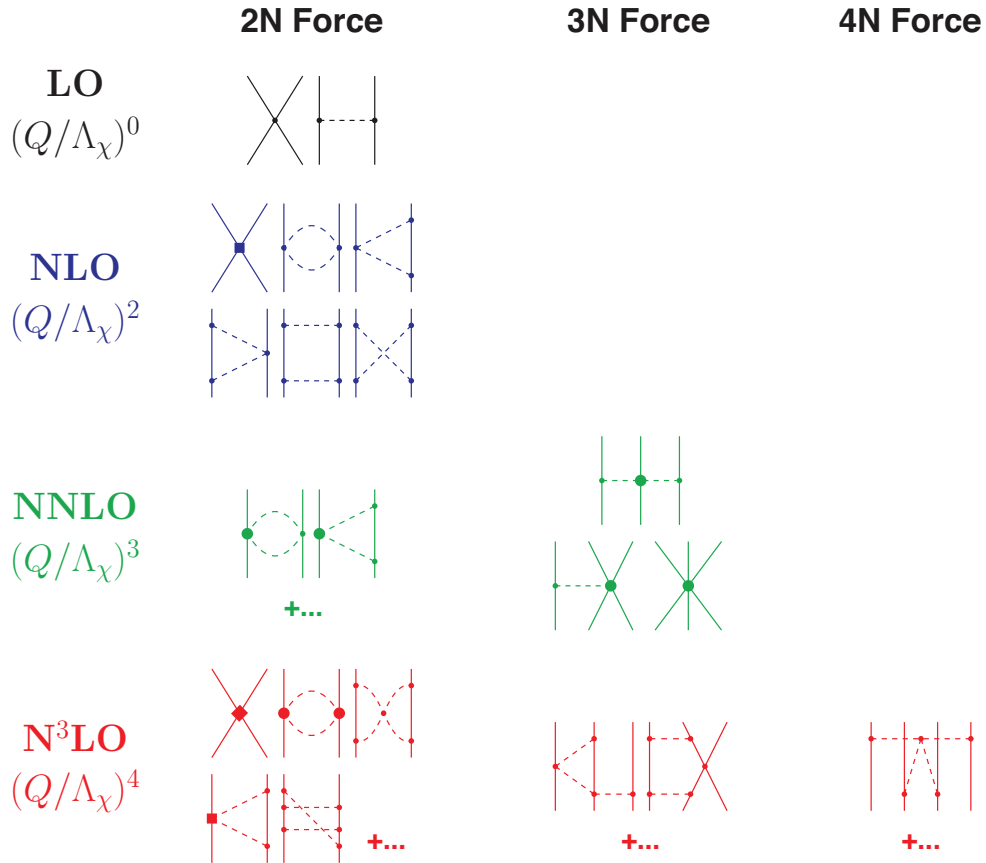


Figure 2: **Hierarchy of nuclear forces in χ EFT [11]:** The interaction potential terms up to the N^3 LO are dedicated to the particle number of the interaction. The dashed lines represent pions and the solid lines nucleons. The small dots, large solid dots, solid squares and solid diamond denote different vertices.

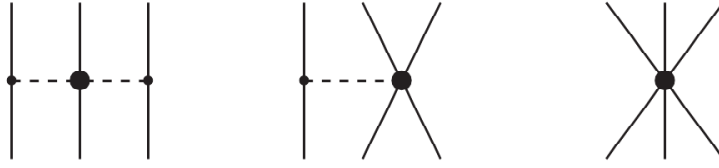


Figure 3: **N²LO terms of the NNN interaction potential**[11]: *The term on the left corresponds to the two-pion exchange depending on the LECs c_1, c_3, c_4 also contained in the NN interaction. In the middle we see the one-pion plus two-nucleon contact term depending on c_D and on the right the three-nucleon contact term depending on c_E .*

are different choices for this regulator function and in our case we use

$$F[q^2; \Lambda] = \exp\left(-\frac{q^{2n}}{\Lambda^{2n}}\right) \quad (12)$$

depending on the momentum transfer q and the cutoff Λ . For the N³LO two-body interaction one has to choose $n = 3$ and for the N²LO three-body interaction $n = 2$. One of the major advantages of χ EFT is that one can construct the NNN interaction in a consistent way. One has to use the same LECs of the NN potential which also appear in the NNN potential and also the regulator function has to be chosen consistently. Up to now the NNN interaction matrix elements are only available from the N²LO, leaving an inconsistency in the many-body calculation when combined with the NN force at N³LO. Except for two LECs, c_D and c_E , this NNN interaction is completely defined by the parameters of the NN interaction at N³LO.

In the following, we concentrate on the N²LO NNN interaction. To produce matrix elements from χ EFT one has to overcome two challenges. First, one has to calculate the operator expressions [10] of the diagrams in Fig. 3. One ends up with three operators depending on a number of LECs. The first term with the two-pion exchange depends on the LECs c_1, c_2 and c_3 already fitted by the N³LO NN interaction. But the parameters c_D of the one-pion exchange plus two-nucleon contact term and c_E of the three-nucleon contact term are not contained in the NN interaction. The procedure for the second task, the calculation of the matrix elements [12] from the operators, is the following. One inserts a regulator function to regularize the momentum integrals. As mentioned above, there are different regulator choices, where we used a regulator depending on the momentum transfer with the cutoff $\Lambda = 500$ MeV. After some non-trivial calculation

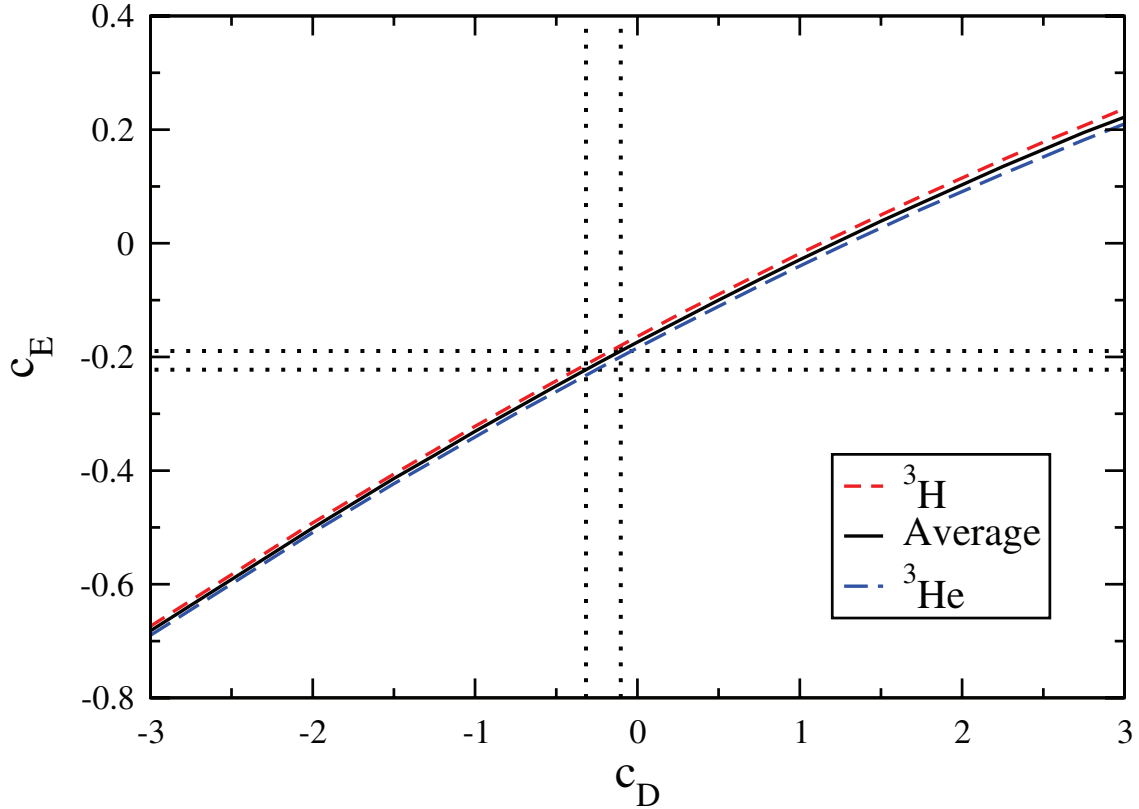


Figure 4: **Fit of the LECs c_D and c_E [13]:** Shown are the fits for c_D and c_E to the binding energies of ${}^3\text{H}$ (red curve) and ${}^3\text{He}$ (blue curve), as well as the average of both fits (black curve). The dotted lines show the regions of the error bars related to the fit of both LECs to the half-life of Triton.

one obtains an expression for the matrix elements depending on c_D and c_E . For the calculations in the second task, the Jacobi states emerge as an appropriate basis. This is why we will deal with matrix elements in Jacobi representation in Sec. 4. What is left is to fit the two LECs to $A \geq 3$ nuclei observables. In our case we adopt the LECs proposed in Ref. [13]. They performed a fit to the binding energies of the $A = 3$ nuclei (${}^3\text{He}$, ${}^3\text{H}$) and the Triton half-life. The fit to the binding energies leads to a curve in the $c_D - c_E$ plane, plotted in Fig. 4. Next they searched the values of the LECs on this trajectory for which the half-life of Triton is reproduced in the best way. From this fit they obtained $c_D = -0.2$ and $c_E = -0.205$.

Note that there are other choices for the regulator and for the c_D and c_E fit leading to different interactions, for example the one used in [14], which differs to some extent to our interaction (used in [15, 16]) in the description of the mid- p -shell nuclei [12].

Moreover, let us assume that the NN interaction from N³LO is sufficient as indicated by the high-precision description of nucleon-nucleon scattering. We still have an incomplete interaction, because only the N²LO is considered for the NNN part and in addition, there are also interaction contributions involving more than three particles. This incompleteness can be absorbed by a phenomenological fit of the parameters c_D and c_E . But it is also possible that one has to choose different parameter sets for different mass regions. Owing to this, one has to explore different choices of the NNN interaction. This is why we plan to investigate the c_D and c_E dependence in the future.

4 Transformation: Jacobi coordinates to m-scheme

The interaction from χ EFT (Chapter 3) is provided by a code [17] of Petr Navrátil in form of matrix elements in an antisymmetrized basis of three-body Jacobi coordinates. For the many-body calculation we will use matrix elements in the m-scheme, therefore, we have to perform a non-trivial basis transformation to get these matrix elements. In the following, we will discuss this transformation and some prerequisites. We start by introducing the two involved basis sets and some mathematical techniques to perform the transformation before we discuss the formal transformation and the implementation in C/C++.

4.1 Jacobi coordinates

The Jacobi coordinates $\vec{\xi}_i$ provide an alternative to the single-nucleon coordinates \vec{r}_i . Both coordinates can be converted into each other by an orthogonal transformation. We work in the isospin formalism and consider nucleons with the same mass m . There is no unique set of Jacobi coordinates, but a number of different sets. For this thesis the following choice will be used [18]

$$\vec{\xi}_0 = \sqrt{\frac{1}{A}}[\vec{r}_1 + \vec{r}_2 + \dots + \vec{r}_A], \quad (13)$$

$$\vec{\xi}_n = \sqrt{\frac{n}{n+1}}\left[\frac{1}{n}(\vec{r}_1 + \vec{r}_2 + \dots + \vec{r}_n) - \vec{r}_{n+1}\right], \quad (14)$$

with $n = 1, 2, \dots, A - 1$ and where A is the number of nucleons of the many-body state one wants to describe.

We are only interested in two- and three-particle states, therefore, we only need the Jacobi coordinates $\vec{\xi}_0, \vec{\xi}_1$ for two particles and also $\vec{\xi}_2$ for three particles. For a three-particle state one obtains the Jacobi coordinates

$$\vec{\xi}_0 = \sqrt{\frac{1}{3}}[\vec{r}_1 + \vec{r}_2 + \vec{r}_3], \quad (15)$$

$$\vec{\xi}_1 = \sqrt{\frac{1}{2}}[\vec{r}_1 - \vec{r}_2], \quad (16)$$

$$\vec{\xi}_2 = \sqrt{\frac{2}{3}}\left[\frac{1}{2}(\vec{r}_1 + \vec{r}_2) - \vec{r}_3\right], \quad (17)$$

which are illustrated in Fig. 5. In the chosen set of Jacobi-coordinates $\vec{\xi}_0$ (see Eq. 13) depends on the number of particles, because it is related to the center of mass of the

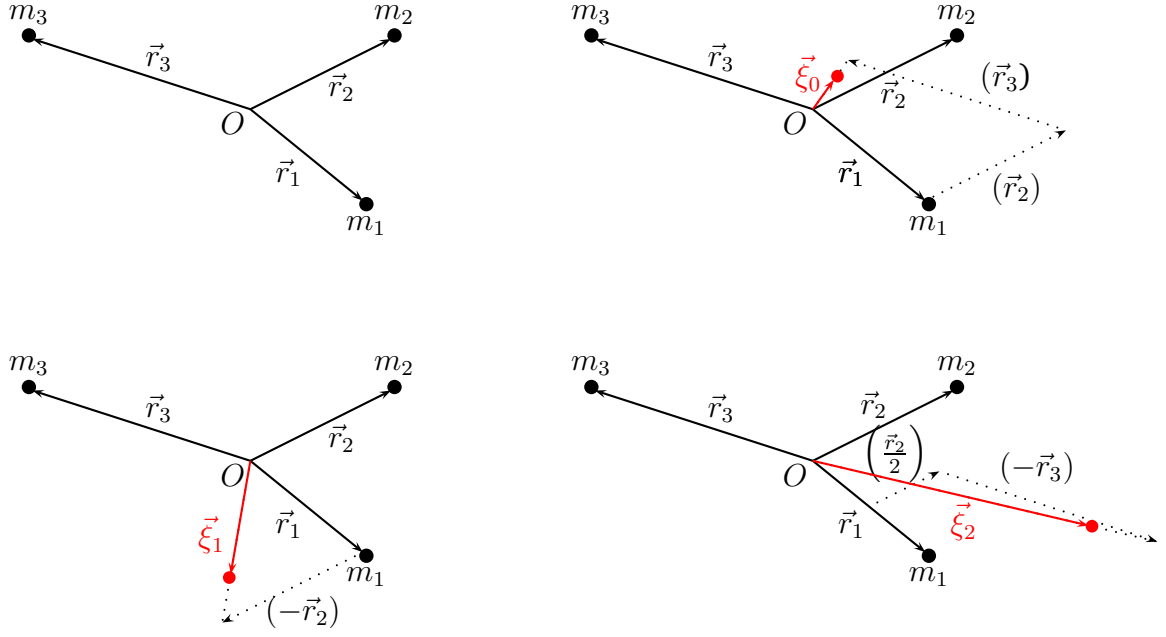


Figure 5: **Jacobi coordinates for three particles:** Top left the Cartesian coordinates are shown. The other three pictures show the construction of the Jacobi coordinates $\vec{\xi}_0$ (top right), $\vec{\xi}_1$ (bottom left) and $\vec{\xi}_2$ (bottom right) out of the Cartesian coordinates. The Jacobi coordinates are constructed by linear combinations of the Cartesian coordinates, indicated by the dotted vectors, which have to be multiplied by certain factors, according to Eq. (15), (16) and (17).

whole system, i.e., it is parallel to the center-of-mass vector. The Jacobi coordinate $\vec{\xi}_1$ is related to the relative coordinate of the first two particles and $\vec{\xi}_2$ to the relative coordinate of the third particle with the center of mass of the first two particles.

Now, after having introduced the Jacobi coordinates we consider the meaning of these coordinates for our quantum mechanical state. Our many-body basis consists of single-particle harmonic oscillator states. We use a single-particle state of the form $|nlm\rangle \otimes |s = \frac{1}{2} m_s\rangle \otimes |t = \frac{1}{2} m_t\rangle$, where the orbital angular momentum and the spin can be coupled with each other. The choice of the coordinates only has an influence on the spatial part. It is characterized by the radial quantum number n , the quantum number l of the orbital angular momentum and the quantum number m corresponding to the z -axis projection of the orbital angular momentum. All these quantum numbers depend on the choice of the coordinate system. For instance, an orbital angular momentum in classical analogy $\vec{l} = \vec{r} \times \vec{p}$ depends on the underlying coordinate system and this holds true for the corresponding quantum numbers as well.

The matrix elements of the χ EFT interaction are given in the basis $\{|n_{cm}l_{cm}\rangle|EiJT\rangle\}^{\mathcal{JM}}$, which will be introduced in Sec. 4.5. However, the state $\{|n_{cm}l_{cm}\rangle|EiJT\rangle\}^{\mathcal{JM}}$ can be expanded in the following three-body basis depending on Jacobi coordinates

$$\{|n_{cm}l_{cm}\rangle|\alpha\rangle\}^{\mathcal{JM}} = \{|n_{cm}l_{cm}\rangle|[(n_{12}l_{12}, s_{ab})j_{12}, (n_3l_3, s_c)j_3]J, [(t_a t_b)t_{ab}, t_c]TM_T\rangle\}^{\mathcal{JM}}, \quad (18)$$

where $n_{cm}l_{cm}$ are the quantum numbers corresponding to the Jacobi coordinate $\vec{\xi}_0$, $n_{12}l_{12}$ to $\vec{\xi}_1$ and n_3l_3 to $\vec{\xi}_2$. A more detailed description of these states will be given in Sec. 4.5. The advantage of the so-called Jacobi basis (18) is that the intrinsic part $|\alpha\rangle$ decouples from the center-of-mass part $|n_{cm}l_{cm}\rangle$, which is not relevant for the interaction. Besides, the basis dimension up to a given energy becomes small compared to the m-scheme and the angular momentum is a good quantum number. For the antisymmetrized Jacobi basis $\{|n_{cm}l_{cm}\rangle|EiJT\rangle\}^{\mathcal{JM}}$ [14] the basis dimension up to a given energy becomes even smaller. But these bases are not very useful in many-body calculations (Chap. 6).

4.2 The m-scheme

The m-scheme basis is an antisymmetrized many-body basis consisting of harmonic-oscillator single-particle states, with quantum numbers defined with respect to single-particle coordinates. In this basis the orbital angular momentum l_i and the spin s_i of each particle are coupled to the angular momentum j_i

$$\begin{aligned} & |(n_1l_1, s_1)j_1m_{j_1}t_1m_{t_1}; (n_2l_2, s_2)j_2m_{j_2}t_2m_{t_2}; \dots; (n_A l_A, s_A)j_A m_{j_A} t_A m_{t_A}\rangle_a \\ & = \sqrt{A!} \hat{\mathcal{A}} |(n_1l_1, s_1)j_1m_{j_1}t_1m_{t_1}\rangle \otimes |(n_2l_2, s_2)j_2m_{j_2}t_2m_{t_2}\rangle \otimes \dots \otimes |(n_A l_A, s_A)j_A m_{j_A} t_A m_{t_A}\rangle, \end{aligned} \quad (19)$$

where $\hat{\mathcal{A}}$ is the antisymmetrizer.

In this basis the quantum numbers $M_J = m_{j_1} + m_{j_2} + \dots + m_{j_A}$ and $M_T = m_{t_1} + m_{t_2} + \dots + m_{t_A}$ are the only good quantum numbers of the many-body basis state. Although the angular momentum is not a good quantum number in this basis, this basis is more convenient for the many-body calculations. Therefore, we will further perform many-body calculations in the m-scheme.

4.3 Coupling and coordinate-transformation formulas

One of the main challenges we will deal with is the transformation of matrix elements from the Jacobi basis (18) to the m-scheme (19). Therefore, several technical formulas will be used which are introduced in this section.

4.3.1 6-j symbols

The Wigner 6-j symbols are related to the coefficients of transformations between different coupling schemes of three angular momenta. Let us consider the state

$|[(j_1 j_2) j_{12}, j_3] j m\rangle$, where j_1 and j_2 couple to j_{12} and j_{12} couples with j_3 to j . If one wants to transform this state into another coupling scheme like $|[j_1, (j_2 j_3) j_{23}] j' m'\rangle$, one has to insert the identity operator in the basis of the new coupling scheme which yields the coefficients $\langle [(j_1 j_2) j_{12}, j_3] j m | [j_1, (j_2 j_3) j_{23}] j' m' \rangle$ which can be calculated from 6-j symbols.

The 6-j symbols are defined by the relations [19]

$$\langle [(j_1 j_2) j_{12}, j_3] j m | [j_1, (j_2 j_3) j_{23}] j' m' \rangle = \delta_{jj'} \delta_{mm'} (-1)^{j_1 + j_2 + j_3 + j} \hat{j}_{12} \hat{j}_{23} \begin{Bmatrix} j_1 & j_2 & j_{12} \\ j_3 & j & j_{23} \end{Bmatrix}, \quad (20)$$

$$\begin{aligned} \langle [(j_1 j_2) j_{12}, j_3] j m | [(j_1 j_3) j_{13}, j_2] j' m' \rangle \\ = \delta_{jj'} \delta_{mm'} (-1)^{j_2 + j_3 + j_{12} + j_{13}} \hat{j}_{12} \hat{j}_{13} \begin{Bmatrix} j_2 & j_1 & j_{12} \\ j_3 & j & j_{13} \end{Bmatrix}, \end{aligned} \quad (21)$$

$$\langle [j_1, (j_2 j_3) j_{23}] j m | [(j_1 j_3) j_{13}, j_2] j' m' \rangle = \delta_{jj'} \delta_{mm'} (-1)^{j_1 + j + j_{23}} \hat{j}_{13} \hat{j}_{23} \begin{Bmatrix} j_1 & j_3 & j_{13} \\ j_2 & j & j_{23} \end{Bmatrix}, \quad (22)$$

with $\hat{j} = \sqrt{2j+1}$.

It is important to note that the total angular momenta quantum numbers j, j' and the corresponding projections m, m' must be equal. The 6-j symbols can be chosen to be real, therefore, one can swap the bra and the ket and obtains the same result. For further symmetry relations see [19].

4.3.2 9-j symbols

The Wigner 9-j symbols (also called Fano coefficients) are related to the transformation coefficients of different coupling schemes of four angular momenta.

They are defined by the relations [19]

$$\begin{aligned} & \langle [(j_1 j_2) j_{12}, (j_3 j_4) j_{34}] j m | [(j_1 j_3) j_{13}, (j_2 j_4) j_{24}] j' m' \rangle \\ &= \delta_{jj'} \delta_{mm'} \hat{j}_{12} \hat{j}_{13} \hat{j}_{24} \hat{j}_{34} \begin{Bmatrix} j_1 & j_2 & j_{12} \\ j_3 & j_4 & j_{34} \\ j_{13} & j_{24} & j \end{Bmatrix}, \end{aligned} \quad (23)$$

$$\begin{aligned} & \langle [(j_1 j_2) j_{12}, (j_3 j_4) j_{34}] j m | [(j_1 j_4) j_{14}, (j_2 j_3) j_{23}] j' m' \rangle \\ &= \delta_{jj'} \delta_{mm'} (-1)^{j_3 + j_4 - j_{34}} \hat{j}_{12} \hat{j}_{14} \hat{j}_{23} \hat{j}_{34} \begin{Bmatrix} j_1 & j_2 & j_{12} \\ j_4 & j_3 & j_{34} \\ j_{14} & j_{23} & j \end{Bmatrix}, \end{aligned} \quad (24)$$

$$\begin{aligned} & \langle [(j_1 j_3) j_{13}, (j_2 j_4) j_{24}] j m | [(j_1 j_4) j_{14}, (j_2 j_3) j_{23}] j' m' \rangle \\ &= \delta_{jj'} \delta_{mm'} (-1)^{j_3 - j_4 - j_{23} + j_{24}} \hat{j}_{13} \hat{j}_{14} \hat{j}_{24} \hat{j}_{23} \begin{Bmatrix} j_1 & j_3 & j_{13} \\ j_4 & j_2 & j_{24} \\ j_{14} & j_{23} & j \end{Bmatrix}, \end{aligned} \quad (25)$$

with $\hat{j} = \sqrt{2j+1}$.

Because the 9-j symbols can be chosen to be real, one can swap the bra and the ket without changing the result. The angular momenta in a row and column of the 9-j symbol fulfill the triangular condition, where the right angular momentum in a row and the lower angular momentum in a column are the coupled angular momenta. The 9-j symbols are invariant under even permutations of columns or rows as well as under transposition. Odd permutations of rows or columns produce a phase factor $(-1)^R$, where R is the sum of all angular momenta in the symbol. For further symmetry relations see [19].

There are different ways to calculate the 9-j symbols. One is to express them by 6-j

symbols

$$\begin{Bmatrix} a & b & c \\ d & e & f \\ g & h & j \end{Bmatrix} = \sum_x (-2)^x (2x+1) \begin{Bmatrix} a & b & c \\ f & j & x \end{Bmatrix} \begin{Bmatrix} d & e & f \\ b & x & h \end{Bmatrix} \begin{Bmatrix} g & h & j \\ x & a & d \end{Bmatrix}. \quad (26)$$

This is how we will implement the 9-j symbols.

4.3.3 Harmonic-oscillator brackets (HOBs)

If one wants to transform between harmonic-oscillator states with quantum numbers defined with respect to different coordinate systems, one can use the harmonic-oscillator brackets or also called Talmi-Moshinsky coefficients. We will call such a transformation, therefore, Talmi-transformation. The HOBs are the scalar product of the spatial part of two two-body states with quantum numbers defined with respect to different coordinate systems. The angular orbital momenta of each state have to be coupled.

In this thesis we will use the HOBs defined by Kammuntavičius [20]

$$|[n_1 l_1(\vec{r}_1), n_2 l_2(\vec{r}_2)]\Lambda\lambda\rangle = \sum_{NL, nl} \langle\langle NL, nl | n_1 l_1, n_2 l_2; \Lambda \rangle\rangle_d |[NL(\vec{R}), nl(\vec{r})]\Lambda\lambda\rangle, \quad (27)$$

with the HOB $\langle\langle NL, nl | n_1 l_1, n_2 l_2; \Lambda \rangle\rangle_d$. The orbital angular momenta l_1, l_2 and L, l couple to Λ with projection λ . Note Eq. (27) is not written in coordinate representation, the coordinate vectors $\vec{r}_1, \vec{r}_2, \vec{R}_1$ and \vec{r} indicate that the radial and the orbital angular momentum quantum numbers n_1, l_1, n_2, l_2, N, L and n, l are defined with respect to this coordinate.

The corresponding coordinate-transformation matrix reads

$$\begin{pmatrix} \vec{R} \\ \vec{r} \end{pmatrix} = \begin{pmatrix} \sqrt{\frac{d}{1+d}} & \sqrt{\frac{1}{1+d}} \\ \sqrt{\frac{1}{1+d}} & -\sqrt{\frac{d}{1+d}} \end{pmatrix} \begin{pmatrix} \vec{r}_1 \\ \vec{r}_2 \end{pmatrix}. \quad (28)$$

The parameter d defines the type of coordinate transformation.

There are three useful symmetry relations and the fact that the HOBs are real, yielding

$$\begin{aligned} & \langle \langle n_1 l_1, n_2 l_2 | NL, nl; \Lambda \rangle \rangle_d \\ & = \langle \langle NL, nl | n_1 l_1, n_2 l_2; \Lambda \rangle \rangle_d, \end{aligned} \quad (29)$$

$$= (-1)^{l_2+L} \langle \langle n_2 l_2, n_1 l_1 | nl, NL; \Lambda \rangle \rangle_d, \quad (30)$$

$$= (-1)^{L-\Lambda} \langle \langle n_2 l_2, n_1 l_1 | NL, nl; \Lambda \rangle \rangle_{\frac{1}{d}}, \quad (31)$$

$$= (-1)^{l_1-\Lambda} \langle \langle n_1 l_1, n_2 l_2 | nl, NL; \Lambda \rangle \rangle_{\frac{1}{d}}. \quad (32)$$

For further symmetry relations see [21].

All symmetry relations can be obtained by analogous derivations. Hence, we will only perform the derivation for one of these relations. First, we insert an identity operator in coordinate representation

$$\begin{aligned} & \langle \langle NL(\vec{R}), nl(\vec{r}) | n_1 l_1(\vec{r}_1), n_2 l_2(\vec{r}_2); \Lambda \rangle \rangle_d \\ & = \frac{1}{2\Lambda+1} \sum_{\lambda} \int \int d^3 r_1 d^3 r_2 \left\{ \phi_{n_1 l_1}(\vec{r}_1) \otimes \phi_{n_2 l_2}(\vec{r}_2) \right\}_{\Lambda\lambda}^{\dagger} \left\{ \phi_{NL}(\vec{R}) \otimes \phi_{nl}(\vec{r}) \right\}_{\Lambda\lambda}, \end{aligned} \quad (33)$$

with a shorthand notation for the coupled wave functions

$$\left\{ \phi_{n_1 l_1}(\vec{r}_1) \otimes \phi_{n_2 l_2}(\vec{r}_2) \right\}_{\Lambda\lambda} = \sum_{m_1 m_2} c \begin{pmatrix} l_1 & l_2 & \Lambda \\ m_1 & m_2 & \lambda \end{pmatrix} \phi_{n_1 l_1 m_1}(\vec{r}_1) \phi_{n_2 l_2 m_2}(\vec{r}_2),$$

where $\phi_{nlm}(\vec{r})$ are the orthonormalized harmonic-oscillator functions [20]. The factor $\frac{1}{2\Lambda+1}$ results from the fact that the HOBs are independent of the projection quantum number λ .

In addition, we recognize that the same transformation matrix combines the coordinates in the following way

$$\begin{pmatrix} -\vec{r} \\ \vec{R} \end{pmatrix} = \begin{pmatrix} \sqrt{\frac{d}{1+d}} & \sqrt{\frac{1}{1+d}} \\ \sqrt{\frac{1}{1+d}} & -\sqrt{\frac{d}{1+d}} \end{pmatrix} \begin{pmatrix} \vec{r}_2 \\ -\vec{r}_1 \end{pmatrix}, \quad (34)$$

where also $\vec{R} = \sqrt{\frac{d}{1+d}}\vec{r}_1 + \sqrt{\frac{1}{1+d}}\vec{r}_2$ and $\vec{r} = \sqrt{\frac{1}{1+d}}\vec{r}_1 - \sqrt{\frac{d}{1+d}}\vec{r}_2$ hold true. Furthermore, it is essential that

$$\left\{ \phi_{e_1 l_1}(\vec{r}_1) \otimes \phi_{e_2 l_2}(\vec{r}_2) \right\}_{\Lambda\lambda} = (-1)^{l_1} (-1)^{l_1+l_2-\Lambda} \left\{ \phi_{e_2 l_2}(\vec{r}_2) \otimes \phi_{e_1 l_1}(-\vec{r}_1) \right\}_{\Lambda\lambda}, \quad (35)$$

$$\left\{ \phi_{EL}(\vec{R}) \otimes \phi_{el}(\vec{r}) \right\}_{\Lambda\lambda} = (-1)^l (-1)^{l+L-\Lambda} \left\{ \phi_{el}(-\vec{r}) \otimes \phi_{EL}(\vec{R}) \right\}_{\Lambda\lambda}. \quad (36)$$

Using these relations we can rewrite Eq. (33) as

$$\begin{aligned} & \langle \langle n_1 l_1(\vec{r}_1), n_2 l_2(\vec{r}_2) | NL(\vec{R}), nl(\vec{r}); \Lambda \rangle \rangle_d \\ &= \frac{1}{2\Lambda+1} \sum_{\lambda} \int \int d^3 r_1 d^3 r_2 \\ & \quad \left\{ \phi_{n_2 l_2}(\vec{r}_2) \otimes \phi_{n_1 l_1}(-\vec{r}_1) \right\}_{\Lambda\lambda}^{\dagger} \left\{ \phi_{nl}(-\vec{r}) \otimes \phi_{NL}(\vec{R}) \right\}_{\Lambda\lambda} (-1)^{l_2+L} \\ &= (-1)^{l_2+L} \langle \langle n_2 l_2(\vec{r}_2), n_1 l_1(-\vec{r}_1) | nl(-\vec{r}), NL(\vec{R}); \Lambda \rangle \rangle_d \\ &= (-1)^{l_2+L} \langle \langle n_2 l_2, n_1 l_1 | nlNL; \Lambda \rangle \rangle_d. \end{aligned} \quad (37)$$

So we obtained the symmetry relation (30). In analogy the other symmetry relations can be derived.

4.4 Two-body Jacobi basis to m-scheme transformation

In this section we will perform the matrix-element transformation from the Jacobi basis to the m-scheme in two-body space. This transformation will be used to produce the two-body m-scheme matrix elements. Moreover, it is a good exercise in view of the transformation in the three-body space.

We aim at the transformation of the following antisymmetrized matrix element of the two-body interaction \hat{V}_{NN} to obtain the formula [22]

$$\begin{aligned} & {}_a \langle \langle (n_1 l_1, s_1) j_1, (n_2 l_2, s_2) j_2 | J T M_T | \hat{V}_{NN} | (n'_1 l'_1, s'_1) j'_1, (n'_2 l'_2, s'_2) j'_2 \rangle \rangle J T M_T \rangle_a \\ &= \hat{j}_1 \hat{j}_2 \hat{j}'_1 \hat{j}'_2 \sum_{LSN\Lambda\nu\lambda,j} \sum_{\nu'\lambda'} \sum_{L'} \hat{L}^2 \hat{L}'^2 \hat{j}^2 \hat{S}^2 (1 - (-1)^{\lambda+S+T}) \\ & \quad \times \begin{Bmatrix} l_1 & l_2 & L \\ s_1 & s_2 & S \\ j_1 & j_2 & J \end{Bmatrix} \begin{Bmatrix} l'_1 & l'_2 & L' \\ s_1 & s_2 & S \\ j'_1 & j'_2 & J \end{Bmatrix} \begin{Bmatrix} \Lambda & \lambda & L \\ S & J & j \end{Bmatrix} \begin{Bmatrix} \Lambda & \lambda' & L' \\ S & J & j \end{Bmatrix} \\ & \quad \times \langle \langle N\Lambda, \nu\lambda | n_1 l_1, n_2 l_2; L \rangle \rangle \langle \langle N\Lambda, \nu'\lambda' | n'_1 l'_1, n'_2 l'_2; L' \rangle \rangle \\ & \quad \times \langle \langle (\nu\lambda, S) j T M_T | \hat{V}_{NN} | (\lambda'\nu', S) j T M_T \rangle \rangle. \end{aligned} \quad (38)$$

In Eq. (38) a coupled antisymmetric m-scheme basis

$\left\{ |[(n_1 l_1, s_1) j_1, (n_2 l_2, s_2) j_2] J M_J T M_T \rangle_a \right\}$ is used on the left-hand side. Note that the used interaction \hat{V}_{NN} is independent of the projection quantum numbers of the angular momenta. To obtain an expression depending on the matrix element represented in the non-antisymmetrized Jacobi basis $|N \Lambda m_\Lambda, (\nu \lambda, S) j m_j T M_T \rangle$ one has to perform the antisymmetrization to get antisymmetric states on the left-hand side

$$\begin{aligned} & {}_a \langle [(n_1 l_1, s_1) j_1, (n_2 l_2, s_2) j_2] J M_J T M_T | \hat{V}_{NN} | [(n'_1 l'_1, s'_1) j'_1, (n'_2 l'_2, s'_2) j'_2] J M_J T M_T \rangle_a \\ &= {}_a \langle [(n_1 l_1, s_1) j_1, (n_2 l_2, s_2) j_2] J M_J T M_T | \\ & \quad \times \hat{V}_{NN} \sqrt{2!} \hat{\mathcal{A}} | [(n'_1 l'_1, s'_1) j'_1, (n'_2 l'_2, s'_2) j'_2] J M_J T M_T \rangle \end{aligned} \quad (39)$$

$$\begin{aligned} &= {}_a \langle [(n_1 l_1, s_1) j_1, (n_2 l_2, s_2) j_2] J M_J T M_T | \hat{\mathcal{A}} \\ & \quad \times \hat{V}_{NN} \sqrt{2!} | [(n'_1 l'_1, s'_1) j'_1, (n'_2 l'_2, s'_2) j'_2] J M_J T M_T \rangle \end{aligned} \quad (40)$$

$$\begin{aligned} &= {}_a \langle [(n_1 l_1, s_1) j_1, (n_2 l_2, s_2) j_2] J M_J T M_T | \\ & \quad \times \hat{V}_{NN} \sqrt{2!} | [(n'_1 l'_1, s'_1) j'_1, (n'_2 l'_2, s'_2) j'_2] J M_J T M_T \rangle \end{aligned} \quad (41)$$

$$\begin{aligned} &= \left[\langle [(n_1 l_1, s_1) j_1, (n_2 l_2, s_2) j_2] J M_J T M_T | - \langle [(n_1 l_1, s_1) j_1, (n_2 l_2, s_2) j_2] J M_J T M_T | \hat{T}_{12} \right] \\ & \quad \times \frac{\sqrt{2!}}{\sqrt{2!}} \hat{V}_{NN} | [(n'_1 l'_1, s'_1) j'_1, (n'_2 l'_2, s'_2) j'_2] J M_J T M_T \rangle \end{aligned} \quad (42)$$

$$\begin{aligned} &= \left[\langle [(n_1 l_1, s_1) j_1, (n_2 l_2, s_2) j_2] J M_J T M_T | \right. \\ & \quad \left. - (-1)^{j_1+j_2-J} (-1)^{T-1} \langle [(n_2 l_2, s_2) j_2, (n_1 l_1, s_1) j_1] J M_J T M_T | \right] \\ & \quad \times \hat{V}_{NN} | [(n'_1 l'_1, s'_1) j'_1, (n'_2 l'_2, s'_2) j'_2] J M_J T M_T \rangle. \end{aligned} \quad (43)$$

To obtain (40) we used the commutator relation $[\hat{V}_{NN}, \hat{\mathcal{A}}] = 0$ and in (41) the projection property $\hat{\mathcal{A}} \cdot \hat{\mathcal{A}} = \hat{\mathcal{A}}$ of the antisymmetrizer. To get (42) we insert the antisymmetrizer

$$\hat{\mathcal{A}} = \frac{1}{A!} \sum_{\mathcal{P}} (-1)^P \hat{\mathcal{P}},$$

where P is the signature of the permutation operator \hat{P} . Finally we apply \hat{T}_{12} , the transposition of particle 1 and 2, obtaining a phase factor [23].

So we have to calculate the following two terms

$$\langle [(n_1 l_1, s_1) j_1, (n_2 l_2, s_2) j_2] J M_J T M_T | \hat{V}_{NN} | [(n'_1 l'_1, s'_1) j'_1, (n'_2 l'_2, s'_2) j'_2] J M_J T M_T \rangle, \quad (44)$$

$$\begin{aligned} & (-1)^{j_1+j_2-J} (-1)^{T-1} \langle [(n_2 l_2, s_2) j_2, (n_1 l_1, s_1) j_1] J M_J T M_T | \hat{V}_{NN} \\ & \times | [(n'_1 l'_1, s'_1) j'_1, (n'_2 l'_2, s'_2) j'_2] J M_J T M_T \rangle. \end{aligned} \quad (45)$$

Due to the length of the formulas we will only transform the bra states of these two terms. The transformation will be performed stepwise by inserting an identity operator in an appropriate basis. The changes will be marked red.

Let us concentrate now on the bra of the first term (44):

$$\begin{aligned} \langle 1 | & := \langle [(n_1 l_1, s_1) j_1, (n_2 l_2, s_2) j_2] J M_J T M_T | \\ & = \sum_{LS} \langle [(n_1 l_1, s_1) j_1, (n_2 l_2, s_2) j_2] J M_J T M_T | [(n_1 l_1, n_2 l_2) L, (s_1 s_2) S] J M_J T M_T \rangle \\ & \times \langle [(n_1 l_1, n_2 l_2) L, (s_1 s_2) S] J M_J T M_T |. \end{aligned} \quad (46)$$

In the next step we can replace the overlap in Eq. (46) by a 9-j symbol via the following relation

$$\begin{aligned} & \langle [(n_1 l_1, s_1) j_1, (n_2 l_2, s_2) j_2] J M_J T M_T | [(n_1 l_1, n_2 l_2) L, (s_1 s_2) S] J M_J T M_T \rangle \\ & = \hat{L} \hat{S} \hat{j}_1 \hat{j}_2 \begin{Bmatrix} l_1 & l_2 & L \\ s_1 & s_2 & S \\ j_1 & j_2 & J \end{Bmatrix} \end{aligned}$$

where $\hat{j} = \sqrt{2j+1}$, leading to

$$\langle 1 | = \sum_{LS} \hat{L} \hat{S} \hat{j}_1 \hat{j}_2 \begin{Bmatrix} l_1 & l_2 & L \\ s_1 & s_2 & S \\ j_1 & j_2 & J \end{Bmatrix} \langle [(n_1 l_1, n_2 l_2) L, (s_1 s_2) S] J M_J T M_T |. \quad (47)$$

Now we expand the bra state in the Jacobi basis $\langle [(N\Lambda, \nu\lambda) L, (s_1 s_2) S] JM_J |$, where N, Λ are radial and orbital angular momentum quantum numbers corresponding to the center-of-mass coordinate and ν, λ the ones corresponding to the relative coordinate. Moreover, we omit the isospin for brevity

$$\begin{aligned} \langle 1 | &= \sum_{N\Lambda\nu\lambda} \sum_{LS} \sum_{L'S'} \hat{L} \hat{S} \hat{j}_1 \hat{j}_2 \begin{Bmatrix} l_1 & l_2 & L \\ s_1 & s_2 & S \\ j_1 & j_2 & J \end{Bmatrix} \langle [(n_1 l_1, n_2 l_2) L, (s_1 s_2) S] JM_J | \\ &\times \langle [(N\Lambda, \nu\lambda) L, (s_1 s_2) S] JM_J | \langle [(N\Lambda, \nu\lambda) L, (s_1 s_2) S] JM_J |. \end{aligned} \quad (48)$$

Next, we introduce the harmonic-oscillator brackets

$$\begin{aligned} &\langle [(n_1 l_1, n_2 l_2) L, (s_1 s_2) S] JM_J | [(N\Lambda, \nu\lambda) L, (s_1 s_2) S] JM_J \rangle \\ &= \langle \langle n_1 l_1, n_2 l_2 | N\Lambda, \nu\lambda; L \rangle \rangle_d \end{aligned} \quad (49)$$

$$= \langle \langle N\Lambda, \nu\lambda | n_1 l_1, n_2 l_2; L \rangle \rangle_d. \quad (50)$$

As mentioned in Sec. 4.3.3 the scalar product (49) describes a transformation of the single-particle coordinates \vec{r}_1 and \vec{r}_2 to the center-of-mass and relative coordinates \vec{r}_{cm} and \vec{r}_{rel} by the linear relation

$$\begin{pmatrix} \vec{r}_1 \\ \vec{r}_2 \end{pmatrix} = \begin{pmatrix} \sqrt{\frac{d}{1+d}} & \sqrt{\frac{1}{1+d}} \\ \sqrt{\frac{1}{1+d}} & -\sqrt{\frac{d}{1+d}} \end{pmatrix} \begin{pmatrix} \vec{r}_{cm} \\ \vec{r}_{rel} \end{pmatrix}, \quad \text{for } d = 1.$$

We omit the index $d = 1$ at the harmonic-oscillator brackets for brevity

$$\begin{aligned} \langle 1 | &= \sum_{N'\Lambda'\nu'\lambda'} \sum_{N\Lambda\nu\lambda} \sum_{LS} \sum_{L'S'} \hat{L} \hat{S} \hat{j}_1 \hat{j}_2 \begin{Bmatrix} l_1 & l_2 & L \\ s_1 & s_2 & S \\ j_1 & j_2 & J \end{Bmatrix} \\ &\times \langle \langle N\Lambda, \nu\lambda | n_1 l_1, n_2 l_2; L \rangle \rangle \langle [(N\Lambda, \nu\lambda) L, (s_1 s_2) S] JM_J |. \end{aligned} \quad (51)$$

Now we expand the bra in the basis $\langle [N\Lambda, (\nu\lambda, S)j]JM_J |$

$$\begin{aligned} \langle 1 | &= \sum_j \sum_{N'\Lambda'\nu'\lambda'} \sum_{LS} \sum_{N\Lambda\nu\lambda} \sum_{L'S'} \hat{L}\hat{S}\hat{j}_1\hat{j}_2 \begin{Bmatrix} l_1 & l_2 & L \\ s_1 & s_2 & S \\ j_1 & j_2 & J \end{Bmatrix} \langle \langle N\Lambda, \nu\lambda | n_1 l_1, n_2 l_2; L \rangle \rangle \\ &\times \langle [(N\Lambda, \nu\lambda)L, (s_1 s_2)S]JM_J | [N\Lambda, (\nu\lambda, S)j]JM_J \rangle \langle [N\Lambda, (\nu\lambda, S)j]JM_J | \rangle. \end{aligned} \quad (52)$$

We can introduce the 6-j symbol using

$$\langle [(N\Lambda, \nu\lambda)L, (s_1 s_2)S]JM_J | [N\Lambda, (\nu\lambda, S)j]JM_J \rangle = (-1)^{\Lambda+\lambda+S+J} \hat{L}\hat{j} \begin{Bmatrix} \Lambda & \lambda & L \\ S & J & j \end{Bmatrix}, \quad (53)$$

leading to

$$\begin{aligned} \langle 1 | &= \sum_j \sum_{N\nu\Lambda\lambda} \sum_{LS} \sum_{N'\nu'\Lambda'\lambda'} \sum_{L'S'} \hat{L}\hat{S}\hat{j}_1\hat{j}_2 \begin{Bmatrix} l_1 & l_2 & L \\ s_1 & s_2 & S \\ j_1 & j_2 & J \end{Bmatrix} \langle \langle N\Lambda, \nu\lambda | n_1 l_1, n_2 l_2; L \rangle \rangle \\ &\times (-1)^{\Lambda+\lambda+S+J} \hat{L}\hat{j} \begin{Bmatrix} \Lambda & \lambda & L \\ S & J & j \end{Bmatrix} \langle [N\Lambda, (\nu\lambda, S)j]JM_J | \rangle. \end{aligned} \quad (54)$$

Now we expand the states in the basis $\langle N\Lambda m_\Lambda, (\nu\lambda, S)jm_j |$ for a complete decoupling of the center-of-mass from the relative part of the states

$$\begin{aligned} \langle 1 | &= \sum_{m_\Lambda m_j} \sum_j \sum_{N\nu\Lambda\lambda} \sum_{LS} \hat{L}^2 \hat{S} \hat{j}_1 \hat{j}_2 \hat{j} (-1)^{\Lambda+\lambda+S+J} \\ &\times \begin{Bmatrix} l_1 & l_2 & L \\ s_1 & s_2 & S \\ j_1 & j_2 & J \end{Bmatrix} \begin{Bmatrix} \Lambda & \lambda & L \\ S & J & j \end{Bmatrix} \langle \langle N\Lambda, \nu\lambda | n_1 l_1, n_2 l_2; L \rangle \rangle \\ &\times \langle [N\Lambda, (\nu\lambda, S)j]JM_J | N\Lambda m_\Lambda, (\nu\lambda, S)jm_j \rangle \langle N\Lambda m_\Lambda, (\nu\lambda, S)jm_j | \rangle. \end{aligned} \quad (55)$$

After introducing the Clebsch-Gordan coefficients

$$\langle [N\Lambda, (\nu\lambda, S)j]JM_J | N\Lambda m_\Lambda, (\nu\lambda, S)jm_j \rangle = c \begin{pmatrix} \Lambda & j & J \\ m_\Lambda & m_j & M_J \end{pmatrix},$$

we obtain

$$\begin{aligned}
\langle 1| &= \sum_{m_\Lambda m_j} \sum_j \sum_{N\nu\Lambda\lambda} \sum_{LS} \hat{L}^2 \hat{S} \hat{j}_1 \hat{j}_2 \hat{j} (-1)^{\Lambda+\lambda+S+J} c \begin{pmatrix} \Lambda & j & J \\ m_\Lambda & m_j & M_J \end{pmatrix} \\
&\times \left\{ \begin{matrix} l_1 & l_2 & L \\ s_1 & s_2 & S \\ j_1 & j_2 & J \end{matrix} \right\} \left\{ \begin{matrix} \Lambda & \lambda & L \\ S & J & j \end{matrix} \right\} \langle \langle N\Lambda, \nu\lambda | n_1 l_1, n_2 l_2; L \rangle \rangle \langle N\Lambda m_\Lambda, (\nu\lambda, S) j m_j |.
\end{aligned} \tag{56}$$

One can perform the analogous steps for the primed quantum numbers of the ket, yielding the term (44)

$$\begin{aligned}
&\langle [(n_1 l_1, s_1) j_1, (n_2 l_2, s_2) j_2] J M_J | \hat{V}_{NN} | [(n'_1 l'_1, s'_1) j'_1, (n'_2 l'_2, s'_2) j'_2] J M_J \rangle \\
&= \sum_{m_\Lambda m_j} \sum_j \sum_{N\nu\Lambda\lambda} \sum_{LS} \hat{L}^2 \hat{S} \hat{j}_1 \hat{j}_2 \hat{j} (-1)^{\Lambda+\lambda+S+J} c \begin{pmatrix} \Lambda & j & J \\ m_\Lambda & m_j & M_J \end{pmatrix} \\
&\times \left\{ \begin{matrix} l_1 & l_2 & L \\ s_1 & s_2 & S \\ j_1 & j_2 & J \end{matrix} \right\} \left\{ \begin{matrix} \Lambda & \lambda & L \\ S & J & j \end{matrix} \right\} \\
&\times \langle \langle N\Lambda, \nu\lambda | n_1 l_1, n_2 l_2; L \rangle \rangle \langle N\Lambda m_\Lambda, (\nu\lambda, S) j m_j | \hat{V}_{NN} \\
&\times \sum_{m'_\Lambda m'_j} \sum_{j'} \sum_{N'\nu'\Lambda'\lambda'} \sum_{L'S'} \hat{L}'^2 \hat{S}' \hat{j}'_1 \hat{j}'_2 \hat{j}' (-1)^{\Lambda'+\lambda'+S'+J'} c \begin{pmatrix} \Lambda' & j' & J \\ m'_\Lambda & m'_j & M_J \end{pmatrix} \\
&\times \left\{ \begin{matrix} l'_1 & l'_2 & L' \\ s'_1 & s'_2 & S' \\ j'_1 & j'_2 & J \end{matrix} \right\} \left\{ \begin{matrix} \Lambda' & \lambda' & L' \\ S' & J & j' \end{matrix} \right\} \\
&\times \langle \langle N'\Lambda', \nu'\lambda' | n'_1 l'_1, n'_2 l'_2; L' \rangle \rangle | N'\Lambda' m'_\Lambda, (\nu'\lambda', S') j' m'_j \rangle,
\end{aligned} \tag{57}$$

We make use of the properties of the NN interaction and remark that only matrix elements between states with equal $S, j, m_j, N, \Lambda, m_\Lambda$ in the bra and ket are nonzero. Because of that we can eliminate sums over $S', j', m'_j, N', \Lambda'$ and m'_Λ using the following condition

$$\begin{aligned} & \langle N\Lambda m_\Lambda, (\nu\lambda, S)jm_j | \hat{V}_{NN} | N'\Lambda'm'_\Lambda, (\nu'\lambda', S')j'm'_j \rangle \\ &= \delta_{SS'} \delta_{NN'} \delta_{\Lambda\Lambda'} \delta_{m_\Lambda m'_\Lambda} \delta_{jj'} \delta_{m_j m'_j} \langle N\Lambda m_\Lambda, (\nu\lambda, S)jm_j | \hat{V}_{NN} | N\Lambda m_\Lambda, (\nu'\lambda' S)jm_j \rangle. \end{aligned} \quad (58)$$

In addition, we can use that the interaction is independent of the projection quantum numbers M_J and m_j . Now we can apply the orthogonality relation of the Clebsch-Gordan coefficients

$$\sum_{m_\Lambda m_j} c \begin{pmatrix} \Lambda & j & J \\ m_\Lambda & m_j & M_J \end{pmatrix} c \begin{pmatrix} \Lambda & j & J \\ m_\Lambda & m_j & M_J \end{pmatrix} = \delta_{JJ} \delta_{M_J M_J} = 1. \quad (59)$$

Inserting both conditions and performing some reordering yields

$$\begin{aligned} & \langle [(n_1 l_1, s_1)j_1, (n_2 l_2, s_2)j_2]J | \hat{V}_{NN} | [(n'_1 l'_1, s'_1)j'_1, (n'_2 l'_2, s'_2)j'_2]J \rangle \\ &= \sum_j \sum_{N\nu\Lambda\lambda} \sum_{LS} \sum_{\nu'\lambda'} \sum_{L'} \hat{L}^2 \hat{L}'^2 \hat{S}^2 \hat{j}^2 \hat{j}_1 \hat{j}_2 \hat{j}'_1 \hat{j}'_2 (-1)^{\Lambda+\lambda+S+J} (-1)^{\Lambda+\lambda'+S+J} \\ & \times \begin{Bmatrix} l_1 & l_2 & L \\ s_1 & s_2 & S \\ j_1 & j_2 & J \end{Bmatrix} \begin{Bmatrix} l'_1 & l'_2 & L' \\ s'_1 & s'_2 & S \\ j'_1 & j'_2 & J \end{Bmatrix} \begin{Bmatrix} \Lambda & \lambda & L \\ S & J & j \end{Bmatrix} \begin{Bmatrix} \Lambda & \lambda' & L' \\ S & J & j \end{Bmatrix} \quad (60) \\ & \times \langle \langle N\Lambda, \nu\lambda | n_1 l_1, n_2 l_2; L \rangle \rangle \langle \langle N\Lambda, \nu'\lambda' | n'_1 l'_1, n'_2 l'_2; L' \rangle \rangle \\ & \times \langle N\Lambda m_\Lambda, (\nu\lambda, S)j | \hat{V}_{NN} | N\Lambda m_\Lambda, (\nu'\lambda', S)j \rangle. \end{aligned}$$

S and J are integer due to $s_1 = s_2 = s'_1 = s'_2 = \frac{1}{2}$ and Λ is integer due to being an orbital angular momentum. Thus, $(-1)^{2\Lambda} = (-1)^{2S} = (-1)^{2J} = +1$ and with the consideration

of the isospin, we obtain the final expression for the first term

$$\begin{aligned}
& \langle [(n_1 l_1, s_1) j_1, (n_2 l_2, s_2) j_2] J T M_T | \hat{V}_{NN} | [(n'_1 l'_1, s_1) j'_1, (n'_2 l'_2, s_2) j'_2] J T M_T \rangle \\
&= \sum_j \sum_{N\nu\Lambda\lambda} \sum_{LS} \sum_{\nu'\lambda'} \sum_{L'} \hat{L}^2 \hat{L}'^2 \hat{S}^2 \hat{j}^2 \hat{j}_1 \hat{j}_2 \hat{j}'_1 \hat{j}'_2 (-1)^{\lambda+\lambda'} \\
&\times \left\{ \begin{matrix} l_1 & l_2 & L \\ s_1 & s_2 & S \\ j_1 & j_2 & J \end{matrix} \right\} \left\{ \begin{matrix} l'_1 & l'_2 & L' \\ s'_1 & s'_2 & S \\ j'_1 & j'_2 & J \end{matrix} \right\} \left\{ \begin{matrix} \Lambda & \lambda & L \\ S & J & j \end{matrix} \right\} \left\{ \begin{matrix} \Lambda & \lambda' & L' \\ S & J & j \end{matrix} \right\} \quad (61) \\
&\times \langle \langle N\Lambda, \nu\lambda | n_1 l_1, n_2 l_2; L \rangle \rangle \langle \langle N\Lambda, \nu'\lambda' | n'_1 l'_1, n'_2 l'_2; L' \rangle \rangle \\
&\times \langle N\Lambda m_\Lambda, (\nu\lambda, S) j T M_T | \hat{V}_{NN} | N\Lambda m_\Lambda, (\nu'\lambda', S) j T M_T \rangle.
\end{aligned}$$

Now we aim at the bra state of the second term (45):

$$\langle 2 | := (-1)^{j_1+j_2-J} (-1)^{T-1} \langle [(n_2 l_2, s_2) j_2, (n_1 l_1, s_1) j_1] J M_J, (t_2 t_1) T M_T | \quad (62)$$

We can swap the isospin $t_1 \leftrightarrow t_2$ with no additional factors due to $t_1 = t_2 = \frac{1}{2}$. Note that we do not change a coupling order, but only rename t_1 and t_2 because they are equal. The isospin part of $\langle 1 |$ and $\langle 2 |$ are equal and we again omit it for brevity. The bra $\langle 2 |$ is exactly the same as $\langle 1 |$ except the factor $(-1)^{j_1+j_2-J} (-1)^{T-1}$ and except that the spatial and spin quantum numbers of particle 1 and 2 are swapped. So we can perform the analogous steps as above also for the bra $\langle 2 |$ of the second term (45) obtaining

$$\begin{aligned}
\langle 2 | &= (-1)^{j_1+j_2-J+T-1} \sum_{m_\Lambda m_j} \sum_j \sum_{N\nu\Lambda\lambda} \sum_{LS} \\
&\times \hat{L}^2 \hat{S}^2 \hat{j}_1 \hat{j}_2 \hat{j} (-1)^{\Lambda+\lambda+S+J} c \left(\begin{matrix} \Lambda & j & J \\ m_\Lambda & m_j & M_J \end{matrix} \right) \\
&\times \left\{ \begin{matrix} l_2 & l_1 & L \\ s_2 & s_1 & S \\ j_2 & j_1 & J \end{matrix} \right\} \left\{ \begin{matrix} \Lambda & \lambda & L \\ S & J & j \end{matrix} \right\} \langle \langle N\Lambda, \nu\lambda | n_2 l_2, n_1 l_1; L \rangle \rangle \langle N\Lambda m_\Lambda, (\nu\lambda, S) j m_j |, \quad (63)
\end{aligned}$$

where have the additional factor and swapped indices in the 9-j symbol and the HOB, compared to (56). Note that in the state $\langle N\Lambda m_\Lambda, (\nu\lambda, S)jm_j |$ the coupling order of the spin $s_1 = \frac{1}{2} = s_2$ to S does not make a difference, because of the same argument as for the isospin part. In the next step we swap the first two columns of the 9-j symbol using the symmetry relation explained in Subsec. 4.3.2

$$\begin{Bmatrix} l_2 & l_1 & L \\ s_2 & s_1 & S \\ j_2 & j_1 & J \end{Bmatrix} = \begin{Bmatrix} l_1 & l_2 & L \\ s_1 & s_2 & S \\ j_1 & j_2 & J \end{Bmatrix} \cdot (-1)^{l_1+s_1+j_1+l_2+s_2+j_2+L+S+J},$$

and transform the HOB with the symmetry relation 31

$$\begin{aligned} \langle\langle N\Lambda, \nu\lambda | n_2 l_2, n_1 l_1; L \rangle\rangle &= \langle\langle n_2 l_2, n_1 l_1 | N\Lambda, \nu\lambda; L \rangle\rangle \\ &= (-1)^{L-\Lambda} \langle\langle n_1 l_1, n_2 l_2 | N\Lambda, \nu\lambda; L \rangle\rangle \\ &= (-1)^{L-\Lambda} \langle\langle N\Lambda, \nu\lambda | n_1 l_1, n_2 l_2; L \rangle\rangle, \end{aligned}$$

yielding

$$\begin{aligned} \langle 2 | &= (-1)^{j_1+j_2-J+T-1} \sum_{m_\Lambda m_j} \sum_j \sum_{N\nu\Lambda\lambda} \sum_{LS} (-1)^{l_1+s_1+j_1+l_2+s_2+j_2+L+S+J} (-1)^{L-\Lambda} \\ &(-1)^{\Lambda+\lambda+S+J} \hat{L}^2 \hat{S} \hat{j}_1 \hat{j}_2 \hat{j} c \begin{pmatrix} \Lambda & j & J \\ m_\Lambda & m_j & M_J \end{pmatrix} \\ &\times \begin{Bmatrix} l_1 & l_2 & L \\ s_1 & s_2 & S \\ j_1 & j_2 & J \end{Bmatrix} \begin{Bmatrix} \Lambda & \lambda & L \\ S & J & j \end{Bmatrix} \langle\langle N\Lambda, \nu\lambda | n_1 l_1, n_2 l_2; L \rangle\rangle \\ &\langle N\Lambda m_\Lambda, (\nu\lambda, S)jm_j |. \end{aligned}$$

Now it is time to look also on the right-hand side of the matrix element. It is exactly the same as derived above (57), so we can use again the properties of the interaction and the orthogonality relation of the Clebsch-Gordan coefficients (59) obtaining the matrix

element

$$\begin{aligned}
& (-1)^{j_1+j_2-J+T-1} \langle [(n_2 l_2, s_2) j_2, (n_1 l_1, s_1) j_1] J | \hat{V}_{NN} | [(n'_1 l'_1, s_1) j'_1, (n'_2 l'_2, s_2) j'_2] J \rangle \\
&= \sum_j \sum_{N\nu\Lambda\lambda} \sum_{LS} \sum_{\nu'\lambda'} \sum_{L'} \hat{L}^2 \hat{L}'^2 \hat{S}^2 \hat{j}^2 \hat{j}_1 \hat{j}_2 \hat{j}'_1 \hat{j}'_2 \\
&\times (-1)^{j_1+j_2-J+T-1} (-1)^{l_1+s_1+j_1+l_2+s_2+j_2+L+S+J} (-1)^{L-\Lambda} (-1)^{\lambda+\lambda'} \\
&\times \begin{Bmatrix} l_1 & l_2 & L \\ s_1 & s_2 & S \\ j_1 & j_2 & J \end{Bmatrix} \begin{Bmatrix} l'_1 & l'_2 & L' \\ s_1 & s_2 & S \\ j'_1 & j'_2 & J \end{Bmatrix} \begin{Bmatrix} \Lambda & \lambda & L \\ S & J & j \end{Bmatrix} \begin{Bmatrix} \Lambda & \lambda' & L' \\ S & J & j \end{Bmatrix} \\
&\times \langle \langle N\Lambda, \nu\lambda | n_1 l_1, n_2 l_2; L \rangle \rangle \langle \langle N\Lambda, \nu'\lambda' | n'_1 l'_1, n'_2 l'_2; L' \rangle \rangle \\
&\times \langle N\Lambda m_\Lambda, (\nu\lambda, S) j | \hat{V}_{NN} | N\Lambda m_\Lambda, (\nu'\lambda', S) j \rangle.
\end{aligned} \tag{64}$$

The last thing to do is to simplify the phase factor, which is the only difference between the result for the first term (61) derived above and our result for the second term (64). Thus we write down the phase factor again

$$\begin{aligned}
& (-1)^{j_1+j_2-J+T-1+l_1+s_1+j_1+l_2+s_2+j_2+L+S+J+L-\Lambda+\lambda+\lambda'} \\
&= (-1)^{2j_1+2j_2} (-1)^{s_1+s_2-1} (-1)^{2L+2S+2J+\Lambda-\Lambda+J-J} (-1)^{\lambda+\lambda'} (-1)^{l_1+l_2-\Lambda} (-1)^{T+S}.
\end{aligned} \tag{65}$$

For the individual phase factors we can use the following properties:

- $(-1)^{2j_1+2j_2}$: Since j_1 and j_2 are half-integral numbers, $2j_i$ are odd numbers and so $2j_1 + 2j_2$ is even and the factor is equal to one.
- $(-1)^{s_1+s_2-1}$: $s_1 = s_2 = \frac{1}{2}$ and $s_1 + s_2 - 1 = 0$ and the factor is equal to one.
- $(-1)^{2L+2S+2J+\Lambda-\Lambda+J-J}$: L , S and J are integer and so this factor is also equal to one.
- $(-1)^{\lambda+\lambda'}$: It is a property of the interaction, that $\lambda' = \lambda \pm 2$ and so the factor is equal to one. This can also be used in (61).

- $(-1)^{l_1+l_2-\Lambda}$: Here we can make use of the energy-conserving condition $2n_1 + l_1 + 2n_2 + l_2 = 2N + \Lambda + 2\nu + \lambda$ and the fact that n_1, n_2, N, ν are integers. Using this we find that the factor is just $(-1)^\lambda$.

So the overall phase factor is $(-1)^{\lambda+S+T}$ and the result of both terms together, considering the isospin, reads

$$\begin{aligned}
& {}_a \langle [(n_1 l_1, s_1) j_1, (n_2 l_2, s_2) j_2] J T M_T | \hat{V}_{NN} | [(n'_1 l'_1, s_1) j'_1, (n'_2 l'_2, s_2) j'_2] J T M_T \rangle_a \\
&= \hat{j}_1 \hat{j}_2 \hat{j}'_1 \hat{j}'_2 \sum_{LSN\Lambda\nu\lambda,j} \sum_{\nu'\lambda'} \sum_{L'} \hat{L}^2 \hat{L}'^2 \hat{j}^2 \hat{S}^2 (1 - (-1)^{\lambda+S+T}) \\
&\times \left\{ \begin{matrix} l_1 & l_2 & L \\ s_1 & s_2 & S \\ j_1 & j_2 & J \end{matrix} \right\} \left\{ \begin{matrix} l'_1 & l'_2 & L' \\ s_1 & s_2 & S \\ j'_1 & j'_2 & J \end{matrix} \right\} \left\{ \begin{matrix} \Lambda & \lambda & L \\ S & J & j \end{matrix} \right\} \left\{ \begin{matrix} \Lambda & \lambda' & L' \\ S & J & j \end{matrix} \right\} \quad (66) \\
&\times \langle \langle N\Lambda, \nu\lambda | n_1 l_1, n_2 l_2; L \rangle \rangle \langle \langle N\Lambda, \nu'\lambda' | n'_1 l'_1, n'_2 l'_2; L' \rangle \rangle \\
&\times \langle (\nu\lambda, S) j T M_T | \hat{V}_{NN} | (\lambda'\nu', S) j T M_T \rangle,
\end{aligned}$$

as we have anticipated from Eq. (38).

4.5 Three-body Jacobi basis to m-scheme transformation

In this section we will derive the transformation of three-body matrix elements from the Jacobi basis to m-scheme [14]

$$\langle E J M_J T M_T i | \hat{V}_{NNN} | E' J M_J T M_T i' \rangle \longrightarrow_a \langle abc | \hat{V}_{NNN} | a' b' c' \rangle_a. \quad (67)$$

Due to the complexity of this transformation, we divide the derivation into several subsections to provide a clear view.

4.5.1 Simplifying the matrix element

We start with the antisymmetrized m-scheme states $|abc\rangle_a$ and transform them stepwise by inserting appropriate identity operators until we have expressed them in the antisym-

metrized Jacobi states $|EJM_JTM_Ti\rangle$. The state $|abc\rangle_a$ is given by

$$|abc\rangle_a = \sqrt{3!}\hat{A}|(n_a l_a, s_a)j_a m_a t_a m_{t_a}\rangle \otimes |(n_b l_b, s_b)j_b m_b t_b m_{t_b}\rangle \otimes |(n_c l_c, s_c)j_c m_c t_c m_{t_c}\rangle, \quad (68)$$

including the center-of-mass part.

It is very important to handle the antisymmetric and non-antisymmetric spaces with great care. First, we consider the non-antisymmetric state

$$|abc\rangle = |(n_a l_a, s_a)j_a m_a t_a m_{t_a}\rangle \otimes |(n_b l_b, s_b)j_b m_b t_b m_{t_b}\rangle \otimes |(n_c l_c, s_c)j_c m_c t_c m_{t_c}\rangle, \quad (69)$$

which we later will project on the antisymmetric space. The first step is to couple the angular momenta to a total angular momentum quantum number \mathcal{J}

$$\begin{aligned} |abc\rangle &= \sum_{J_{ab} M_{ab}} \sum_{\mathcal{J} \mathcal{M}_{\mathcal{J}}} c \begin{pmatrix} j_a & j_b & J_{ab} \\ m_a & m_b & M_{ab} \end{pmatrix} c \begin{pmatrix} J_{ab} & j_c & \mathcal{J} \\ M_{ab} & m_c & \mathcal{M}_{\mathcal{J}} \end{pmatrix} \\ &\times \{[(n_a l_a, s_a)j_a, (n_b l_b, s_b)j_b]J_{ab}, (n_c l_c, s_c)j_c\} \mathcal{J} \mathcal{M}_{\mathcal{J}}, t_a m_{t_a} t_b m_{t_b} t_c m_{t_c} \} \end{aligned} \quad (70)$$

In the second step we use the following identity operator

$$\hat{1} = \sum_{n_{cm} l_{cm} \alpha} \{ |n_{cm} l_{cm}\rangle \otimes |\alpha\rangle \}^{\mathcal{J} \mathcal{M}_{\mathcal{J}}} \{ \langle n_{cm} l_{cm}| \otimes \langle \alpha| \}^{\mathcal{J} \mathcal{M}_{\mathcal{J}}}, \quad (71)$$

where $|\alpha\rangle = |[(n_{12} l_{12}, s_{ab})j_{12}, (n_3 l_3, s_c)j_3]J, [(t_a t_b) t_{ab}, t_c] T M_T\rangle$ is the relative part of the Jacobi state (see Eq. (18)) and the sum \sum_{α} denotes the sum over

$$\{n_{12}, l_{12}, s_{ab}, j_{12}, n_3, l_3, j_3, J, t_{ab}, T, M_T\}. \quad (72)$$

The state $|\alpha\rangle$ is antisymmetric under the exchange of particle 1 and 2, see Appendix A.1. In the following, quantum numbers with characters as index correspond to Cartesian coordinates, while quantum numbers with integers as index correspond to Jacobi coordinates. Of course, this notation is not always strictly obeyed for intermediate quantum numbers, if angular momenta of both coordinate spaces can couple to them.

Because the states we are dealing with are coupled to \mathcal{J} , $\mathcal{M}_{\mathcal{J}}$ as good quantum num-

bers, the sums over \mathcal{J} , $\mathcal{M}_{\mathcal{J}}$ vanish. Inserting (71) into (70) yields

$$\begin{aligned}
|abc\rangle &= \sum_{J_{ab}M_{ab}} \sum_{\mathcal{J}\mathcal{M}_{\mathcal{J}}} \sum_{n_{cm}l_{cm}} \sum_{\alpha} c \begin{pmatrix} j_a & j_b & J_{ab} \\ m_a & m_b & M_{ab} \end{pmatrix} c \begin{pmatrix} J_{ab} & j_c & \mathcal{J} \\ M_{ab} & m_c & \mathcal{M}_{\mathcal{J}} \end{pmatrix} \\
&\times T \begin{bmatrix} a & b & c & J_{ab} & J & \mathcal{J} \\ n_{cm} & l_{cm} & n_{12} & l_{12} & n_3 & l_3 \\ s_{ab} & j_{12} & j_3 & t_{ab} & T & M_T \end{bmatrix} \{|n_{cm}l_{cm}\rangle \otimes |\alpha\rangle\}^{\mathcal{J}\mathcal{M}_{\mathcal{J}}},
\end{aligned} \tag{73}$$

with the T -coefficient

$$\begin{aligned}
&T \begin{bmatrix} a & b & c & J_{ab} & J & \mathcal{J} \\ n_{cm} & l_{cm} & n_{12} & l_{12} & n_3 & l_3 \\ s_{ab} & j_{12} & j_3 & t_{ab} & T & M_T \end{bmatrix} \\
&= \{|n_{cm}l_{cm}\rangle \otimes \langle\alpha|\}^{\mathcal{J}\mathcal{M}_{\mathcal{J}}} \\
&\times \{|[(n_a l_a, s_a)j_a, (n_b l_b, s_b)j_b]J_{ab}, (n_c l_c, s_c)j_c\}^{\mathcal{J}\mathcal{M}_{\mathcal{J}}; t_a m_{t_a} t_b m_{t_b} t_c m_{t_c}} \\
&:= \{|n_{cm}l_{cm}\rangle \otimes \langle\alpha|\}^{\mathcal{J}\mathcal{M}_{\mathcal{J}}} \{|[|a\rangle \otimes |b\rangle]^{J_{ab}} \otimes |c\rangle\}^{\mathcal{J}\mathcal{M}_{\mathcal{J}}}.
\end{aligned} \tag{74}$$

The arrangement of the quantum numbers in the argument of the T -coefficient has no physical meaning. We will come back to the calculation of this T -coefficient later. Next we make use of the projection operator \hat{P}_{antisym} , which is equivalent to the antisymmetrizer \hat{A}

$$\hat{P}_{\text{antisym}} = \sum_{n_{cm}l_{cm}} \sum_{EJ} \sum_{TM_T} \sum_{\mathcal{J}\mathcal{M}_{\mathcal{J}}} \sum_i \{|n_{cm}l_{cm}\rangle \otimes |EiJTM_T\rangle\}^{\mathcal{J}\mathcal{M}_{\mathcal{J}}} \{|n_{cm}l_{cm}\rangle \otimes \langle EiTJTM_T|\}^{\mathcal{J}\mathcal{M}_{\mathcal{J}}}. \tag{75}$$

The auxiliary index i labels the state within the set of antisymmetrized states for total energy quantum number E , angular momentum J and isospin T of the relative part.

We have to consider the overlap

$$\begin{aligned}
& \{ \langle \tilde{n}_{cm} \tilde{l}_{cm} | \otimes \langle \tilde{E} i \tilde{J} \tilde{T} \tilde{M}_T | \rangle \}^{\mathcal{J} \mathcal{M}_{\mathcal{J}}} \{ |n_{cm} l_{cm} \rangle \otimes |\alpha \rangle \}^{\mathcal{J} \mathcal{M}_{\mathcal{J}}} \\
&= \delta_{\mathcal{J} \tilde{\mathcal{J}}} \delta_{\mathcal{M}_{\mathcal{J}} \tilde{\mathcal{M}}_{\mathcal{J}}} \delta_{n_{cm} \tilde{n}_{cm}} \delta_{l_{cm} \tilde{l}_{cm}} \delta_{J \tilde{J}} \delta_{T \tilde{T}} \delta_{M_T \tilde{M}_T} \delta_{E, 2n_{12} + l_{12} + 2n_3 + l_3} \\
&\times \{ \langle n_{cm} l_{cm} | \otimes \langle E i J T M_T | \rangle \}^{\mathcal{J} \mathcal{M}_{\mathcal{J}}} \{ |n_{cm} l_{cm} \rangle \otimes |\alpha \rangle \}^{\mathcal{J} \mathcal{M}_{\mathcal{J}}} \\
&= \delta_{\mathcal{J} \tilde{\mathcal{J}}} \delta_{\mathcal{M}_{\mathcal{J}} \tilde{\mathcal{M}}_{\mathcal{J}}} \delta_{n_{cm} \tilde{n}_{cm}} \delta_{l_{cm} \tilde{l}_{cm}} \delta_{J \tilde{J}} \delta_{T \tilde{T}} \delta_{M_T \tilde{M}_T} \delta_{E, 2n_{12} + l_{12} + 2n_3 + l_3} c_{\alpha, i}
\end{aligned} \tag{76}$$

with the coefficients of fractional parentage (CFPs)

$$c_{\alpha, i} := \{ \langle n_{cm} l_{cm} | \otimes \langle E i J T M_T | \rangle \}^{\mathcal{J} \mathcal{M}_{\mathcal{J}}} \{ |n_{cm} l_{cm} \rangle \otimes |\alpha \rangle \}^{\mathcal{J} \mathcal{M}_{\mathcal{J}}} .$$

If we plug (75) into (73) and use (76), we antisymmetrize the states on the left and right hand side

$$\begin{aligned}
\hat{A} |abc \rangle &= \frac{1}{\sqrt{3!}} |abc \rangle_a \\
&= \sum_{J_{ab}} \sum_{\mathcal{J}} \sum_{n_{cm} l_{cm}} \sum_{\alpha} \sum_i c \begin{pmatrix} j_a & j_b & J_{ab} \\ m_a & m_b & M_{ab} \end{pmatrix} c \begin{pmatrix} J_{ab} & j_c & \mathcal{J} \\ M_{ab} & m_c & \mathcal{M}_{\mathcal{J}} \end{pmatrix} \\
&\times T \begin{bmatrix} a & b & c & J_{ab} & J & \mathcal{J} \\ n_{cm} & l_{cm} & n_{12} & l_{12} & n_3 & l_3 \\ s_{ab} & j_{12} & j_3 & t_{ab} & T & M_T \end{bmatrix} c_{\alpha, i} \{ |n_{cm} l_{cm} \rangle \otimes |E i J T M_T \rangle \}^{\mathcal{J} \mathcal{M}_{\mathcal{J}}} ,
\end{aligned} \tag{77}$$

with the energy quantum number $E = 2n_{12} + l_{12} + 2n_3 + l_3$ from the Kronecker delta and $M_{ab} = m_a + m_b$, $\mathcal{M}_{\mathcal{J}} = M_{12} + m_c$ from properties of the Clebsch-Gordan coefficients. As the last step we decouple the center-of-mass part and the relative part of

$\{|n_{cm}l_{cm}\rangle|EiJTM_T\rangle\}^{\mathcal{J}\mathcal{M}\mathcal{J}}$ and obtain for the antisymmetric m-scheme state

$$\begin{aligned}
|abc\rangle_a &= \sqrt{6} \sum_{J_{ab}} \sum_{\mathcal{J}} \sum_{n_{cm}l_{cm}} \sum_{\alpha} \sum_i \sum_{m_{cm}M_J} \\
&\times c \begin{pmatrix} j_a & j_b & J_{ab} \\ m_a & m_b & M_{ab} \end{pmatrix} c \begin{pmatrix} J_{ab} & j_c & \mathcal{J} \\ M_{ab} & m_c & \mathcal{M}_{\mathcal{J}} \end{pmatrix} c \begin{pmatrix} l_{cm} & J & \mathcal{J} \\ m_{cm} & M_J & \mathcal{M}_{\mathcal{J}} \end{pmatrix} \quad (78) \\
&T \begin{bmatrix} a & b & c & J_{ab} & J & \mathcal{J} \\ n_{cm} & l_{cm} & n_{12} & l_{12} & n_3 & l_3 \\ s_{ab} & j_{12} & j_3 & t_{ab} & T & M_T \end{bmatrix} c_{\alpha,i} |n_{cm}l_{cm}m_{cm}\rangle \otimes |EiJM_JTM_T\rangle.
\end{aligned}$$

Now we can write down the interaction matrix element

$$\begin{aligned}
&{}_a \langle abc | \hat{V}_{NNN} | a'b'c' \rangle_a \\
&= 6 \sum_{J_{ab}} \sum_{\mathcal{J}} \sum_{n_{cm}l_{cm}} \sum_{\alpha} \sum_i \sum_{m_{cm}M_J} \sum_{J'_{ab}} \sum_{\mathcal{J}'} \sum_{n'_{cm}l'_{cm}} \sum_{\alpha'} \sum_{i'} \sum_{m'_{cm}M'_J} \\
&\times c \begin{pmatrix} j_a & j_b & J_{ab} \\ m_a & m_b & M_{ab} \end{pmatrix} c \begin{pmatrix} J_{ab} & j_c & \mathcal{J} \\ M_{ab} & m_c & \mathcal{M}_{\mathcal{J}} \end{pmatrix} c \begin{pmatrix} l_{cm} & J & \mathcal{J} \\ m_{cm} & M_J & \mathcal{M}_{\mathcal{J}} \end{pmatrix} \\
&\times c \begin{pmatrix} j'_a & j'_b & J'_{ab} \\ m'_a & m'_b & M'_{ab} \end{pmatrix} c \begin{pmatrix} J'_{ab} & j'_c & \mathcal{J}' \\ M'_{ab} & m'_c & \mathcal{M}'_{\mathcal{J}} \end{pmatrix} c \begin{pmatrix} l'_{cm} & J' & \mathcal{J}' \\ m'_{cm} & M'_J & \mathcal{M}'_{\mathcal{J}} \end{pmatrix} \quad (79) \\
&\times T \begin{bmatrix} a & b & c & J_{ab} & J & \mathcal{J} \\ n_{cm} & l_{cm} & n_{12} & l_{12} & n_3 & l_3 \\ s_{ab} & j_{12} & j_3 & t_{ab} & T & M_T \end{bmatrix} T \begin{bmatrix} a' & b' & c' & J'_{ab} & J' & \mathcal{J}' \\ n'_{cm} & l'_{cm} & n'_{12} & l'_{12} & n'_3 & l'_3 \\ s'_{ab} & j'_{12} & j'_3 & t'_{ab} & T & M_T \end{bmatrix} \\
&\times c_{\alpha,i} c_{\alpha',i'} \langle n_{cm}l_{cm}m_{cm} | n'_{cm}l'_{cm}m'_{cm} \rangle \langle EiJM_JTM_T | \hat{V}_{NNN} | E'i'J'M'_JT'M'_T \rangle,
\end{aligned}$$

where we used the fact that the interaction does not affect the center-of-mass part of the state. For further simplification we make use of

$$\langle n_{cm}l_{cm}m_{cm} | n'_{cm}l'_{cm}m'_{cm} \rangle = \delta_{n_{cm}n'_{cm}} \delta_{l_{cm}l'_{cm}} \delta_{m_{cm}m'_{cm}}, \quad (80)$$

and of properties of the interaction which imply

$$\begin{aligned}
& \langle EiJM_JTM_T | \hat{V}_{NNN} | E'i'J'M_JT'M_T \rangle \\
& = \langle EiJM_JTM_T | \hat{V}_{NNN} | E'i'JM_JTM_T \rangle \delta_{J'J} \delta_{M'_J M_J} \delta_{T'T} \delta_{M'_T M_T}.
\end{aligned} \tag{81}$$

Using this we eliminate sums in (79) corresponding to the Kronecker deltas

$$\begin{aligned}
& {}_a \langle abc | \hat{V}_{NNN} | a'b'c' \rangle_a \\
& = 6 \sum_{J_{ab}} \sum_{\mathcal{J}} \sum_{n_{cm} l_{cm}} \sum_{\alpha} \sum_i \sum_{m_{cm} M_J} \sum_{J'_{ab}} \sum_{\mathcal{J}'} \sum_{\bar{\alpha}'} \sum_{i'} \\
& \times c \begin{pmatrix} j_a & j_b & J_{ab} \\ m_a & m_b & M_{ab} \end{pmatrix} c \begin{pmatrix} J_{ab} & j_c & \mathcal{J} \\ M_{ab} & m_c & \mathcal{M}_{\mathcal{J}} \end{pmatrix} c \begin{pmatrix} l_{cm} & J & \mathcal{J} \\ m_{cm} & M_J & \mathcal{M}_{\mathcal{J}} \end{pmatrix} \\
& \times c \begin{pmatrix} j'_a & j'_b & J'_{ab} \\ m'_a & m'_b & M'_{ab} \end{pmatrix} c \begin{pmatrix} J'_{ab} & j'_c & \mathcal{J}' \\ M'_{ab} & m'_c & \mathcal{M}'_{\mathcal{J}'} \end{pmatrix} c \begin{pmatrix} l_{cm} & J & \mathcal{J}' \\ m_{cm} & M_J & \mathcal{M}'_{\mathcal{J}'} \end{pmatrix} \\
& \times T \begin{bmatrix} a & b & c & J_{ab} & J & \mathcal{J} \\ n_{cm} & l_{cm} & n_{12} & l_{12} & n_3 & l_3 \\ s_{ab} & j_{12} & j_3 & t_{ab} & T & M_T \end{bmatrix} T \begin{bmatrix} a' & b' & c' & J'_{ab} & J & \mathcal{J}' \\ n_{cm} & l_{cm} & n'_{12} & l'_{12} & n'_3 & l'_3 \\ s'_{ab} & j'_{12} & j'_3 & t'_{ab} & T & M_T \end{bmatrix} \\
& \times c_{\alpha,i} c_{\alpha',i'} \langle EiJM_JTM_T | \hat{V}_{NNN} | E'i'JM_JTM_T \rangle,
\end{aligned} \tag{82}$$

where \sum_{α} again denotes a sum over $\{n_{12}, l_{12}, s_{ab}, j_{12}, n_3, l_3, j_3, J, t_{ab}, T\}$ and $\sum_{\bar{\alpha}'}$ denotes a sum over

$\{n'_{12}, l'_{12}, s'_{ab}, j'_{12}, n'_3, l'_3, j'_3, t'_{ab}\}$. Furthermore, the Jacobi matrix elements are independent of M_J and we can use the orthogonality relation of the Clebsch-Gordan coefficients

$$\sum_{m_{cm} M_J} c \begin{pmatrix} l_{cm} & J & \mathcal{J} \\ m_{cm} & M_J & \mathcal{M}_{\mathcal{J}} \end{pmatrix} c \begin{pmatrix} l_{cm} & J & \mathcal{J}' \\ m_{cm} & M_J & \mathcal{M}'_{\mathcal{J}'} \end{pmatrix} = \delta_{\mathcal{J}\mathcal{J}'} \delta_{\mathcal{M}_{\mathcal{J}}\mathcal{M}'_{\mathcal{J}'}} \tag{83}$$

and the interaction matrix element finally reads

$$\begin{aligned}
& {}_a \langle abc | \hat{V}_{NNN} | a' b' c' \rangle_a \\
&= 6 \sum_{J_{ab}} \sum_{\mathcal{J}} \sum_{n_{cm} l_{cm}} \sum_{\alpha} \sum_i \sum_{J'_{ab}} \sum_{\tilde{\alpha}'} \sum_{i'} \\
&\times c \begin{pmatrix} j_a & j_b & J_{ab} \\ m_a & m_b & M_{ab} \end{pmatrix} c \begin{pmatrix} J_{ab} & j_c & \mathcal{J} \\ M_{ab} & m_c & \mathcal{M}_{\mathcal{J}} \end{pmatrix} \\
&\times c \begin{pmatrix} j'_a & j'_b & J'_{ab} \\ m'_a & m'_b & M'_{ab} \end{pmatrix} c \begin{pmatrix} J'_{ab} & j'_c & \mathcal{J} \\ M'_{ab} & m'_c & \mathcal{M}_{\mathcal{J}} \end{pmatrix} \tag{84} \\
&\times T \begin{bmatrix} a & b & c & J_{ab} & J & \mathcal{J} \\ n_{cm} & l_{cm} & n_{12} & l_{12} & n_3 & l_3 \\ s_{ab} & j_{12} & j_3 & t_{ab} & T & M_T \end{bmatrix} T \begin{bmatrix} a' & b' & c' & J'_{ab} & J & \mathcal{J} \\ n_{cm} & l_{cm} & n'_{12} & l'_{12} & n'_3 & l'_3 \\ s'_{ab} & j'_{12} & j'_3 & t'_{ab} & T & M_T \end{bmatrix} \\
&\times c_{\alpha, i} c_{\alpha', i'} \langle E i J T M_T | \hat{V}_{NNN} | E' i' J T M_T \rangle.
\end{aligned}$$

Or, with all quantum numbers shown explicitly,

$$\begin{aligned}
& {}_a \langle abc | \hat{V}_{NNN} | a' b' c' \rangle_a \\
&= 6 \sum_{J_{ab} J'_{ab}} \sum_{\mathcal{J}} \sum_{n_{cm} l_{cm}} \sum_{n_{12} n'_{12}} \sum_{l_{12} l'_{12}} \sum_{n_3 n'_3} \sum_{l_3 l'_3} \sum_{s_{ab} s'_{ab}} \sum_{j_{12} j'_{12}} \sum_{j_3 j'_3} \sum_{t_{ab} t'_{ab}} \sum_J \sum_T \sum_{i i'} \\
&\times c \begin{pmatrix} j_a & j_b & J_{ab} \\ m_a & m_b & M_{ab} \end{pmatrix} c \begin{pmatrix} J_{ab} & j_c & \mathcal{J} \\ M_{ab} & m_c & \mathcal{M}_{\mathcal{J}} \end{pmatrix} \\
&\times c \begin{pmatrix} j'_a & j'_b & J'_{ab} \\ m'_a & m'_b & M'_{ab} \end{pmatrix} c \begin{pmatrix} J'_{ab} & j'_c & \mathcal{J} \\ M'_{ab} & m'_c & \mathcal{M}_{\mathcal{J}} \end{pmatrix} \\
&\times T \begin{bmatrix} a & b & c & J_{ab} & J & \mathcal{J} \\ n_{cm} & l_{cm} & n_{12} & l_{12} & n_3 & l_3 \\ s_{ab} & j_{12} & j_3 & t_{ab} & T & M_T \end{bmatrix} T \begin{bmatrix} a' & b' & c' & J'_{ab} & J & \mathcal{J} \\ n_{cm} & l_{cm} & n'_{12} & l'_{12} & n'_3 & l'_3 \\ s'_{ab} & j'_{12} & j'_3 & t'_{ab} & T & M_T \end{bmatrix} \\
&\times c_{\alpha, i} \begin{bmatrix} n_{12} & l_{12} & n_3 & l_3 \\ s_{ab} & j_{12} & j_3 & J \\ t_{ab} & T & M_T & i \end{bmatrix} c_{\alpha', i'} \begin{bmatrix} n'_{12} & l'_{12} & n'_3 & l'_3 \\ s'_{ab} & j'_{12} & j'_3 & J \\ t'_{ab} & T & M_T & i' \end{bmatrix} \\
&\times \langle E i J T M_T | \hat{V}_{NNN} | E' i' J T M_T \rangle,
\end{aligned} \tag{85}$$

where in addition the quantum-number dependence of the CFPs, indicated by the α - and i -index, are illustrated in the squared brackets. Moreover, there are the relations

$$M_{ab} = m_a + m_b \tag{86}$$

$$M'_{ab} = m'_a + m'_b \tag{87}$$

$$\mathcal{M}_{\mathcal{J}} = m_a + m_b + m_c \tag{88}$$

$$m_{t_{ab}} = m_{t_a} + m_{t_b} \tag{89}$$

$$M_T = m_{t_{ab}} + m_{t_c} \tag{90}$$

$$E = 2n_{12} + l_{12} + n_3 + l_3. \tag{91}$$

4.5.2 Calculating the T-coefficient

To calculate the T-coefficient

$$\begin{aligned}
T & \begin{bmatrix} a & b & c & J_{ab} & J & \mathcal{J} \\ n_{cm} & l_{cm} & n_{12} & l_{12} & n_3 & l_3 \\ s_{ab} & j_{12} & j_3 & t_{ab} & T & M_T \end{bmatrix} \\
& = \{ \langle n_{cm} l_{cm} | \otimes \langle \alpha | \}^{\mathcal{J}\mathcal{M}\mathcal{J}} | \{ \{ |a\rangle \otimes |b\rangle \}^{J_{ab}} \otimes |c\rangle \}^{\mathcal{J}\mathcal{M}\mathcal{J}} \}
\end{aligned} \tag{92}$$

we express the states $| \{ \{ |a\rangle \otimes |b\rangle \}^{J_{ab}} \otimes |c\rangle \}^{\mathcal{J}\mathcal{M}\mathcal{J}}$ in terms of the states $\{ |n_{cm} l_{cm}\rangle \otimes |\alpha\rangle \}^{\mathcal{J}\mathcal{M}\mathcal{J}}$. Starting with

$$\begin{aligned}
& | \{ \{ |a\rangle \otimes |b\rangle \}^{J_{ab}} \otimes |c\rangle \}^{\mathcal{J}\mathcal{M}\mathcal{J}} \\
& = | \{ [(n_a l_a, s_a) j_a, (n_b l_b, s_b) j_b] J_{ab}, (n_c l_c, s_c) j_c \} \mathcal{J}\mathcal{M}\mathcal{J}, t_a m_{t_a} t_b m_{t_b} t_c m_{t_c} \rangle, \tag{93}
\end{aligned}$$

we couple the isospins t_a, t_b, t_c to T, M_T using two Clebsch-Gordan coefficients

$$\begin{aligned}
& | \{ \{ |a\rangle \otimes |b\rangle \}^{J_{ab}} \otimes |c\rangle \}^{\mathcal{J}\mathcal{M}\mathcal{J}} \\
& = \sum_{t_{ab} m_{t_{ab}}} \sum_{T M_T} c \begin{pmatrix} t_a & t_b & t_{ab} \\ m_{t_a} & m_{t_b} & m_{t_{ab}} \end{pmatrix} c \begin{pmatrix} t_{ab} & t_c & T \\ m_{t_{ab}} & m_{t_c} & M_T \end{pmatrix} \\
& \times | \{ [(n_a l_a, s_a) j_a, (n_b l_b, s_b) j_b] J_{ab}, (n_c l_c, s_c) j_c \} \mathcal{J}\mathcal{M}\mathcal{J}, [(t_a t_b) t_{ab}, t_c] T M_T \rangle. \tag{94}
\end{aligned}$$

In the next steps the isospin part will not be changed anymore, so we omit it for brevity. In the following we have to carry out a number of unitary transformations by inserting appropriate identity operators. We do this stepwise and collect the resulting factors at the end in (117). To keep track of the transformations we show the involved quantum numbers before each transformation step.

$$[(n_a l_a, s_a) j_a, (n_b l_b, s_b) j_b] J_{ab} \longrightarrow [(n_a l_a, n_b l_b) L_{ab}, (s_a s_b) s_{ab}] J_{ab}$$

We aim at the separation of the center-of-mass part of the state, so we have to do Talmi-transformations. The first Talmi-transformation will introduce the coordinate of the center-of-mass of the first two particles and the corresponding relative coordinate. Before doing this we have to change the jj -coupling of particles 1 and 2 into LS -coupling.

This can be achieved by inserting a suitable identity operator in (94)

$$\begin{aligned}
& |\{[(n_a l_a, s_a) j_a, (n_b l_b, s_b) j_b] J_{ab}, (n_c l_c, s_c) j_c\} \mathcal{J} \mathcal{M}_{\mathcal{J}} \rangle \\
&= \sum_{L_{ab} s_{ab}} |\{[(n_a l_a, n_b l_b) L_{ab}, (s_a s_b) s_{ab}] J_{ab}, (n_c l_c, s_c) j_c\} \mathcal{J} \mathcal{M}_{\mathcal{J}} \rangle \\
&\quad \times \langle \{[(n_a l_a, n_b l_b) L_{ab}, (s_a s_b) s_{ab}] J_{ab}, (n_c l_c, s_c) j_c\} \mathcal{J} \mathcal{M}_{\mathcal{J}} | \\
&\quad \times |\{[(n_a l_a, s_a) j_a, (n_b l_b, s_b) j_b] J_{ab}, (n_c l_c, s_c) j_c\} \mathcal{J} \mathcal{M}_{\mathcal{J}} \rangle,
\end{aligned} \tag{95}$$

and the overlap can be replaced by

$$\begin{aligned}
& \langle \{[(n_a l_a, n_b l_b) L_{ab}, (s_a s_b) s_{ab}] J_{ab}, (n_c l_c, s_c) j_c\} \mathcal{J} \mathcal{M}_{\mathcal{J}} | \\
& \times |\{[(n_a l_a, s_a) j_a, (n_b l_b, s_b) j_b] J_{ab}, (n_c l_c, s_c) j_c\} \mathcal{J} \mathcal{M}_{\mathcal{J}} \rangle \\
&= \left\{ \begin{array}{ccc} l_a & l_b & L_{ab} \\ s_a & s_b & s_{ab} \\ j_a & j_b & J_{ab} \end{array} \right\} \hat{j}_a \hat{j}_b \hat{L}_{ab} \hat{S}_{ab},
\end{aligned}$$

yielding

$$\begin{aligned}
& |\{[(n_a l_a, s_a) j_a, (n_b l_b, s_b) j_b] J_{ab}, (n_c l_c, s_c) j_c\} \mathcal{J} \mathcal{M}_{\mathcal{J}} \rangle \\
&= \sum_{L_{ab} s_{ab}} \left\{ \begin{array}{ccc} l_a & l_b & L_{ab} \\ s_a & s_b & s_{ab} \\ j_a & j_b & J_{ab} \end{array} \right\} \hat{j}_a \hat{j}_b \hat{L}_{ab} \hat{S}_{ab} \\
&\quad \times |\{[(n_a l_a, n_b l_b) L_{ab}, (s_a s_b) s_{ab}] J_{ab}, (n_c l_c, s_c) j_c\} \mathcal{J} \mathcal{M}_{\mathcal{J}} \rangle.
\end{aligned} \tag{96}$$

$$(n_a l_a, n_b l_b) L_{ab} \longrightarrow (\mathcal{N}_{12} \mathcal{L}_{12}(\mathbf{c}\vec{\mathbf{m}}_{ab}), n_{12} l_{12}(\vec{\xi}_1)) L_{ab}$$

Now we carry out a Talmi-transformation which transforms the single-particle coordinates \vec{r}_a and \vec{r}_b into the coordinate of the center-of-mass $\mathbf{c}\vec{\mathbf{m}}_{ab}$ of the first two particles,

and their relative Jacobi coordinate $\vec{\xi}_1$. The corresponding transformation matrix reads

$$\begin{pmatrix} \vec{\mathbf{m}}_{ab} \\ \vec{\xi}_1 \end{pmatrix} = \begin{pmatrix} \sqrt{\frac{1}{2}} & \sqrt{\frac{1}{2}} \\ \sqrt{\frac{1}{2}} & -\sqrt{\frac{1}{2}} \end{pmatrix} \begin{pmatrix} \vec{r}_a \\ \vec{r}_b \end{pmatrix} \quad (97)$$

which corresponds to HOBs with parameter $d = 1$. The result of this transformation is given by

$$\begin{aligned} & | \{ [(n_a l_a, n_b l_b) L_{ab}, (s_a s_b) s_{ab}] J_{ab}, (n_c l_c, s_c) j_c \} \mathcal{J} \mathcal{M}_{\mathcal{J}} \rangle \\ &= \sum_{\mathcal{N}_{12} \mathcal{L}_{12}} \sum_{n_{12} l_{12}} \langle \langle \mathcal{N}_{12} \mathcal{L}_{12}, n_{12} l_{12} | n_a l_a, n_b l_b; L_{ab} \rangle \rangle_1 \\ & \times | \{ [(\mathcal{N}_{12} \mathcal{L}_{12}(\vec{\mathbf{m}}_{ab}), n_{12} l_{12}(\vec{\xi}_1)) L_{ab}, (s_a s_b) s_{ab}] J_{ab}, (n_c l_c s_c) j_c \} \mathcal{J} \mathcal{M}_{\mathcal{J}} \rangle . \end{aligned} \quad (98)$$

The coordinates again indicate which basis the quantum numbers correspond to and will be omitted in the following.

$$[(L_{ab} s_{ab}) J_{ab}, (l_c s_c) j_c] \mathcal{J} \longrightarrow [(L_{ab} l_c) \mathcal{L}, (s_{ab} s_c) S] \mathcal{J}$$

We change the coupling scheme from jj -coupling to LS -coupling to prepare the next Talmi-transformation

$$\begin{aligned} & | \{ [(\mathcal{N}_{12} \mathcal{L}_{12}, n_{12} l_{12}) L_{ab}, (s_a s_b) s_{ab}] J_{ab}, (n_c l_c, s_c) j_c \} \mathcal{J} \mathcal{M}_{\mathcal{J}} \rangle \\ &= \sum_{\mathcal{L} S} | \{ [(\mathcal{N}_{12} \mathcal{L}_{12}, n_{12} l_{12}) L_{ab}, n_c l_c] \mathcal{L}, [(s_a s_b) s_{ab}, s_c] S \} \mathcal{J} \mathcal{M}_{\mathcal{J}} \rangle \\ & \times \langle \{ [(\mathcal{N}_{12} \mathcal{L}_{12}, n_{12} l_{12}) L_{ab}, n_c l_c] \mathcal{L}, [(s_a s_b) s_{ab}, s_c] S \} \mathcal{J} \mathcal{M}_{\mathcal{J}} | \\ & \times | \{ [(\mathcal{N}_{12} \mathcal{L}_{12}, n_{12} l_{12}) L_{ab}, (s_a s_b) s_{ab}] J_{ab}, (n_c l_c, s_c) j_c \} \mathcal{J} \mathcal{M}_{\mathcal{J}} \rangle . \end{aligned} \quad (99)$$

Again, the overlap can be replaced by a 9-j symbol

$$\begin{aligned}
& \langle \{[(\mathcal{N}_{12}\mathcal{L}_{12}, n_{12}l_{12})L_{ab}, n_cl_c]\mathcal{L}, [(s_as_b)s_{ab}, s_c]S\}\mathcal{J}\mathcal{M}_{\mathcal{J}} | \\
& \times | \{[(\mathcal{N}_{12}\mathcal{L}_{12}, n_{12}l_{12})L_{ab}, (s_as_b)s_{ab}]J_{ab}, (n_cl_c, s_c)j_c\}\mathcal{J}\mathcal{M}_{\mathcal{J}} \rangle \\
& = \left\{ \begin{array}{ccc} L_{ab} & l_c & \mathcal{L} \\ s_{ab} & s_c & S \\ J_{ab} & j_c & \mathcal{J} \end{array} \right\} \hat{\mathcal{L}}\hat{S}\hat{J}_{ab}\hat{j}_c,
\end{aligned} \tag{100}$$

yielding

$$\begin{aligned}
& | \{[(\mathcal{N}_{12}\mathcal{L}_{12}, n_{12}l_{12})L_{ab}, (s_as_b)s_{ab}]J_{ab}, (n_cl_c, s_c)j_c\}\mathcal{J}\mathcal{M}_{\mathcal{J}} \rangle \\
& = \sum_{\mathcal{L}S} \left\{ \begin{array}{ccc} L_{ab} & l_c & \mathcal{L} \\ s_{ab} & s_c & S \\ J_{ab} & j_c & \mathcal{J} \end{array} \right\} \hat{\mathcal{L}}\hat{S}\hat{J}_{ab}\hat{j}_c \\
& \times | \{[(\mathcal{N}_{12}\mathcal{L}_{12}, n_{12}l_{12})L_{ab}, n_cl_c]\mathcal{L}, [(s_as_b)s_{ab}, s_c]S\}\mathcal{J}\mathcal{M}_{\mathcal{J}} \rangle.
\end{aligned} \tag{101}$$

$$[(\mathcal{N}_{12}\mathcal{L}_{12}, n_{12}l_{12})L_{ab}, n_cl_c]\mathcal{L} \longrightarrow [(\mathcal{N}_{12}\mathcal{L}_{12}, n_cl_c)\Lambda, n_{12}l_{12}]\mathcal{L}$$

Before we can carry out the second Talmi-transformation, which will lead us to the complete set of Jacobi coordinates, we have to couple \mathcal{L}_{12} with l_c

$$\begin{aligned}
& | \{[(\mathcal{N}_{12}\mathcal{L}_{12}, n_{12}l_{12})L_{ab}, n_cl_c]\mathcal{L}, [(s_as_b)s_{ab}, s_c]S\}\mathcal{J}\mathcal{M}_{\mathcal{J}} \rangle \\
& = \sum_{\Lambda} | \{[(\mathcal{N}_{12}\mathcal{L}_{12}, n_cl_c)\Lambda, n_{12}l_{12}]\mathcal{L}, [(s_as_b)s_{ab}, s_c]S\}\mathcal{J}\mathcal{M}_{\mathcal{J}} \rangle \\
& \times \langle \{[(\mathcal{N}_{12}\mathcal{L}_{12}, n_cl_c)\Lambda, n_{12}l_{12}]\mathcal{L}, [(s_as_b)s_{ab}, s_c]S\}\mathcal{J}\mathcal{M}_{\mathcal{J}} | \\
& \times | \{[(\mathcal{N}_{12}\mathcal{L}_{12}, n_{12}l_{12})L_{ab}, n_cl_c]\mathcal{L}, [(s_as_b)s_{ab}, s_c]S\}\mathcal{J}\mathcal{M}_{\mathcal{J}} \rangle.
\end{aligned} \tag{102}$$

Because we have a reordering of three angular momenta this time, we can replace the overlap introducing a 6-j symbol

$$\begin{aligned}
& \langle \{[(\mathcal{N}_{12}\mathcal{L}_{12}, n_c l_c)\Lambda, n_{12}l_{12}]\mathcal{L}, [(s_a s_b) s_{ab} s_c]S\} \mathcal{J} \mathcal{M}_{\mathcal{J}} | \\
& \times | \{[(\mathcal{N}_{12}\mathcal{L}_{12}, n_{12}l_{12})L_{ab}, n_c l_c]\mathcal{L}, [(s_a s_b) s_{ab}, s_c]S\} \mathcal{J} \mathcal{M}_{\mathcal{J}} \rangle \\
& = (-1)^{l_c + l_{12} + \Lambda + L_{ab}} \hat{\Lambda} \hat{L}_{ab} \begin{Bmatrix} l_c & \mathcal{L}_{12} & \Lambda \\ l_{12} & \mathcal{L} & L_{ab} \end{Bmatrix},
\end{aligned} \tag{103}$$

yielding

$$\begin{aligned}
& | \{[(\mathcal{N}_{12}\mathcal{L}_{12}, n_{12}l_{12})L_{ab}, n_c l_c]\mathcal{L}, [(s_a s_b) s_{ab}, s_c]S\} \mathcal{J} \mathcal{M}_{\mathcal{J}} \rangle \\
& = \sum_{\Lambda} (-1)^{l_c + l_{12} + \Lambda + L_{ab}} \hat{\Lambda} \hat{L}_{ab} \begin{Bmatrix} l_c & \mathcal{L}_{12} & \Lambda \\ l_{12} & \mathcal{L} & L_{ab} \end{Bmatrix} \\
& \times | \{[(\mathcal{N}_{12}\mathcal{L}_{12}, n_c l_c)\Lambda, n_{12}l_{12}]\mathcal{L}, [(s_a s_b) s_{ab}, s_c]S\} \mathcal{J} \mathcal{M}_{\mathcal{J}} \rangle.
\end{aligned} \tag{104}$$

$$(\mathcal{N}_{12}\mathcal{L}_{12}(\mathbf{c}\vec{\mathbf{m}}_{ab}), n_c l_c(\vec{r}_c))\Lambda \longrightarrow (n_{cm} l_{cm}(\vec{\xi}_0), n_3 l_3(\vec{\xi}_2))\Lambda$$

Now we carry out the second Talmi-transformation that transforms the coordinates $\mathbf{c}\vec{\mathbf{m}}_{ab}$ and \vec{r}_c into the center-of-mass coordinate $\vec{\xi}_0$ of the three particles and the Jacobi coordinate $\vec{\xi}_2$. Here the transformation matrix reads

$$\begin{pmatrix} \vec{\xi}_0 \\ \vec{\xi}_2 \end{pmatrix} = \begin{pmatrix} \sqrt{\frac{2}{3}} & \sqrt{\frac{1}{3}} \\ \sqrt{\frac{1}{3}} & -\sqrt{\frac{2}{3}} \end{pmatrix} \begin{pmatrix} \mathbf{c}\vec{\mathbf{m}}_{ab} \\ \vec{r}_c \end{pmatrix} \tag{105}$$

and corresponds to HOBs with parameter $d = 2$. The result is given by

$$\begin{aligned}
& | \{[(\mathcal{N}_{12}\mathcal{L}_{12}, n_c l_c)\Lambda, n_{12}l_{12}]\mathcal{L}, [(s_a s_b) s_{ab} s_c]S\} \mathcal{J} \mathcal{M}_{\mathcal{J}} \rangle \\
& = \sum_{n_{cm} l_{cm}} \sum_{n_3 l_3} \langle \langle n_{cm} l_{cm}, n_3 l_3 | \mathcal{N}_{12}\mathcal{L}_{12}, n_c l_c; \Lambda \rangle \rangle_2 \\
& \times | \{[(n_{cm} l_{cm}(\vec{\xi}_0), n_3 l_3(\vec{\xi}_2))\Lambda, n_{12}l_{12}]\mathcal{L}, [(s_a s_b) s_{ab}, s_c]S\} \mathcal{J} \mathcal{M}_{\mathcal{J}} \rangle.
\end{aligned} \tag{106}$$

$$[(n_{cm}l_{cm}(\vec{\xi}_0), n_3l_3(\vec{\xi}_2))\Lambda, n_{12}l_{12}]\mathcal{L} \longrightarrow [n_{cm}l_{cm}, (n_3l_3, n_{12}l_{12})L]\mathcal{L}$$

Recoupling of the orbital angular momenta yields

$$\begin{aligned} & | \{ [(n_{cm}l_{cm}, n_3l_3)\Lambda, n_{12}l_{12}]\mathcal{L}, [(s_a s_b) s_{ab}, s_c] S \} \mathcal{J} \mathcal{M}_{\mathcal{J}} \rangle \\ &= \sum_L | \{ [(n_{cm}l_{cm}, (n_3l_3, n_{12}l_{12})L)\mathcal{L}, [(s_a s_b) s_{ab}, s_c] S \} \mathcal{J} \mathcal{M}_{\mathcal{J}} \rangle \\ &\times \langle \{ [(n_{cm}l_{cm}, (n_3l_3, n_{12}l_{12})L)\mathcal{L}, [(s_a s_b) s_{ab}, s_c] S \} \mathcal{J} \mathcal{M}_{\mathcal{J}} | \\ &\times | \{ [(n_{cm}l_{cm}, n_3l_3)\Lambda, n_{12}l_{12}]\mathcal{L}, [(s_a s_b) s_{ab}, s_c] S \} \mathcal{J} \mathcal{M}_{\mathcal{J}} \rangle . \end{aligned} \tag{107}$$

Here the overlap can be substituted by

$$\begin{aligned} & \langle \{ [(n_{cm}l_{cm}, (n_3l_3, n_{12}l_{12})L)\mathcal{L}, [(s_a s_b) s_{ab}, s_c] S \} \mathcal{J} \mathcal{M}_{\mathcal{J}} | \\ &\times | \{ [(n_{cm}l_{cm}, n_3l_3)\Lambda, n_{12}l_{12}]\mathcal{L}, [(s_a s_b) s_{ab}, s_c] S \} \mathcal{J} \mathcal{M}_{\mathcal{J}} \rangle \\ &= (-1)^{l_{cm}+l_3+l_{12}+\mathcal{L}} \hat{\Lambda} \hat{L} \begin{Bmatrix} l_{cm} & l_3 & \Lambda \\ l_{12} & \mathcal{L} & L \end{Bmatrix} , \end{aligned} \tag{108}$$

yielding

$$\begin{aligned} & | \{ [(n_{cm}l_{cm}, n_3l_3)\Lambda, n_{12}l_{12}]\mathcal{L}, [(s_a s_b) s_{ab}, s_c] S \} \mathcal{J} \mathcal{M}_{\mathcal{J}} \rangle \\ &= \sum_L (-1)^{l_{cm}+l_3+l_{12}+\mathcal{L}} \hat{\Lambda} \hat{L} \begin{Bmatrix} l_{cm} & l_3 & \Lambda \\ l_{12} & \mathcal{L} & L \end{Bmatrix} \\ &\times | \{ [n_{cm}l_{cm}, (n_3l_3, n_{12}l_{12})L)\mathcal{L}, [(s_a s_b) s_{ab}, s_c] S \} \mathcal{J} \mathcal{M}_{\mathcal{J}} \rangle . \end{aligned} \tag{109}$$

$$[(n_{cm}l_{cm}, L)\mathcal{L}, S]\mathcal{J} \longrightarrow [n_{cm}l_{cm}, (L, S)J]\mathcal{J}$$

Inserting the corresponding identity operator leads to

$$\begin{aligned} & | \{ [(n_{cm}l_{cm}, (n_3l_3, n_{12}l_{12})L_3)\mathcal{L}, [(s_a s_b) s_{ab}, s_c]S]\mathcal{J}\mathcal{M}_{\mathcal{J}} \rangle \\ &= \sum_J | \{ n_{cm}l_{cm}, [(n_3l_3, n_{12}l_{12})L, [(s_a s_b) s_{ab}, s_c]S]J\}\mathcal{J}\mathcal{M}_{\mathcal{J}} \rangle \end{aligned} \quad (110)$$

$$\times \langle \{ n_{cm}l_{cm}, [(n_3l_3, n_{12}l_{12})L, [(s_a s_b) s_{ab}, s_c]S]J\}\mathcal{J}\mathcal{M}_{\mathcal{J}} |$$

$$\times | \{ [(n_{cm}l_{cm}, (n_3l_3, n_{12}l_{12})L)\mathcal{L}, [(s_a s_b) s_{ab}, s_c]S]\mathcal{J}\mathcal{M}_{\mathcal{J}} \rangle$$

and the overlap can be replaced by

$$\begin{aligned} & \langle \{ n_{cm}l_{cm}, [(n_3l_3, n_{12}l_{12})L, [(s_a s_b) s_{ab}, s_c]S]J\}\mathcal{J}\mathcal{M}_{\mathcal{J}} | \\ & \times | \{ [(n_{cm}l_{cm}, (n_3l_3, n_{12}l_{12})L)\mathcal{L}, [(s_a s_b) s_{ab}, s_c]S]\mathcal{J}\mathcal{M}_{\mathcal{J}} \rangle \end{aligned} \quad (111)$$

$$= (-1)^{l_{cm}+L+S+J} \hat{\mathcal{L}} \hat{\mathcal{J}} \left\{ \begin{array}{ccc} l_{cm} & L & \mathcal{L} \\ S & \mathcal{J} & J \end{array} \right\},$$

yielding

$$\begin{aligned} & | \{ [(n_{cm}l_{cm}, (n_3l_3, n_{12}l_{12})L_3)\mathcal{L}, [(s_a s_b) s_{ab}, s_c]S]\mathcal{J}\mathcal{M}_{\mathcal{J}} \rangle \\ &= \sum_J (-1)^{l_{cm}+L+S+J} \hat{\mathcal{L}} \hat{\mathcal{J}} \left\{ \begin{array}{ccc} l_{cm} & L & \mathcal{L} \\ S & \mathcal{J} & J \end{array} \right\} \end{aligned} \quad (112)$$

$$\times | \{ n_{cm}l_{cm}, [(n_3l_3, n_{12}l_{12})L, [(s_a s_b) s_{ab}, s_c]S]J\}\mathcal{J}\mathcal{M}_{\mathcal{J}} \rangle .$$

$$[(n_3 l_3, n_{12} l_{12})L, [s_{ab} s_c]S]J \longrightarrow [(n_3 l_3, s_c)j_3, (n_{12} l_{12}, s_{ab})j_{12}]J$$

The final transformation leads to the coupling structure of the state $|\alpha\rangle$

$$\begin{aligned} & |\{n_{cm} l_{cm}, [(n_3 l_3, n_{12} l_{12})L, [(s_a s_b) s_{ab}, s_c]S]J\} \mathcal{J} \mathcal{M}_{\mathcal{J}}\rangle \\ &= \sum_{j_{12} j_3} |\{n_{cm} l_{cm}, [(n_3 l_3, s_c)j_3, (n_{12} l_{12}, s_{ab})j_{12}]J\} \mathcal{J} \mathcal{M}_{\mathcal{J}}\rangle \\ &\times \langle \{n_{cm} l_{cm}, [(n_3 l_3, s_c)j_3, (n_{12} l_{12}, s_{ab})j_{12}]J\} \mathcal{J} \mathcal{M}_{\mathcal{J}} | \\ &\times |\{n_{cm} l_{cm}, [(n_3 l_3, n_{12} l_{12})L, [(s_a s_b) s_{ab}, s_c]S]J\} \mathcal{J} \mathcal{M}_{\mathcal{J}}\rangle. \end{aligned} \quad (113)$$

We can replace the overlap by a 9-j symbol

$$\begin{aligned} & \langle \{n_{cm} l_{cm}, [(n_3 l_3, s_c)j_3, (n_{12} l_{12}, s_{ab})j_{12}]J\} \mathcal{J} \mathcal{M}_{\mathcal{J}} | \\ & \times |\{n_{cm} l_{cm}, [(n_3 l_3, n_{12} l_{12})L, [(s_a s_b) s_{ab}, s_c]S]J\} \mathcal{J} \mathcal{M}_{\mathcal{J}}\rangle \\ &= (-1)^{s_{ab}+s_c-S} \hat{L} \hat{j}_3 \hat{j}_{12} \hat{S} \begin{Bmatrix} l_3 & l_{12} & L \\ s_c & s_{ab} & S \\ j_3 & j_{12} & J \end{Bmatrix} \end{aligned} \quad (114)$$

$$= (-1)^{s_{ab}+s_c-S} \hat{L} \hat{j}_3 \hat{j}_{12} \hat{S} \begin{Bmatrix} l_{12} & l_3 & L \\ s_{ab} & s_c & S \\ j_{12} & j_3 & J \end{Bmatrix} (-1)^{l_{12}+l_3+L+s_{ab}+s_c+S+j_{12}+j_3+J}. \quad (115)$$

In the previous equation a symmetry relation of the 9-j symbol was used. Additionally, we change the coupling order from $(j_3 j_{12})$ into $(j_{12} j_3)$ and collect a phase $(-1)^{j_3+j_{12}-J}$. Then we can simplify the phase factors, because some combinations of quantum numbers are even, and we obtain the phase $(-1)^{l_3+l_{12}+L}$. Altogether the result of this trans-

formation reads

$$\begin{aligned}
& |\{n_{cm}l_{cm}, [(n_3l_3, n_{12}l_{12})L, [(s_a s_b)s_{ab}, s_c]S]J\}\mathcal{J}\mathcal{M}_{\mathcal{J}}\rangle \\
&= \sum_{j_{12}j_3} (-1)^{l_3+l_{12}+L} \hat{L}\hat{j}_3\hat{j}_{12}\hat{S} \left\{ \begin{array}{ccc} l_{12} & l_3 & L \\ s_{ab} & s_c & S \\ j_{12} & j_3 & J \end{array} \right\} \tag{116}
\end{aligned}$$

$$\times |\{n_{cm}l_{cm}, [(n_{12}l_{12}, s_{ab})j_{12}, (n_3l_3, s_c)j_3]J\}\mathcal{J}\mathcal{M}_{\mathcal{J}}\rangle.$$

The complete result of the transformation $\{ \{|a\rangle \otimes |b\rangle\}^{J_{ab}} \otimes |c\rangle\}^{\mathcal{J}} \longrightarrow \{|n_{cm}l_{cm}\rangle \otimes |\alpha\rangle\}^{\mathcal{J}}$

is given by

$$\begin{aligned}
& \{ \{ |a\rangle \otimes |b\rangle \}^{J_{ab}} \otimes |c\rangle \}^{\mathcal{J}} \\
&= \sum_{t_{ab} m_{t_{ab}}} \sum_{TM_T} \sum_{L_{ab} s_{ab}} \sum_{\mathcal{N}_{12} \mathcal{L}_{12}} \sum_{n_{12} l_{12}} \sum_{\mathcal{L} S} \sum_{\Lambda} \sum_{n_{cm} l_{cm}} \sum_{n_3 l_3} \sum_L \sum_J \sum_{j_{12} j_3} \\
&\times \delta_{2\mathcal{N}_{12} + \mathcal{L}_{12} + 2n_{12} + l_{12}, 2n_a + l_a + 2n_b + l_b} \delta_{2n_{cm} + l_{cm} + 2n_3 + l_3, 2\mathcal{N}_{12} + \mathcal{L}_{12} + 2n_c + l_c} \\
&\times (-1)^{l_c + l_{12} + \Lambda + L_{ab}} (-1)^{l_{cm} + l_3 + l_{12} + \mathcal{L}} (-1)^{l_{cm} + L + S + \mathcal{J}} (-1)^{l_3 + l_{12} + L} \\
&\times \hat{j}_a \hat{j}_b \hat{j}_c \hat{L}_{ab}^2 \hat{s}_{ab} \hat{J}_{ab} \hat{\mathcal{L}}^2 \hat{S}^2 \hat{\Lambda}^2 \hat{L}^2 \hat{J} \hat{j}_{12} \hat{j}_3 \\
&\times c \begin{pmatrix} t_a & t_b & t_{ab} \\ m_{t_a} & m_{t_b} & m_{t_{ab}} \end{pmatrix} c \begin{pmatrix} t_{ab} & t_c & T \\ m_{t_{ab}} & m_{t_c} & M_T \end{pmatrix} \tag{117} \\
&\times \begin{Bmatrix} l_a & l_b & L_{ab} \\ s_a & s_b & s_{ab} \\ j_a & j_b & J_{ab} \end{Bmatrix} \begin{Bmatrix} L_{ab} & l_c & \mathcal{L} \\ s_{ab} & s_c & S \\ J_{ab} & j_c & \mathcal{J} \end{Bmatrix} \begin{Bmatrix} l_{12} & l_3 & L \\ s_{ab} & s_c & S \\ j_{12} & j_3 & J \end{Bmatrix} \\
&\times \begin{Bmatrix} l_c & \mathcal{L}_{12} & \Lambda \\ l_{12} & \mathcal{L} & L_{ab} \end{Bmatrix} \begin{Bmatrix} l_{cm} & l_3 & \Lambda \\ l_{12} & \mathcal{L} & L \end{Bmatrix} \begin{Bmatrix} l_{cm} & L & \mathcal{L} \\ S & \mathcal{J} & J \end{Bmatrix} \\
&\times \langle \langle \mathcal{N}_{12} \mathcal{L}_{12}, n_{12} l_{12} | n_a l_a, n_b l_b; L_{ab} \rangle \rangle_1 \langle \langle n_{cm} l_{cm}, n_3 l_3 | \mathcal{N}_{12} \mathcal{L}_{12}, n_c l_c; \Lambda \rangle \rangle_2 \\
&\times \{ |n_{cm} l_{cm}\rangle \otimes |\alpha\rangle \}^{\mathcal{J}}
\end{aligned}$$

Multiplying (117) with $\{ \langle n'_{cm} l'_{cm} | \otimes \langle \alpha' | \}^{\mathcal{J}}$ generates Kronecker deltas

$$\delta_{n'_{cm} n_{cm}} \delta_{l'_{cm} l_{cm}} \delta_{n'_{12} n_{12}} \delta_{l'_{12} l_{12}} \delta_{s'_{ab} s_{ab}} \delta_{j'_{12} j_{12}} \delta_{n'_3 n_3} \delta_{l'_3 l_3} \delta_{j'_3 j_3} \delta_{J' J} \delta_{t'_{ab} t_{ab}} \delta_{m'_{t'_{ab}} m_{t_{ab}}} \delta_{T' T} \delta_{M'_T M_T} \tag{118}$$

which eliminate the corresponding summations, leading to

$$\begin{aligned}
& \{ \langle n_{cm} l_{cm} | \otimes \langle \alpha | \}^{\mathcal{J}} \{ \{ |a\rangle \otimes |b\rangle \}^{J_{ab}} \otimes |c\rangle \}^{\mathcal{J}} \\
&= \sum_{L_{ab}} \sum_{\mathcal{N}_{12}} \sum_{\mathcal{L}_{12}} \sum_{\mathcal{L}} \sum_S \sum_{\Lambda} \sum_L \\
&\times (-1)^{l_c + l_{12} + \Lambda + L_{ab}} (-1)^{l_{cm} + l_3 + l_{12} + \mathcal{L}} (-1)^{l_{cm} + L + S + \mathcal{J}} (-1)^{l_3 + l_{12} + L} \\
&\times \delta_{2\mathcal{N}_{12} + \mathcal{L}_{12} + 2n_{12} + l_{12}, 2n_a + l_a + 2n_b + l_b} \delta_{2n_{cm} + l_{cm} + 2n_3 + l_3, 2\mathcal{N}_{12} + \mathcal{L}_{12} + 2n_c + l_c} \\
&\times \hat{j}_a \hat{j}_b \hat{j}_c \hat{L}_{ab}^2 \hat{s}_{ab} \hat{J}_{ab} \hat{\mathcal{L}}^2 \hat{S}^2 \hat{\Lambda}^2 \hat{L}^2 \hat{J} \hat{j}_{12} \hat{j}_3 \\
&\times c \begin{pmatrix} t_a & t_b & t_{ab} \\ m_{t_a} & m_{t_b} & m_{t_{ab}} \end{pmatrix} c \begin{pmatrix} t_{ab} & t_c & T \\ m_{t_{ab}} & m_{t_c} & M_T \end{pmatrix} \\
&\times \begin{Bmatrix} l_a & l_b & L_{ab} \\ s_a & s_b & s_{ab} \\ j_a & j_b & J_{ab} \end{Bmatrix} \begin{Bmatrix} L_{ab} & l_c & \mathcal{L} \\ s_{ab} & s_c & S_3 \\ J_{ab} & j_c & \mathcal{J} \end{Bmatrix} \begin{Bmatrix} l_{12} & l_3 & L \\ s_{ab} & s_c & S \\ j_{12} & j_3 & J \end{Bmatrix} \\
&\times \begin{Bmatrix} l_c & \mathcal{L}_{12} & \Lambda \\ l_{12} & \mathcal{L} & L_{ab} \end{Bmatrix} \begin{Bmatrix} l_{cm} & l_3 & \Lambda \\ l_{12} & \mathcal{L} & L \end{Bmatrix} \begin{Bmatrix} l_{cm} & L & \mathcal{L} \\ S & \mathcal{J} & J \end{Bmatrix} \\
&\times \langle \langle \mathcal{N}_{12} \mathcal{L}_{12}, n_{12} l_{12} | n_a l_a, n_b l_b; L_{ab} \rangle \rangle_1 \langle \langle n_{cm} l_{cm}, n_3 l_3 | \mathcal{N}_{12} \mathcal{L}_{12}, n_c l_c; \Lambda \rangle \rangle_2.
\end{aligned} \tag{119}$$

Here we dropped the primes and used the additional constraints $m_{t_{ab}} = m_{t_a} + m_{t_b}$, $M_T = m_{t_{ab}} + m_{t_c}$ from the Clebsch-Gordan coefficients. Moreover, we can eliminate the sum over \mathcal{N}_{12} with help of the first Kronecker delta $\delta_{2\mathcal{N}_{12} + \mathcal{L}_{12} + 2n_{12} + l_{12}, 2n_a + l_a + 2n_b + l_b}$. Then the second Kronecker delta reads

$$\delta_{2n_a + l_a + 2n_b + l_b - 2n_{12} - l_{12} + 2n_c + l_c, 2n_{cm} + l_{cm} + 2n_3 + l_3} \tag{120}$$

and our final result for the T-coefficient is

$$\begin{aligned}
& T \begin{bmatrix} a & b & c & J_{ab} & J & \mathcal{J} \\ n_{cm} & l_{cm} & n_{12} & l_{12} & n_3 & l_3 \\ s_{ab} & j_{12} & j_3 & t_{ab} & T & M_T \end{bmatrix} \\
&= \{ \langle n_{cm} l_{cm} | \otimes \langle \alpha | \}^{\mathcal{J}} \{ \{ |a\rangle \otimes |b\rangle \}^{J_{ab}} \otimes |c\rangle \}^{\mathcal{J}} \\
&= \sum_{L_{ab}} \sum_{\mathcal{L}_{12}} \sum_{\mathcal{L}} \sum_S \sum_{\Lambda} \sum_L (-1)^{l_c + \Lambda + L_{ab} + \mathcal{L} + S + l_{12} + \mathcal{J}} \\
&\times \delta_{2n_a + l_a + 2n_b + l_b - 2n_{12} - l_{12} + 2n_c + l_c, 2n_{cm} + l_{cm} + 2n_3 + l_3} \\
&\times \hat{j}_a \hat{j}_b \hat{j}_c \hat{L}_{ab}^2 \hat{s}_{ab} \hat{J}_{ab} \hat{\mathcal{L}}^2 \hat{S}^2 \hat{\Lambda}^2 \hat{L}^2 \hat{j}_{12} \hat{j}_3 \\
&\times c \begin{pmatrix} t_a & t_b & t_{ab} \\ m_{t_a} & m_{t_b} & m_{t_{ab}} \end{pmatrix} c \begin{pmatrix} t_{ab} & t_c & T \\ m_{t_{ab}} & m_{t_c} & M_T \end{pmatrix} \\
&\times \begin{Bmatrix} l_a & l_b & L_{ab} \\ s_a & s_b & s_{ab} \\ j_a & j_b & J_{ab} \end{Bmatrix} \begin{Bmatrix} L_{ab} & l_c & \mathcal{L} \\ s_{ab} & s_c & S \\ J_{ab} & j_c & \mathcal{J} \end{Bmatrix} \begin{Bmatrix} l_{12} & l_3 & L \\ s_{ab} & s_c & S \\ j_{12} & j_3 & J \end{Bmatrix} \\
&\times \begin{Bmatrix} l_c & \mathcal{L}_{12} & \Lambda \\ l_{12} & \mathcal{L} & L_{ab} \end{Bmatrix} \begin{Bmatrix} l_{cm} & l_3 & \Lambda \\ l_{12} & \mathcal{L} & L \end{Bmatrix} \begin{Bmatrix} l_{cm} & L & \mathcal{L} \\ S & \mathcal{J} & J \end{Bmatrix} \\
&\times \langle \langle \mathcal{N}_{12} \mathcal{L}_{12}, n_{12} l_{12} | n_a l_a, n_b l_b; L_{ab} \rangle \rangle_1 \langle \langle n_{cm} l_{cm}, n_3 l_3 | \mathcal{N}_{12} \mathcal{L}_{12}, n_c l_c; \Lambda \rangle \rangle_2,
\end{aligned} \tag{121}$$

where we also simplified the phase factor. This is also the result of reference [14].

4.6 Implementation of the three-body basis transformation

In this section we discuss the implementation of the three-body Jacobi to m-scheme transformation, considering the problems and limits of the transformation. The whole implementation is too complicated to describe it in this thesis, for a more detailed dis-

discussion of some implementation issues see the appendix. Our aim is to use the NNN Jacobi interaction matrix elements from χ EFT and the CFPs up to a certain three-body energy limit E_{3max} and produce a file containing the m-scheme matrix elements up to that energy limit. This file serves as input for many-body calculations, like those discussed at the end of this thesis.

First of all, we consider Eq. (84), which we have to implement. Most important for the implementation of our formulas is that we try to arrange the sums in order to avoid multiple calculation of the same term. Besides, one should put the computationally intensive terms as far out as possible in the hierarchy of summations to minimize the number of evaluations. If we arrange (84) considering these circumstances, we obtain

$$\begin{aligned}
& {}_a \langle abc | \hat{V}_{NNN} | a'b'c' \rangle_a \\
&= 6 \sum_{\mathcal{J}} \sum_{n_{cm} l_{cm}} \\
&\times \sum_{\alpha} \sum_{J_{ab}} c \begin{pmatrix} j_a & j_b & J_{ab} \\ m_a & m_b & M_{ab} \end{pmatrix} c \begin{pmatrix} J_{ab} & j_c & \mathcal{J} \\ M_{ab} & m_c & \mathcal{M}_{\mathcal{J}} \end{pmatrix} \\
&\times T \begin{bmatrix} a & b & c & J_{ab} & J & \mathcal{J} \\ n_{cm} & l_{cm} & n_{12} & l_{12} & n_3 & l_3 \\ s_{ab} & j_{12} & j_3 & t_{ab} & T & M_T \end{bmatrix} \\
&\times \sum_{\bar{\alpha}'} \sum_{J'_{ab}} c \begin{pmatrix} j'_a & j'_b & J'_{ab} \\ m'_a & m'_b & M'_{ab} \end{pmatrix} c \begin{pmatrix} J'_{ab} & j'_c & \mathcal{J} \\ M'_{ab} & m'_c & \mathcal{M}_{\mathcal{J}} \end{pmatrix} \\
&\times T \begin{bmatrix} a' & b' & c' & J'_{ab} & J & \mathcal{J} \\ n_{cm} & l_{cm} & n'_{12} & l'_{12} & n'_3 & l'_3 \\ s'_{ab} & j'_{12} & j'_3 & t'_{ab} & T & M_T \end{bmatrix} \\
&\times \sum_i c_{\alpha,i} \sum_{i'} c_{\alpha',i'} \langle E i J T M_T | \hat{V}_{NNN} | E' i' J T M_T \rangle,
\end{aligned} \tag{122}$$

where the T -coefficients, the computationally most demanding terms, are outside and the sum are arranged in an efficient manner. In order to accelerate the evaluation further, we precompute the T -coefficients and save them combined with the Clebsch-Gordans in a new quantity called \tilde{T} -coefficient

$$\begin{aligned} \tilde{T}(a, b, c, \mathcal{J}, l_{cm}, \alpha) &= \sum_{J_{ab}} c \begin{pmatrix} j_a & j_b & J_{ab} \\ m_a & m_b & M_{ab} \end{pmatrix} c \begin{pmatrix} J_{ab} & j_c & \mathcal{J} \\ M_{ab} & m_c & \mathcal{M}_{\mathcal{J}} \end{pmatrix} \\ &\times T \begin{bmatrix} a & b & c & J_{ab} & J & \mathcal{J} \\ n_{cm} & l_{cm} & n_{12} & l_{12} & n_3 & l_3 \\ s_{ab} & j_{12} & j_3 & t_{ab} & T & M_T \end{bmatrix}, \end{aligned} \quad (123)$$

which is kept in memory.

Remember a, b, c are collective indices for the quantum numbers of the single-particle states and α is a collective index for the Jacobi quantum numbers $n_{12}, l_{12}, s_{ab}, j_{12}, n_3, l_3, j_3, J, t_{ab}, T$. The M_T dependence of α can be neglected because M_T is already determined by the m-scheme basis. Besides, also the n_{cm} dependence of the T - and \tilde{T} -coefficient vanishes owing to the Kronecker delta (120).

The new expression for the m-scheme matrix-element as it is used in the computation reads

$$\begin{aligned} &{}_a \langle abc | \hat{V}_{NNN} | a' b' c' \rangle_a \\ &= 6 \sum_{\mathcal{J}} \sum_{n_{cm} l_{cm}} \sum_{\alpha} \tilde{T}(a, b, c, \mathcal{J}, l_{cm}, \alpha) \sum_{\tilde{\alpha}'} \tilde{T}(a', b', c', \mathcal{J}', l'_{cm}, \alpha') \\ &\times \sum_i c_{\alpha, i} \sum_{i'} c_{\alpha', i'} \langle E i J T M_T | \hat{V}_{NNN} | E' i' J T M_T \rangle. \end{aligned} \quad (124)$$

After precomputing of the \tilde{T} -coefficients we end up with the CFPs, the Jacobi matrix elements and the \tilde{T} -coefficients, saved to memory. To determine the m-scheme matrix elements we just have to loop over a couple of indices and read out the right values from memory. The massive memory consumption of the \tilde{T} -coefficients is the major limitation of formula (124). In Fig. 6 we illustrate that already for a three-body energy larger than $E_{3max} = 8$ the memory required for the \tilde{T} -coefficients becomes larger than 16 GB. Similarly, the set of m-scheme matrix elements, that needs to be kept in RAM for the many-body calculations, exceeds 16 GB for $E_{3max} > 8$ as shown in Fig. 7. Due to the

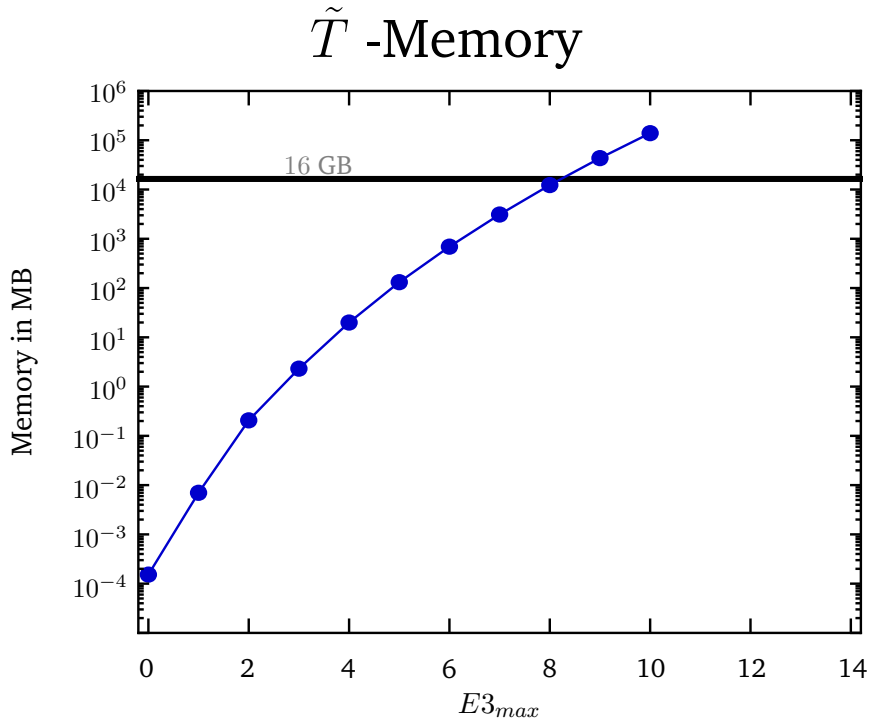


Figure 6: **Memory requirements for the \tilde{T} -coefficient:** The figure shows the memory requirements of the nonzero $\tilde{T}(a, b, c, \mathcal{J}, l_{cm}, \alpha)$ up to the three-body energy limit E_{3max} . To find the right \tilde{T} -coefficient we used a memory scheme where apart from \tilde{T} also $\mathcal{J}, l_{cm}, \alpha$ are saved. Note that it is a logarithmic plot.

Matrix-Element Memory

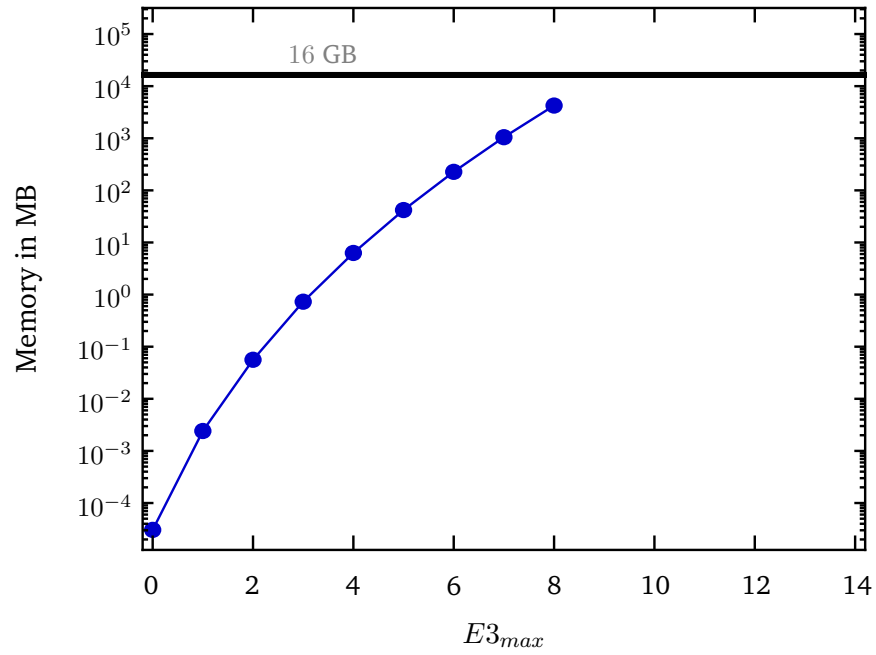


Figure 7: **Memory requirements for the m-scheme matrix elements:** The figure shows the memory requirements of the nonzero m-scheme interaction matrix elements up to the three-body energy limit E_{3max} . The matrix elements are saved in double precision. Note that it is a logarithmic plot.

exponential growth of the required memory with increasing energy E_{3max} we have to apply a new concept, discussed in the next subsection.

4.6.1 Implementation of the J -coupling

A remedy for the limitations discussed in the previous subsection is a simple trick. We save the matrix elements in a J -coupled representation and decouple them on the fly during the many-body calculation. Because the coupled basis has a smaller dimension, we have a smaller number of matrix elements.

We adopt a very simple coupling scheme:

First, we jj -couple the particles 1 and 2 of the m -scheme state as well as their isospin.

Next, we couple the resulting J_{ab} with j_c and t_{ab} with t_c , yielding

$$\begin{aligned}
& {}_a \langle \{[(n_a l_a, s_a) j_a, j_b] J_{ab}, (n_c l_c, s_c) j_c\} \mathcal{J} \mathcal{M}_{\mathcal{J}} ; [(t_a t_b) t_{ab}, t_c] T M_T | \\
&= \sum_{m_a m_b m_c} \sum_{m_{t_a} m_{t_b} m_{t_c}} c \begin{pmatrix} j_a & j_b & J_{ab} \\ m_a & m_b & M_{ab} \end{pmatrix} c \begin{pmatrix} t_a & t_b & t_{ab} \\ m_{t_a} & m_{t_b} & m_{t_{ab}} \end{pmatrix} \\
& \times c \begin{pmatrix} J_{ab} & j_c & \mathcal{J} \\ M_{ab} & m_c & \mathcal{M}_{\mathcal{J}} \end{pmatrix} c \begin{pmatrix} t_{ab} & t_c & T \\ m_{t_{ab}} & m_{t_c} & M_T \end{pmatrix} \\
& \times {}_a \langle (n_a l_a, s_a) j_a m_a t_a m_{t_a} (n_b l_b, s_b) j_b m_b t_b m_{t_b} (n_c l_c, s_c) j_c m_c t_c m_{t_c} |,
\end{aligned} \tag{125}$$

with $M_{ab} = m_a + m_b$, $\mathcal{M}_{\mathcal{J}} = M_{ab} + m_c$, $m_{t_{ab}} = m_{t_a} + m_{t_b}$ and $M_T = m_{t_{ab}} + m_{t_c}$. For the matrix elements in the J-coupled basis we obtain

$$\begin{aligned}
& {}_a \langle [(ab)J_{ab}, c] \mathcal{J} \mathcal{M}_{\mathcal{J}} ; [(t_a t_b)t_{ab}, t_c] T M_T | \hat{V}_{NNN} \\
& \times |[(a'b')J'_{ab}, c'] \mathcal{J} \mathcal{M}_{\mathcal{J}} ; [(t_a t_b)t'_{ab}, t_c] T M_T \rangle_a \\
& = \sum_{m_a m_b m_c} \sum_{m_{t_a} m_{t_b} m_{t_c}} \sum_{m'_a m'_b m'_c} \sum_{m'_{t_a} m'_{t_b} m'_{t_c}} \\
& \times c \begin{pmatrix} j_a & j_b & J_{ab} \\ m_a & m_b & M_{ab} \end{pmatrix} c \begin{pmatrix} t_a & t_b & t_{ab} \\ m_{t_a} & m_{t_b} & m_{t_{ab}} \end{pmatrix} \\
& \times c \begin{pmatrix} J_{ab} & j_c & \mathcal{J} \\ M_{ab} & m_c & \mathcal{M}_{\mathcal{J}} \end{pmatrix} c \begin{pmatrix} t_{ab} & t_c & T \\ m_{t_{ab}} & m_{t_c} & M_T \end{pmatrix} c \begin{pmatrix} j'_a & j'_b & J'_{ab} \\ m'_a & m'_b & M'_{ab} \end{pmatrix} \\
& \times c \begin{pmatrix} t'_a & t'_b & t'_{ab} \\ m'_{t_a} & m'_{t_b} & m'_{t_{ab}} \end{pmatrix} c \begin{pmatrix} J'_{ab} & j'_c & \mathcal{J} \\ M'_{ab} & m'_c & \mathcal{M}_{\mathcal{J}} \end{pmatrix} c \begin{pmatrix} t'_{ab} & t'_c & T \\ m'_{t_{ab}} & m'_{t_c} & M_T \end{pmatrix} \\
& \times {}_a \langle abc | \hat{V}_{NNN} | a'b'c' \rangle_a,
\end{aligned} \tag{126}$$

where one has to insert (124) for the m-scheme matrix elements. Now one can apply the orthogonality relation of the Clebsch-Gordan coefficients

$$\sum_{m_1 m_2} c \begin{pmatrix} j_1 & j_2 & j_{12} \\ m_1 & m_2 & m_{12} \end{pmatrix} c \begin{pmatrix} j_1 & j_2 & \tilde{j}_{12} \\ m_1 & m_2 & \tilde{m}_{12} \end{pmatrix} = \delta_{j_{12} \tilde{j}_{12}} \delta_{m_{12} \tilde{m}_{12}}, \tag{127}$$

to the Clebsch-Gordans obtained from the J-coupling and those contained in the \tilde{T} -coefficients of the m-scheme matrix element. In the expression for the J-coupled matrix elements this leads to a vanishing of all Clebsch Gordans and sums over m -quantum numbers as well as of the sums over j_{12} , j'_{12} , t_{ab} and t'_{ab} .

In the following, interaction matrix elements will be expressed in the J -coupled basis

$${}_a \langle [(ab)J_{ab} t_{ab}, c] \mathcal{J} T | = {}_a \langle \{[(n_a l_a, s_a) j_a, j_b] J_{ab}, (n_c l_c, s_c) j_c\} \mathcal{J} | \langle [(t_a t_b)t_{ab}, t_c] T |,$$

where $\mathcal{M}_{\mathcal{J}}$ and M_T are omitted, because the initial Jacobi matrix elements are independent of those quantum numbers. Note that the M_T independence of the Jacobi matrix elements of the NNN interaction is only an approximation. After dropping the M_T quantum number and applying the orthogonality relation of the Clebsch-Gordan coefficients, we obtain the following expression for the J -coupled matrix elements

$$\begin{aligned}
& {}_a \langle [(ab)J_{ab}t_{ab}, c] \mathcal{J}T | \hat{V}_{NNN} | [(a'b')J'_{ab}t'_{ab}, c'] \mathcal{J}T \rangle_a \\
&= 6 \sum_{n_{cm} l_{cm}} \sum_{n_{12} n'_{12}} \sum_{l_{12} l'_{12}} \sum_{n_3 n'_3} \sum_{l_3 l'_3} \sum_{s_{ab} s'_{ab}} \sum_{j_{12} j'_{12}} \sum_{j_3 j'_3} \sum_J \sum_{ii'} \\
&\times T_J \begin{bmatrix} \tilde{a} & \tilde{b} & \tilde{c} & J_{ab} & J & \mathcal{J} \\ n_{cm} & l_{cm} & n_{12} & l_{12} & n_3 & l_3 \\ s_{ab} & j_{12} & j_3 & & & \end{bmatrix} T_J \begin{bmatrix} \tilde{a}' & \tilde{b}' & \tilde{c}' & J'_{ab} & J & \mathcal{J} \\ n_{cm} & l_{cm} & n'_{12} & l'_{12} & n'_3 & l'_3 \\ s'_{ab} & j'_{12} & j'_3 & & & \end{bmatrix} \quad (128) \\
&\times c_{\alpha, i} \begin{bmatrix} n_{12} & l_{12} & n_3 & l_3 \\ s_{ab} & j_{12} & j_3 & J \\ t_{ab} & T & & i \end{bmatrix} c_{\alpha', i'} \begin{bmatrix} n'_{12} & l'_{12} & n'_3 & l'_3 \\ s'_{ab} & j'_{12} & j'_3 & J \\ t'_{ab} & T & & i' \end{bmatrix} \\
&\times \langle E i J T | \hat{V}_{NNN} | E' i' J T \rangle,
\end{aligned}$$

with the T_J -coefficient

$$\begin{aligned}
& T_J \begin{bmatrix} \tilde{a} & \tilde{b} & \tilde{c} & J_{ab} & J & \mathcal{J} \\ n_{cm} & l_{cm} & n_{12} & l_{12} & n_3 & l_3 \\ s_{ab} & j_{12} & j_3 & & & \end{bmatrix} \\
&= \{ \langle n_{cm} l_{cm} | \otimes \langle \alpha | \}^{\mathcal{J}} | [(ab) J_{ab} t_{ab}, c] \mathcal{J} T \rangle \\
&= \sum_{L_{ab}} \sum_{\mathcal{L}_{12}} \sum_{\mathcal{L}} \sum_S \sum_{\Lambda} \sum_L (-1)^{l_c + \Lambda + L_{ab} + \mathcal{L} + S + l_{12} + \mathcal{J}} \\
&\times \delta_{2n_a + l_a + 2n_b + l_b + 2n_c + l_c, 2n_{cm} + l_{cm} + 2n_{12} + l_{12} + 2n_3 + l_3} \\
&\times \hat{j}_a \hat{j}_b \hat{j}_c \hat{L}_{ab}^2 \hat{s}_{ab} \hat{J}_{ab} \hat{\mathcal{L}}^2 \hat{S}^2 \hat{\Lambda}^2 \hat{L}^2 \hat{J} \hat{j}_{12} \hat{j}_3 \\
&\times \begin{Bmatrix} l_a & l_b & L_{ab} \\ s_a & s_b & s_{ab} \\ j_a & j_b & J_{ab} \end{Bmatrix} \begin{Bmatrix} L_{ab} & l_c & \mathcal{L} \\ s_{ab} & s_c & S \\ J_{ab} & j_c & \mathcal{J} \end{Bmatrix} \begin{Bmatrix} l_{12} & l_3 & L \\ s_{ab} & s_c & S \\ j_{12} & j_3 & J \end{Bmatrix} \\
&\times \begin{Bmatrix} l_c & \mathcal{L}_{12} & \Lambda \\ l_{12} & \mathcal{L} & L_{ab} \end{Bmatrix} \begin{Bmatrix} l_{cm} & l_3 & \Lambda \\ l_{12} & \mathcal{L} & L \end{Bmatrix} \begin{Bmatrix} l_{cm} & L & \mathcal{L} \\ S & \mathcal{J} & J \end{Bmatrix} \\
&\times \langle \langle \mathcal{N}_{12} \mathcal{L}_{12}, n_{12} l_{12} | n_a l_a, n_b l_b; L_{ab} \rangle \rangle_1 \langle \langle n_{cm} l_{cm}, n_3 l_3 | \mathcal{N}_{12} \mathcal{L}_{12}, n_c l_c; \Lambda \rangle \rangle_2.
\end{aligned} \tag{129}$$

Note that due to the vanished Clebsch-Gordans there is no direct t_{ab} and T dependence of the T_J -coefficient, even the quantum numbers appear in the scalar product $\{ \langle n_{cm} l_{cm} | \otimes \langle \alpha | \}^{\mathcal{J}} | [(ab) J_{ab} t_{ab}, c] \mathcal{J} T \rangle$. Again, the n_{cm} dependence vanishes owing to the Kronecker delta in (129). In Eq. (128) and (129) the single particle indices $\tilde{a}, \tilde{b}, \tilde{c}$ now only correspond to the quantum numbers $n_a l_a j_a, n_b l_b j_b, n_c l_c j_c$. The single-particle m quantum numbers have disappeared, which decreases the basis dimension. The improvements resulting from the J-coupling regarding the memory needed to store the T_J -coefficients and the J-coupled matrix elements are illustrated in Fig. 8 and 9, respectively. After the J -coupling the memory needed for storing both quantities for $E_{3max} = 8$ is now in the range of some MB, far away from the initial 16 GB of the m-scheme version.

The limit of 16 GB is now reached at $E_{3max} = 12$.

4.6.2 Problems and limits of the implementation

Even if we use the J -coupled matrix elements, the required memory shows a polynomial increase with E_{3max} , which is illustrated in Fig. 8 and 9. So with the new improvements we still have the same type of limitation, but now at a higher energy, what is very important for the convergence of the many-body calculations, as we will see in Sec. 6. Besides this limitation, there are also other problems occurring with increasing energy.

For instance, to accelerate the transformation code we precompute not only the T_J -coefficients, but also the occurring 6-j and 9-j symbols as well as the Clebsch-Gordan coefficients and the harmonic oscillator brackets. All these precomputed quantities have to fit into the memory and their size also increases polynomially with E_{3max} . In a word, there are also many other quantities used for the implementation of the transformation which increase with the energy, due to this one has to be very careful with the memory management.

At the moment we are able to perform the transformation code for $E_{3max} = 12$, this basis space is already larger than any other space used for the three-body interaction. In addition, we plan to expand our transformation code to a basis space corresponding to $E_{3max} = 16$ for nodes with 16 GB RAM. In order to achieve this we will split our transformation to several nodes so that just a part of the T_J -coefficients have to be imported to the RAM of one node. At this energy also the limit of the many-body calculation code is reached. For $E_{3max} > 14$ the number of m-scheme matrix elements becomes so large, that the eigenvalue problem cannot be solved anymore (depending on the many-body method and on the observed nuclei).

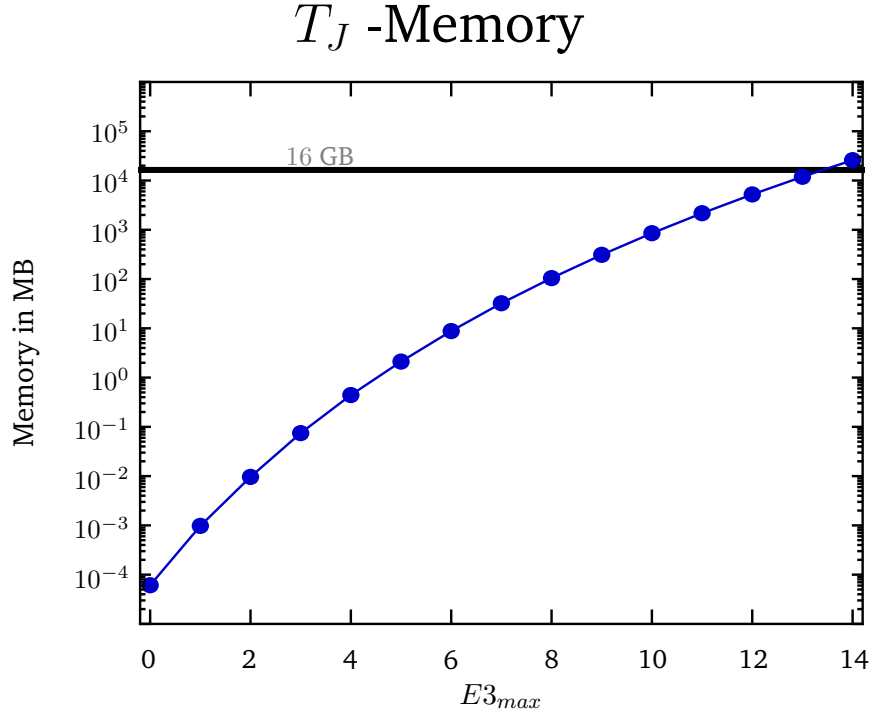


Figure 8: **Memory requirements for the T_J -coefficient:** The figure shows the memory requirements of the nonzero $T_J(a, b, c, \mathcal{J}, l_{cm}, \alpha)$ up to the three-body energy limit $E3_{max}$. To find the right \tilde{T} -coefficient we used a memory scheme where besides T_J also the indices $\mathcal{J}, l_{cm}, \alpha$ are saved. Note that it is a logarithmic plot.

J-Coupled Matrix-Element Memory

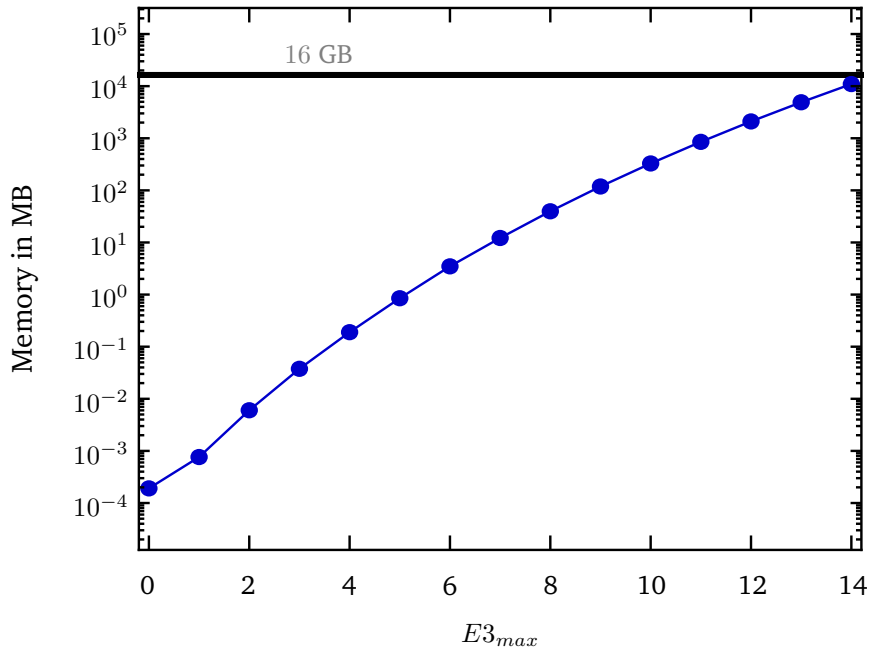


Figure 9: **Memory requirements for the J-coupled m-scheme matrix elements:** *The figure shows the memory requirements of the J-coupled m-scheme interaction matrix elements up to the three-body energy limit $E3_{max}$. The matrix elements are saved in double precision. Note that it is a logarithmic plot.*

5 Similarity renormalization group (SRG)

The topic of this section is the similarity renormalization group (SRG) transformation, which is used to make the χ EFT interaction softer to accelerate the convergence of the many-body calculations. In the first subsection we describe the basic concepts of the SRG, in the second we describe the application of the SRG transformation to the three-body interaction, in the third section we explain the implementation of the SRG evolution and finally in the fourth section we show the impact of the SRG transformation to the form of the Hamilton matrix.

5.1 Basic concepts

Besides the unitary correlation operator method (UCOM) [24] the SRG method provides an alternative way to handle short-range correlations by pre-diagonalization of the interaction in momentum space [25], leading to a phase-shift equivalent potential. As in the UCOM, the basic idea of SRG is to transform an initial Hamiltonian \hat{H}_0 by an unitary transformation

$$\hat{H}_\alpha = \hat{U}_\alpha^\dagger \hat{H}_0 \hat{U}_\alpha, \quad (130)$$

with the α -dependent unitary operator \hat{U}_α . Unitary transformations do not change the spectrum of the Hamiltonian.

In order to obtain a diagonalization of the Hamiltonian \hat{H}_α in a particular basis representation, a renormalization group flow equation [26] is formulated that induces a continuous flow of \hat{H}_α to a diagonal form with increasing flow parameter α . How such a transformation must be structured is shown in the following and also in [27]. The derivative of the Hamiltonian is given by

$$\frac{d\hat{H}_\alpha}{d\alpha} = \frac{d}{d\alpha}(\hat{U}_\alpha^\dagger \hat{H}_0 \hat{U}_\alpha) = \frac{d\hat{U}_\alpha^\dagger}{d\alpha} \hat{H}_0 \hat{U}_\alpha + \hat{U}_\alpha^\dagger \hat{H}_0 \frac{d\hat{U}_\alpha}{d\alpha}, \quad (131)$$

with

$$\hat{U}_\alpha^\dagger \hat{U}_\alpha = \hat{\mathbb{1}} \Rightarrow \frac{d}{d\alpha}(\hat{U}_\alpha^\dagger \hat{U}_\alpha) = 0 \Rightarrow \frac{d}{d\alpha} \hat{U}_\alpha^\dagger = -\hat{U}_\alpha^\dagger \frac{d\hat{U}_\alpha}{d\alpha} \hat{U}_\alpha^\dagger,$$

leading to

$$\frac{d\hat{H}_\alpha}{d\alpha} = -\hat{U}_\alpha^\dagger \frac{d\hat{U}_\alpha}{d\alpha} \hat{U}_\alpha^\dagger \hat{H}_0 \hat{U}_\alpha + \hat{U}_\alpha^\dagger \hat{H}_0 \hat{U}_\alpha \hat{U}_\alpha^\dagger \frac{d\hat{U}_\alpha}{d\alpha}, \quad (132)$$

where we replaced $\frac{d}{d\alpha} \hat{U}_\alpha^\dagger$ in the first term and inserted an identity operator in the second term. Introducing the anti-Hermitian generator $\hat{\eta}_\alpha = -\hat{U}_\alpha^\dagger \frac{d\hat{U}_\alpha}{d\alpha} = -\hat{\eta}_\alpha^\dagger$ one obtains the following initial-value problem

$$\frac{d\hat{H}_\alpha}{d\alpha} = [\hat{\eta}_\alpha, \hat{H}_\alpha], \quad \text{with} \quad \hat{H}_0 = \hat{H}_{\alpha=0}. \quad (133)$$

Generally, one can transform an arbitrary operator \hat{O} by the SRG flow equation

$$\frac{d\hat{O}_\alpha}{d\alpha} = [\hat{\eta}_\alpha, \hat{O}_\alpha], \quad (134)$$

where the generator has the general form $\hat{\eta}_\alpha = [\hat{\xi}, \hat{H}_\alpha]$. We have to keep in mind that the generator $\hat{\eta}_\alpha$ depends on the Hamiltonian \hat{H}_α . Because of this dependence one always has to evolve the Hamiltonian to transform an arbitrary operator. There are various choices for the generator $\hat{\eta}_\alpha$, i.e., for the operator $\hat{\xi}$ entering the generator.

Let us concentrate again on the evolution of the Hamiltonian. The choice of $\hat{\eta}_\alpha$ determines the basis in which the Hamiltonian is pre-diagonalized [28]. In general, for a many-body basis $\{|i\rangle\}$, the generator

$$\hat{\eta}_\alpha = [\text{diag}(\hat{H}_\alpha), \hat{H}_\alpha], \quad \text{with} \quad \text{diag}(\hat{H}_\alpha) = \sum_i |i\rangle \langle i| \hat{H}_\alpha |i\rangle \langle i|, \quad (135)$$

is an evident choice for the diagonalization of the Hamiltonian with respect to the basis $\{|i\rangle\}$.

In the following we use the generator $\hat{\eta}_\alpha = (2\mu)^2 [\hat{T}_{int}, \hat{H}_\alpha]$ with the intrinsic kinetic energy operator

$$\hat{T}_{int} = \hat{T} - \hat{T}_{cm} \quad (136)$$

$$= \frac{1}{2\mu} \hat{q}^2, \quad (137)$$

with the total kinetic energy operator \hat{T} and the center-of-mass kinetic energy operator \hat{T}_{cm} . In Eq. (137) we assume equal proton and neutron masses and thus a reduced nucleon mass $\mu = \frac{m_N}{2}$. In an A -body space the kinetic energy operator for equal proton

and neutron masses is given by

$$\hat{T}_{int} = \frac{1}{A\mu} \sum_{i<j} \hat{q}_{ij}^2, \quad (138)$$

with the relative momentum operator $\hat{q}_{ij} = \frac{\hat{p}_i - \hat{p}_j}{2}$ for the particles i and j .

The flow equation with this generator is given by

$$\frac{d\hat{H}_\alpha}{d\alpha} = [\hat{\eta}_\alpha, \hat{H}_\alpha] = (2\mu)^2 \left([\hat{T}_{int}, \hat{H}_\alpha] \hat{H}_\alpha - \hat{H}_\alpha [\hat{T}_{int}, \hat{H}_\alpha] \right), \quad (139)$$

$$= (2\mu)^2 \left(\hat{T}_{int} \hat{H}_\alpha \hat{H}_\alpha - 2 \cdot \hat{H}_\alpha \hat{T}_{int} \hat{H}_\alpha + \hat{H}_\alpha \hat{H}_\alpha \hat{T}_{int} \right). \quad (140)$$

The occurrence of the intrinsic kinetic energy \hat{T}_{int} in the flow equation leads to a decoupling of the high- and low-momentum parts of the Hamiltonian \hat{H}_α , which causes a softer and more convergent potential [29]. For instance, in two-body space the generator leads to a diagonalization of the Hamiltonian in a LS -coupled relative-momentum basis $\left\{ |q(LS)JM_T M_T\rangle \right\}$. Since we do not plan to use basis states in momentum space, but in harmonic-oscillator space, our generator does not lead to an exact diagonal Hamiltonian, but to a pre-diagonalization through the SRG evolution (see Sec. 5.4). More important is that a SRG transformation slides the effects of the interaction to lower energetic basis spaces. So that we can describe also high-energetic effects in a low-energetic basis space and thus accelerate the convergence behavior with the energy.

5.2 Application to the NN+NNN interaction and subtraction procedure

We apply the SRG transformation to the NN+NNN interaction and discuss the occurring problems. Because we will only deal with operators in this section, we omit the hat notation. First, we consider the initial Hamiltonian H_0 with two- and three-body interactions, which we obtained from chiral effective field theory

$$H_0 = T_0^{int} + V_0^{NN} + V_0^{NNN}. \quad (141)$$

We have to deal with different one-, two- and three-body interaction operators, which also can be SRG transformed, as well as induced interaction contributions. To keep track of the various interaction operators and matrix elements of this section we will introduce

the following notation:

- The index below indicates the kind of interaction and the upper index in squared brackets indicates the “irreducible” n -body contributions of the operator, where n corresponds to the smallest particle number of a basis, which is necessary to represent the operator completely. For instance, the untransformed NN interaction operator $V_{NN}^{[2]}$ has an irreducible two-body part. To denote that the operator is SRG transformed we will use a tilde. In addition we will also deal with matrix elements of an operator, this means an operator in a certain basis representation. To indicate a matrix element we will use angle brackets with an upper index in round brackets denoting the particle number of the representing basis. For instance $\langle \tilde{V}_{NN}^{[3]} \rangle^{(4)}$ are the matrix elements of the irreducible three-body part of the SRG-transformed NN interaction represented in a four-body basis.

Equation (141) in the upper notation reads

$$H^{[2,3]} = T_{int}^{[2]} + V_{NN}^{[2]} + V_{NNN}^{[3]}. \quad (142)$$

One of the challenging features of the SRG is that a transformation of an irreducible n -body interaction $V^{[n]}$ leads to an interaction $\tilde{V}^{[n,n+1,\dots,A]} = \tilde{V}^{[n]} + \tilde{V}^{[n+1]} + \dots$, which contains also irreducible m -body interactions, with $n \leq m \leq A$ [30]. If we apply the SRG transformation to the irreducible two-body part of the interaction we do not just obtain an irreducible two-body part in the SRG-transformed interaction, but also an induced irreducible three-body part. This makes the transformation more complicated, because it is necessary to distinguish between the irreducible two- and three-body parts of our untransformed Hamiltonian (see Appendix A.3).

First of all, we list some basic properties of the SRG transformation, which are necessary to understand our SRG approach:

- As already mentioned a SRG-transformed irreducible n -body interaction contains also irreducible m -body contributions with $n \leq m \leq A$. Note that the irreducible one-body contributions of an operator are invariant under the SRG transformation, but induces irreducible m -body contributions with $2 \leq m \leq A$ [24]. For instance, the SRG transformation of the kinetic energy operator $T^{[1]}$, which is an irreducible one-body operator, yields $\tilde{T}^{[1,2,\dots,A]} = T^{[1]} + \tilde{T}^{[2]} + \tilde{T}^{[3]} + \dots$, where the irreducible one-body contribution $T^{[1]}$ stay unchanged.

- Let us have a look at the SRG-transformed intrinsic kinetic energy operator

$$\begin{aligned}\tilde{T}_{int}^{[2,\dots,A]} &= \tilde{T}_{int}^{[2]} + \tilde{T}_{int}^{[3]} + \tilde{T}_{int}^{[4]} + \dots, \\ &= T_{int}^{[2]} + \left(\tilde{T}_{int}^{[2]} - T_{int}^{[2]}\right) + \tilde{T}_{int}^{[3]} + \tilde{T}_{int}^{[4]} + \dots,\end{aligned}$$

where $T_{int}^{[2]}$ is the untransformed intrinsic kinetic energy operator and $\tilde{T}_{int}^{[k]}$, with $k \geq 2$, are the irreducible k -body parts of the SRG-transformed intrinsic kinetic energy. We point out that $\tilde{T}_{int}^{[2]}$ contains the induced part as well as the SRG-transformed genuine irreducible two-body contributions. For brevity we will absorb the induced terms $\tilde{T}_{int}^{[k]}$, with $k \geq 3$ as well as the term $\left(\tilde{T}_{int}^{[2]} - T_{int}^{[2]}\right)$ in the NN terms of the nucleon interactions.

- To solve the initial-value problem of the flow equation, one has to represent the interaction operators in an appropriate basis and perform the SRG evolution for the individual matrix elements

$$\begin{aligned}\frac{d\langle i|H_\alpha|i'\rangle}{d\alpha} &= (2\mu)^2 \left(\sum_{j,j'} \langle i|T_{int}|j\rangle \langle j|H_\alpha|j'\rangle \langle j'|H_\alpha|i'\rangle \right. \\ &\quad - 2 \cdot \sum_{j,j'} \langle i|H_\alpha|j\rangle \langle j|T_{int}|j'\rangle \langle j'|H_\alpha|i'\rangle \\ &\quad \left. + \sum_{j,j'} \langle i|H_\alpha|j\rangle \langle j|H_\alpha|j'\rangle \langle j'|T_{int}|i'\rangle \right),\end{aligned}\tag{143}$$

where $|i\rangle$ are the n -body basis states.

If one uses a n -body basis, with $n < A$, for this evolution one discards all higher-order interaction than the n -body order.

- By the phrase ‘‘SRG evolution in a n -body basis’’ we mean that during the SRG evolution the operators are represented in a special basis by inserting several identity operators, see Eq. (143). These identity operators should be constructed in an A -body Hilbert space for an A particle system, to consider all induced interaction parts up to the irreducible A -body contribution. The problem is that we cannot insert the complete n -body identity operator $\hat{1} = \sum |i\rangle \langle i|$, because it consists of an infinite number of basis states $|i\rangle$. Therefore, we have to restrict the basis space. For example in the three-body space we use the Jacobi basis states $\{|n_{cm}l_{cm}\rangle \otimes |EiJT\rangle\}^{\mathcal{J}\mathcal{M}\mathcal{J}}$ (see Chapter 4) up to a certain energy quantum num-

ber $E_{3max}^{(SRG)} \geq 2n_{cm} + l_{cm} + E$ and for a two-body space we use the Jacobi basis states up to the energy quantum number $E_{2max}^{(SRG)}$. This limited basis states span the model space. The energy quantum-number limit and the corresponding model space must be large enough, so that the effect of the neglected basis states approximately vanishes. Due to this we have to investigate the convergence of the many-body calculations for interactions SRG transformed in different model spaces. The model space of an A -body basis would be too large to achieve such a convergence, moreover we will only use irreducible two- and three-body interaction contributions for the many-body calculation, therefore, we restrict the SRG evolution to a two- and three-body space.

- To solve the initial-value problem (133) one evolves α (see Sec. 5.3), with a sufficient small step size. In our implementation we use a Runge–Kutta method with an adaptive step size. During every evolution step higher-order interactions are induced and with rising α -parameter these higher-order induced contributions increase [30].
- For a certain energy limit the model space in Jacobi basis is smaller than the model space in the m -scheme basis, therefore, we will perform the SRG transformation in the two- and three-body Jacobi basis.

To construct the SRG-transformed Hamiltonian in a form, where the irreducible two- and three-body contributions are separated

$$\tilde{H}^{[2,3]} = T_{int}^{[2]} + \tilde{V}_{NN}^{[2]} + (\tilde{V}_{NN}^{[3]} + \tilde{V}_{NNN}^{[3]}), \quad (144)$$

one can use the intrinsic kinetic energy operator $T_{int}^{[2]}$ of the initial Hamiltonian, because the corresponding induced terms $\tilde{T}_{int}^{[3]}$ as well as $(\tilde{T}_{int}^{[2]} - T_{int}^{[2]})$ will be absorbed in $\tilde{V}_{NN}^{[2]}$ and $\tilde{V}_{NN}^{[3]}$, respectively, to abbreviate the expression for the transformed Hamiltonian $\tilde{H}^{[2,3]}$.

The irreducible two-body part $\tilde{V}_{NN}^{(2)}$ results from a SRG transformation of the genuine NN interaction in the two-body space, this means one inserts identity operators in a two-body Hilbert space (see Subsec. 5.3.1), which is equivalent to a projection to the two-body space, so that the induced irreducible three-body part is discarded.

The irreducible three-body contributions are more complicated, because they consist of $\tilde{V}_{NN}^{[3]}$ the induced irreducible three-body contribution from the NN interaction, as well as of the genuine three-body interaction, which is SRG transformed in three-body space $\tilde{V}_{NNN}^{[3]}$. First, one considers the initial matrix elements $\langle V_{NN+NNN}^{[2,3]} \rangle^{(3)} := \langle V_{NN}^{[2]} \rangle^{(3)} +$

$\langle \tilde{V}_{NNN}^{[3]} \rangle^{(3)}$ given in a three-body Jacobi basis and perform a SRG transformation in three-body space (see Subsec. 5.3.2), obtaining the matrix elements $\langle \tilde{V}_{NN+NNN}^{[2,3]} \rangle^{(3)} = \langle \tilde{V}_{NN}^{[2]} \rangle^{(3)} + \langle \tilde{V}_{NN}^{[3]} \rangle^{(3)} + \langle \tilde{V}_{NNN}^{[3]} \rangle^{(3)}$. At this point we got the SRG-transformed matrix elements $\langle \tilde{V}_{NN+NNN}^{[2,3]} \rangle^{(3)}$ and $\langle \tilde{V}_{NN}^{[2]} \rangle^{(2)}$ in Jacobi basis representation. In the next step we transform these matrix elements to the m-scheme (or J-coupled scheme see Chapter 4) and convert the two-body m-scheme matrix elements $\langle \tilde{V}_{NN}^{[2]} \rangle^{(2)}$ to $\langle \tilde{V}_{NN}^{[2]} \rangle^{(3)}$ in the three-body m-scheme basis (see Appendix A.2). Next we perform a subtraction of the NN interaction matrix elements from the NN+NNN interaction matrix elements in the three-body m-scheme to obtain the m-scheme matrix elements $\langle \tilde{V}_{NN+NNN}^{[3]} \rangle^{(3)} := \langle \tilde{V}_{NN}^{[3]} \rangle^{(3)} + \langle \tilde{V}_{NNN}^{[3]} \rangle^{(3)}$

$$\begin{aligned} \langle \tilde{V}_{NN+NNN}^{[3]} \rangle^{(3)} &= \langle \tilde{V}_{NN+NNN}^{[2,3]} \rangle^{(3)} - \langle \tilde{V}_{NN}^{[2]} \rangle^{(3)} \\ &= \langle \tilde{V}_{NN}^{[3]} \rangle^{(3)} + \langle \tilde{V}_{NNN}^{[3]} \rangle^{(3)}. \end{aligned} \quad (145)$$

Note that the operator $\tilde{V}_{NN+NNN}^{[3]}$ does not contain an irreducible two-body contribution, but only an irreducible three-body contribution.

Due to the fact that the NN+NNN interaction matrix elements $\langle \tilde{V}_{NN+NNN}^{[3]} \rangle^{(3)}$ of the isospin projection M_T , which is an approximation, also the $\langle \tilde{V}_{NN}^{[2]} \rangle^{(2)}$ matrix elements has to be M_T independent to perform the subtraction consistently. Thus, the $\langle \tilde{V}_{NN}^{[2]} \rangle^{(2)}$ matrix elements for the SRG subtraction and for the many-body calculation will not be the same, because we want to include the isospin projection dependence of the NN interaction (like the Coulomb interaction and the isospin breaking of the strong interaction) in the many-body calculation. In other words we consider the M_T dependence of the irreducible two-body contribution $\tilde{V}_{NN}^{[2]}$, but not of the irreducible three-body contributions $\tilde{V}_{NN}^{[3]}$ and $\tilde{V}_{NNN}^{[3]}$. The consistency is an important issue one has to take account of for the subtraction procedure. For the subtraction the α parameter and the model space for the SRG evolution has to be the same for all involved interactions. Thus, the limits $E_{2max}^{(SRG)}$ and $E_{3max}^{(SRG)}$, for the two- and three-body basis states, have to be equal, and we will call this limit $E_{max}^{(SRG)} := E_{2max}^{(SRG)} = E_{3max}^{(SRG)}$ in the following. Note that the SRG model spaces for the subtraction have to be the same, but the SRG model space, for irreducible two-body interactions used in the many-body calculation, can be chosen much larger.

As outlook we want to mention that the subtraction could also be performed in the Jacobi basis. This also enable to perform a consistent subtraction, if one uses a more flexible model space spanned by basis states with a limited energy quantum number $E_{max}^{(SRG)}(J)$, where the limit depends on the angular momentum J of the intrinsic Jacobi state. Because the effect of a SRG model space part to a certain target state does not

only depend on the energy of the model space part, but also depends on the angular momentum. For instance one would expect that effect of the SRG model space part to the ground state of a light nuclei is basically determined by the basis states with a small angular momentum. Therefore, it is adequate to use a SRG model space with large energy quantum-number limits $E_{max}^{(SRG)}(J)$ for basis states with small angular momentum and decline the limit with increasing angular momentum. These SRG transformations are a budding subject we want to investigate in the future.

5.3 Implementation of the SRG evolution

Now that we have discussed the basic procedure to obtain the SRG matrix elements, we will have a closer look at the implementation of the SRG evolution. As we know from Section 5.2 we have to perform separate calculations, a transformation of $V_{NN}^{[2]}$ with M_T dependence to obtain $\langle \tilde{V}_{NN}^{[2]} \rangle^{(2)}$, a SRG transformation of $V_{NN}^{[2]}$ without M_T dependence for the subtraction and a SRG run with $V_{NN+NNN}^{[2,3]}$. In the following we do not differentiate between the first two runs. Remember that the irreducible two- and three-body contributions from the intrinsic kinetic energy, caused by the SRG transformation, are included in the NN interaction terms.

5.3.1 SRG transformation of $V_{NN}^{[2]}$

We perform the SRG evolution in the two-body Jacobi basis, therefore, the NNN interaction part will not be considered and we use the Hamiltonian $H_\alpha^{[2]} = T_{int}^{[2]} + V_{\alpha,NN}^{[2]}$. The flow equation for $H_\alpha^{[2]}$ is given by

$$\begin{aligned} \frac{dH_\alpha^{[2]}}{d\alpha} &= [\eta_\alpha^{[2]}, H_\alpha^{[2]}] = (2\mu)^2 [[T_{int}^{[2]}, H_\alpha^{[2]}], H_\alpha^{[2]}], \\ &= (2\mu)^2 \left(T_{int}^{[2]} H_\alpha^{[2]} H_\alpha^{[2]} - 2H_\alpha^{[2]} T_{int}^{[2]} H_\alpha^{[2]} + H_\alpha^{[2]} H_\alpha^{[2]} T_{int}^{[2]} \right), \end{aligned} \quad (146)$$

where we skipped the tilde notation and indicate the α dependence directly by the lower index.

A representation of (146) in the model space of the two-body Jacobi basis (see Eq. (143)) leads to some matrix multiplications and additions on the right-hand side. The two-body Jacobi matrix elements of the kinetic energy $\langle T_{int}^{[2]} \rangle^{(2)}$ and the Hamiltonian $\langle H_\alpha^{[2]} \rangle^{(2)}$ are stored to memory so the evaluation of (146) is easy to perform, providing

the matrix elements of the derivative $\left\langle \frac{dH_\alpha^{[2]}}{d\alpha} \right\rangle^{(2)}$. As mentioned before, we use a Runge-Kutta method, but for simplification we will show the procedure with an Euler algorithm to point out the principle. Let us start with the matrix element $\langle H_\alpha^{[2]} \rangle^{(2)}$ of a Hamiltonian evolved to the parameter α . In the Euler algorithm we multiply the matrix element $\left\langle \frac{dH_\alpha^{[2]}}{d\alpha} \right\rangle^{(2)}$ with the step size of α to obtain the change $\Delta \langle H_\alpha^{[2]} \rangle^{(2)}$ of the Hamilton matrix element during one evolution step, this change we can add to the initial Hamilton matrix element $\langle H_\alpha^{[2]} \rangle^{(2)}$ and get the Hamilton matrix element $\langle H_{\alpha+\Delta\alpha}^{[2]} \rangle^{(2)}$ evolved to the parameter $\alpha + \Delta\alpha$

$$\langle H_{\alpha+\Delta\alpha}^{[2]} \rangle^{(2)} = \langle H_\alpha^{[2]} \rangle^{(2)} + \Delta \langle H_\alpha^{[2]} \rangle^{(2)} = \langle H_\alpha^{[2]} \rangle^{(2)} + \left\langle \frac{dH_\alpha^{[2]}}{d\alpha} \right\rangle^{(2)} \Delta\alpha. \quad (147)$$

This can be iterated until the desired α value is reached. It is crucial to realize that, for the SRG evolution of a single Hamilton matrix element $\langle H_\alpha^{[2]} \rangle^{(2)}$, all other Hamilton matrix elements are needed. Therefore, one has to transform all Hamilton matrix elements simultaneously.

Finally we subtract the kinetic energy matrix element $\langle T_{int}^{[2]} \rangle^{(2)}$ from the SRG-transformed Hamilton matrix element $\langle H_\alpha^{[2]} \rangle^{(2)}$ yielding the matrix element $\langle V_{\alpha,NN}^{[2]} \rangle^{(2)}$ of the SRG-transformed NN interaction.

5.3.2 SRG transformation of $V_{NN+NNN}^{[2,3]}$

The SRG evolution of $V_{NN+NNN}^{[2,3]}$ has to be performed in three-body space to take the three-body interaction into account. The corresponding flow equation reads

$$\begin{aligned} \frac{dH_\alpha^{[2,3]}}{d\alpha} &= [\eta_\alpha^{[2,3]}, H_\alpha^{[2,3]}] = (2\mu)^2 [[T_{int}^{[2]}, H_\alpha^{[2,3]}], H_\alpha^{[2,3]}], \\ &= (2\mu)^2 \left(T_{int}^{[2]} H_\alpha^{[2,3]} H_\alpha^{[2,3]} - 2H_\alpha^{[2,3]} T_{int}^{[2]} H_\alpha^{[2,3]} + H_\alpha^{[2,3]} H_\alpha^{[2,3]} T_{int}^{[2]} \right), \end{aligned} \quad (148)$$

with $H_\alpha^{[2,3]} = T_{int}^{[2]} + V_{\alpha,NN+NNN}^{[2,3]} = T_{int}^{[2]} + V_{\alpha,NN}^{[2]} + V_{\alpha,NN}^{[3]} + V_{\alpha,NNN}^{[3]}$.

We can perform the α -evolution in the same way as above, using a model space of a three-body Jacobi basis instead of a two-body Jacobi basis. But the model space size becomes very large in the three-body basis and we cannot perform the SRG evolution of the complete Hamilton matrix due to the limited available memory. This is one of the reasons we perform the SRG transformation for every TJP -block separately (Fig. 10). Owing to the properties of the nuclear interaction, only matrix elements between states with the same total isospin T , angular momentum J and parity P are nonzero, thus the

Hamilton matrix exhibits a block structure in the three-body Jacobi basis representation. A separated SRG evolution of all these TJP -blocks is equivalent to the SRG evolution of the complete Hamilton matrix. After the SRG evolution and the kinetic energy subtraction we obtain the matrix elements $\langle V_{\alpha, NN+NNN}^{[2,3]} \rangle^{(3)}$ containing the genuine two- and three-body interactions, as well as the induced irreducible two- and three-body contributions of the intrinsic kinetic energy and the induced irreducible three-body contribution from the two-body interaction.

$$\langle EiJT|\hat{H}|\tilde{E}\tilde{i}\tilde{J}\tilde{T}\rangle \equiv \left(\begin{array}{c} \boxed{TJP} \\ \boxed{T'J'P'} \\ \boxed{T''J''P''} \\ \boxed{\dots} \end{array} \right)$$

Figure 10: **Representation of the Hamiltonian in antisymmetrized Jacobi basis:** *The Hamiltonian only connects Jacobi states with same total isospin T , angular momentum J and parity P . Thence, the matrix of the Hamiltonian in antisymmetric Jacobi representation exhibits a TJP -block structure.*

5.4 Diagonalization of the interaction matrix

We will investigate the diagonalization properties of the implemented SRG transformation. Therefore, we examine the antisymmetrized three-body Jacobi matrix elements $\langle V_{\alpha, NN+NNN}^{[2,3]} \rangle^{(3)} = \langle EiJT|V_{\alpha, NN+NNN}^{[2,3]}|E'i'JT\rangle$ of the SRG transformed NN+NNN interaction. As mentioned in Subsec. 5.3.2 we can divide the Hamilton matrix into TJP -blocks and perform the SRG transformation separately. The subtraction of the intrinsic kinetic energy matrix from the Hamilton matrix yields the interaction matrix. In Fig. 11 this interaction matrix for the TJP -block, with $T = \frac{1}{2}$, $J = \frac{1}{2}$ and $P = +1$ is illustrated for different SRG evolution parameters α . The states with different energy quantum number E and E' of the bra and ket become decoupled with increasing α parameter. This means that the corresponding absolute value of the matrix elements decreases. The strength of the decoupling grows with the difference between E and E' . This leads to a more diagonal form of the TJP -block. Note that there is no unique choice of the CFPs (see Appendix A.1), thus, there is no unique choice for the antisymmetrized Ja-

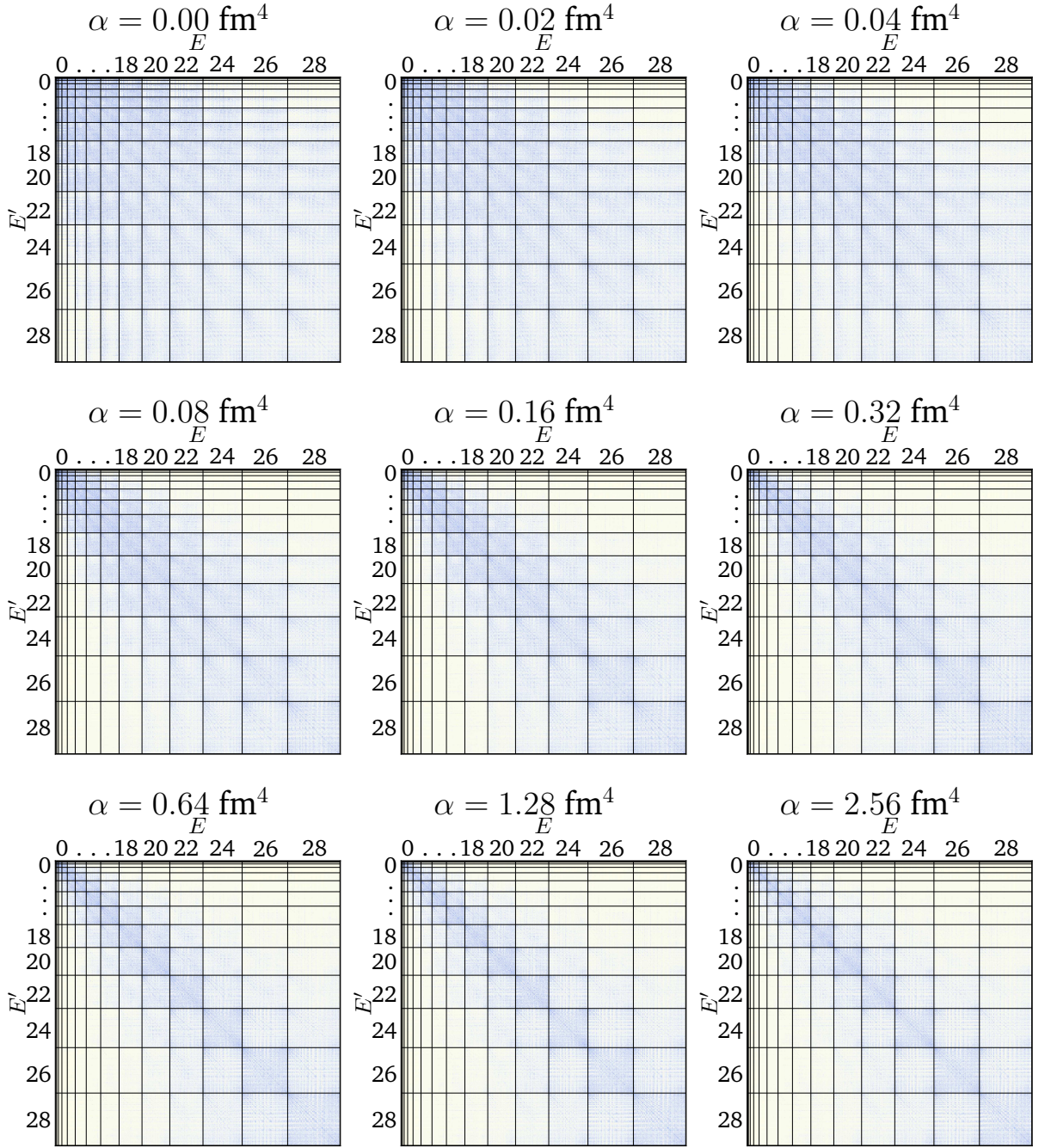


Figure 11: **TJP-block structure through the SRG transformation:** The figure shows the absolute value of the matrix elements $\langle V_{\alpha, NN+NNN}^{[2,3]} \rangle^{(3)} = \langle EiJT | V_{\alpha, NN+NNN}^{[2,3]} | E'i'JT \rangle$ of the NN+NNN interaction in Jacobi basis. The illustrated matrices correspond to the TJP-block with $T = \frac{1}{2}$, $J = \frac{1}{2}$ and $P = +1$, for the SRG parameter $\alpha = 0.00 \text{ fm}^4$, $\alpha = 0.02 \text{ fm}^4$, $\alpha = 0.04 \text{ fm}^4$, $\alpha = 0.08 \text{ fm}^4$, $\alpha = 0.16 \text{ fm}^4$, $\alpha = 0.32 \text{ fm}^4$, $\alpha = 0.64 \text{ fm}^4$, $\alpha = 1.28 \text{ fm}^4$ and $\alpha = 2.56 \text{ fm}^4$. For the SRG transformation a model space corresponding to $E_{max}^{(SRG)} = 28$ is used. The grid lines denote the areas for a given energy quantum number E and E' of the bra and ket Jacobi state, respectively. The more the blue color of a matrix element is saturated the larger is the corresponding absolute value.

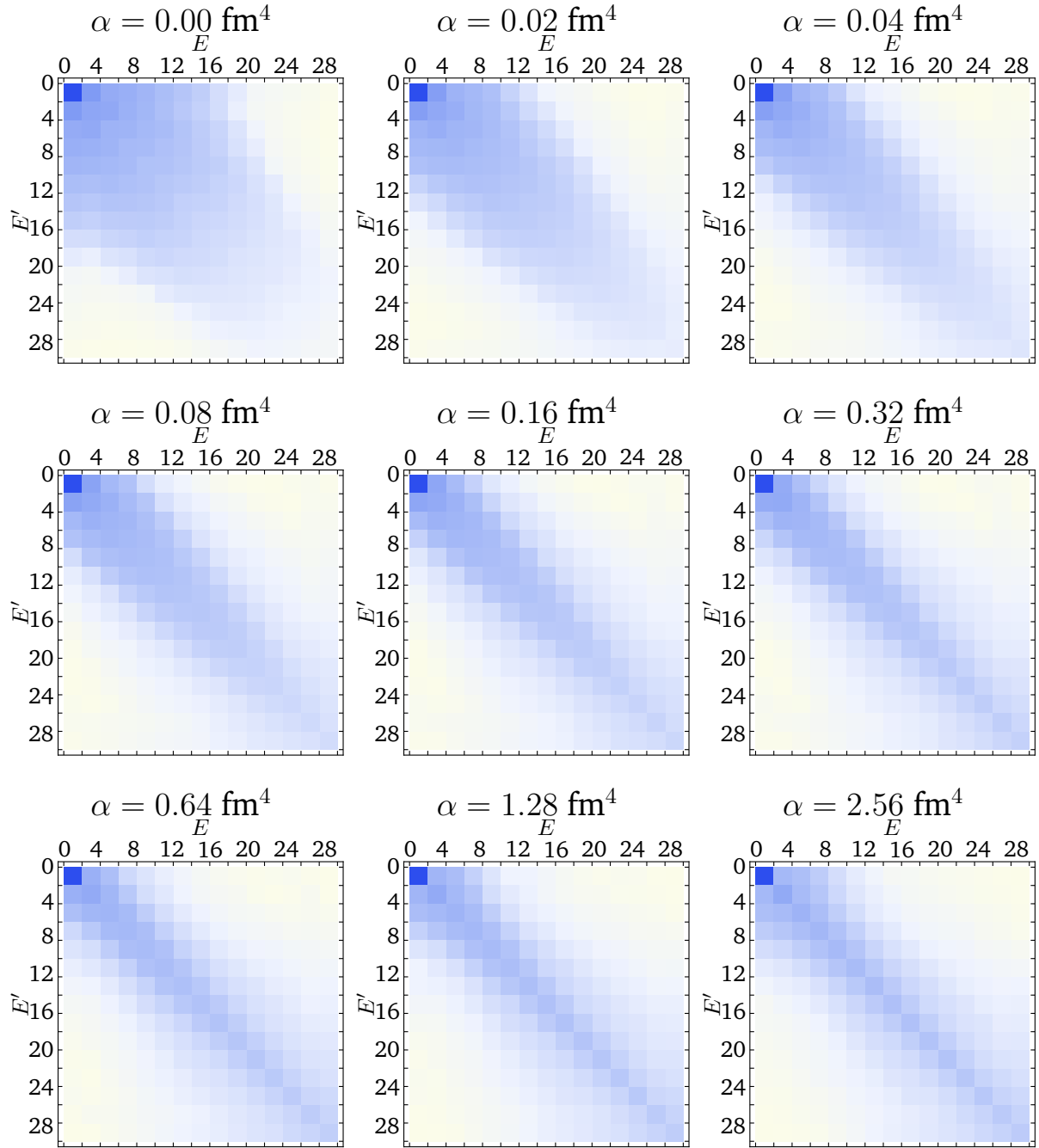


Figure 12: **TJP-block structure through the SRG transformation:** The figure shows the same TJP-block as in Fig. 11 the absolute value of the matrix elements $\langle V_{\alpha, NN+NNN}^{[2,3]} \rangle^{(3)} = \langle EiJT | V_{\alpha, NN+NNN}^{[2,3]} | E'i'JT \rangle$ is now averaged for the E - E' -region. The illustrated matrices correspond to the SRG parameter $\alpha = 0.00 \text{ fm}^4$, $\alpha = 0.02 \text{ fm}^4$, $\alpha = 0.04 \text{ fm}^4$, $\alpha = 0.08 \text{ fm}^4$, $\alpha = 0.16 \text{ fm}^4$, $\alpha = 0.32 \text{ fm}^4$, $\alpha = 0.64 \text{ fm}^4$, $\alpha = 1.28 \text{ fm}^4$ and $\alpha = 2.56 \text{ fm}^4$. The more the blue color of an E - E' -region is saturated the larger is the corresponding averaged absolute value.

cobi basis. Owing to this the matrix elements of an $E-E'$ -region of the TJP -block can show also completely different behavior, depending on the choice of the CFPs. The $E-E'$ -regions correspond to the parts of the TJP -block, where the bra has the energy quantum number E and the ket has the energy quantum number E' . These areas are indicated by the grid lines in Fig. 11. The general properties of the SRG transformation can be observed more adequately, treating the $E-E'$ -regions as a whole. Figure 12 shows the averaged absolute value of the $E-E'$ -areas. As already observed also the averaged absolute values of the $E-E'$ -regions transform to a more diagonal form with increasing α -parameter. In addition we can find that the averaged absolute values for the diagonal $E-E'$ -regions decrease with increasing E . Besides, it seems as if the transformation to a diagonal form slows down after a certain α parameter value. For the finite α parameters we will use in the following the SRG transformation does not provide a complete diagonalization of the interaction matrix elements in the antisymmetrized Jacobi basis, but a pre-diagonalization.

6 Many-body methods

The aim of the different many-body methods employed in this thesis is to solve the eigenvalue problem

$$\hat{H}|\psi_n\rangle = E_n|\psi_n\rangle, \quad (149)$$

derived from the stationary Schrödinger equation, with the many-body Hamilton operator \hat{H} , the n -th eigenstate $|\psi_n\rangle$ and the corresponding energy eigenvalue E_n . The Hamiltonian contains the SRG-transformed NN plus NNN interactions from χ EFT. Before we come to the results (see Chapter 7), we will discuss the basic ideas of the many-body methods used, we point out their range of application, as well as their advantages and disadvantages. The first many-body method is the importance truncated no-core shell model (IT-NCSM), which is an extension of the no-core shell model (NCSM). Both are exact ab initio approaches and will be discussed in Sec. 6.1. The second method we use is the Hartree-Fock method, which is an approximate approach and will be discussed in Sec. 6.2.

6.1 Exact ab initio approaches

Exact ab initio approaches are very important for modern nuclear structure theory. They are necessary to investigate the properties of new interactions and they provide a connection between QCD-based interactions and nuclear structure observables. Moreover, they establish a reference point for approximative methods.

Two methods are particularly successful in describing nuclei up to the mid-p-shell region, the Green's functions Monte Carlo approach (GFMC) [31, 32] and the no-core shell model (NCSM) [17, 33, 34]. First, we want to concentrate on the NCSM to establish a basis for the explanation of the IT-NCSM.

6.1.1 No-core shell model (NCSM)

The NCSM is a special case of a configuration interaction (CI) approach. A conventional CI calculation would use a model space spanned by all Slater determinants build from a finite set of single-particle states. For instance one can use the single-particle states of the harmonic-oscillator up to a maximum energy quantum number e_{max} , where $e = 2n + l$, with the radial quantum number n and the orbital angular momentum l of a harmonic-oscillator single-particle state. In the limit $e_{max} \rightarrow \infty$ one approaches the

exact solution of the eigenvalue problem (149).

In the NCSM the model space is defined in a different way. Also in the NCSM the model space is spanned by Slater determinants $|\phi_\nu\rangle$ consisting of harmonic-oscillator single-particle states, but not every Slater determinant, which can be constructed from a finite set of single-particle states, is used. Instead the NCSM model space is spanned by the Slater determinants up to a certain many-body excitation energy $N_{max}\hbar\Omega$ with respect to the unperturbed Slater determinant $|\phi_0\rangle$. Here, Ω is the frequency associated with the harmonic oscillator basis. The unperturbed Slater determinant consists of the single-particle configurations with the lowest possible energy allowed by the Pauli principle. For illustration of the NCSM model space, we depict an exemplary configuration for a Slater determinant of ^{16}O in Fig. 13. From the unperturbed configuration one proton is excited by $1\hbar\Omega$ from the p-shell ($e = 1$) into the sd-shell ($e = 2$) and one neutron is excited from the s-shell ($e = 0$) by $3\hbar\Omega$, so the whole Slater determinant is excited by $4\hbar\Omega$ and is included in every NCSM model space with $N_{max} \geq 4$. The exact solution of the eigenvalue problem (149) is systematically approached for $N_{max} \rightarrow \infty$.

The NCSM has many advantages that we will discuss now. Due to the special many-body basis truncation and the use of the harmonic-oscillator basis for the single-particle states, the center-of-mass motion separates from the intrinsic motion, which is necessary to obtain translationally invariant intrinsic many-body eigenstates. Furthermore, the variational principle holds. Thus the energy eigenvalues of a NCSM calculation provide an upper bound for the exact solution of (149) for a given Hamiltonian. Moreover, the energy eigenvalues decrease with increasing size of the model space defined by N_{max} . Because the contribution of a many-body configuration to a low-energy state typically decreases with increasing unperturbed excitation energy, the energy eigenvalues converge with N_{max} . The NCSM is applicable for closed as well as open-shell nuclei and treats ground and excited eigenstates at the same footing. Moreover, the NCSM calculation does not only provide the energy eigenvalues E_n , but the eigenstates $|\psi_n\rangle$ as well. The eigenstates are expressed as a superposition of the many-body basis states $|\phi_\nu\rangle$

$$|\psi_n\rangle = \sum_{\nu} C_{\nu}^n |\phi_{\nu}\rangle, \quad (150)$$

where the coefficients C_{ν}^n , determined by the solution of the eigenvalue problem, define the eigenvector. Therefore, in principle every nuclear structure observable of the low-energy states can be extracted.

A disadvantage of the NCSM is the fast growth of the model space size with N_{max} and

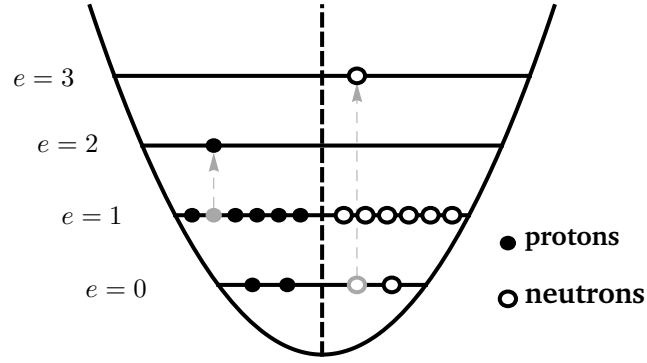


Figure 13: **NCSM model space**: The figure shows an exemplary $4\hbar\Omega$ excited configuration for the protons (disks) and neutrons (circles) of ^{16}O arranged in an harmonic-oscillator potential. The illustrated orbits correspond to an energy quantum number $e = 2n + l$.

with the nucleon number A . Nowadays one can handle model space dimensions up to the order of 10^9 or even 10^{10} with massive parallelization. For a NCSM calculation of ^{16}O in a $N_{max} = 8$ model space the dimension is in the order of 10^9 , but a $8\hbar\Omega$ model space is not sufficient to obtain energy convergence, therefore, the NCSM is limited to mid-p-shell nuclei.

6.1.2 Importance truncated no-core shell model (IT-NCSM)

The importance truncated no-core shell model (IT-NCSM) [35, 36, 37] is based on bases the NCSM and extends the range of applicability to larger model spaces. The NCSM and the full CI method use a global truncation of the many-body basis, which do not account for the specific properties of the Hamiltonian and of the investigated states. As a result the model spaces contain a substantial number of basis states that are irrelevant for the description of the investigated states. The importance truncation scheme uses an additional truncation in order to neglect these irrelevant basis states from the model space, by considering to properties of the Hamiltonian and the target states. Generally the idea of importance selection, pioneered in quantum chemistry in the 1970s, can be applied to any CI method. In nuclear structure theory the application to the NCSM is at the moment the most successful approach.

Let us consider the basic concept of the IT-NCSM. We start with an approximation of the target state, called reference state $|\psi_{ref}\rangle$, carrying the correct quantum numbers of the

target state

$$|\psi_{ref}\rangle = \sum_{\nu \in \mathcal{M}_{ref}} C_{\nu}^{(ref)} |\phi_{\nu}\rangle. \quad (151)$$

The reference state is a superposition of the basis states $|\phi_{\nu}\rangle$ spanning the reference space \mathcal{M}_{ref} , which is a subspace of the $N_{max}\hbar\Omega$ model space $\mathcal{M}_{N_{max}}$ of the NCSM. For instance one can obtain the reference state $|\psi_{ref}\rangle$ from a NCSM calculation in a $2\hbar\Omega$ reference space. The next element is a priori measure for the relevance of the individual basis states $|\phi_{\nu}\rangle$ in $\mathcal{M}_{N_{max}}$, which are not contained in \mathcal{M}_{ref} . Based on the reference state, multi-configuration perturbation theory provides a natural framework for assessing the importance of these basis states. From the amplitudes of first order perturbation to the reference state, one obtains the dimensionless measure of the importance

$$\begin{aligned} \kappa_{\nu} &= -\frac{\langle \phi_{\nu} | \hat{H} | \psi_{ref} \rangle}{\varepsilon_{\nu} - \varepsilon_{ref}}, \\ &= -\sum_{\mu \in \mathcal{M}_{ref}} C_{\mu}^{(ref)} \frac{\langle \phi_{\nu} | \hat{H} | \phi_{\mu} \rangle}{\varepsilon_{\nu} - \varepsilon_{ref}}, \end{aligned} \quad (152)$$

where ε_{ν} can be obtained in the simplest case at the level of the independent particle picture (Møller-Pleset-type formulation). In this formulation we set $\varepsilon_{\nu} := \varepsilon_{ref} + \Delta\varepsilon_{\nu}$, where $\Delta\varepsilon_{\nu}$ corresponds to the excitation energy of $\langle \phi_{\nu} |$ to the unperturbed ground state. Alternatively, in an Epstein-Nesbet partitioning, the energy ε_{ν} is defined by the expectation value of the Hamiltonian

$$\varepsilon_{\nu} = \langle \phi_{\nu} | \hat{H} | \phi_{\nu} \rangle. \quad (153)$$

Although definition (153) appears to be the more natural choice we use the simpler Møller-Pleset-type formulation to obtain the energy ε_{ν} , because the formulation choice has no significant influence on the importance-truncated model space and for our application computational efficiency is the prime concern. Due to implementation reasons we use the SRG-transformed Hamiltonian $\hat{H}_{\alpha}^{[1,2]} = \hat{T}_{int}^{[1]} + \hat{V}_{\alpha,NN}^{[2]}$ for the importance measure in (152), without irreducible three-body contributions. We will discuss this point at the end of the subsection.

Only those basis states with an absolute value of the importance measure $|\kappa_{\nu}|$ larger than a certain threshold $\kappa_{min} \geq 0$ are included in the importance-truncated model space. Due to the importance measure we do not have to solve the eigenvalue problem in the $\mathcal{M}_{N_{max}}$

model space to determine the relevance of the individual basis states, but we are able to estimate the relevance a priori. In the importance-truncated model space we solve the eigenvalue problem. The resulting eigenstate provides a better approximation for the target state and is used as new reference state. With the new reference state one can iterate the previous steps, obtaining again an importance truncated model space and after the eigenvalue solution a better approximation for the target state. This procedure can be iterated until the reference state and energy converge.

In the following we use a sequential construction of the model space, which we will discuss now. Again we start with the first reference state $|\psi_{ref}^{(1)}\rangle$ obtained from a NCSM calculation in a $2\hbar\Omega$ model space as reference space $\mathcal{M}_{ref}^{(1)}$, where the upper index in angle brackets indicate the number of iterations. Next we extend the model space $\mathcal{M}_{ref}^{(1)}$ by $2\hbar\Omega$ excitations and obtain a $4\hbar\Omega$ model space, where we perform an a priori importance selection of the basis states. Note that we use an Hamiltonian with irreducible two- but without three-body contributions, therefore, only basis states $|\phi_\nu\rangle$ which can be produced by 1p1h- and 2p2h-excitations of the basis states in the reference space, have an importance measure $\kappa_\nu \neq 0$ and can be included to the importance truncated model space $\mathcal{M}_{ref}^{(2)}$. In $\mathcal{M}_{ref}^{(2)}$ one can solve the eigenvalue problem obtaining $|\psi_{ref}^{(2)}\rangle$. Again we extend the reference model space $\mathcal{M}_{ref}^{(2)}$ by $2\hbar\Omega$ excitations, obtaining a $6\hbar\Omega$ model space and perform the importance measure with respect to $|\psi_{ref}^{(2)}\rangle$ yielding the new importance truncated model space $\mathcal{M}_{ref}^{(3)}$ and so on. These steps can be sequentially iterated until the $N_{max}\hbar\Omega$ space is reached for which the eigenenergy converges.

The importance threshold κ_{min} has an essential role. For the limit $\kappa_{min} \rightarrow 0$ the importance truncated model space corresponds to the NCSM model space. The aim of the IT-NCSM is to reproduce the results of the full NCSM calculation, therefore, we calculate the eigenenergies or other nuclear structure observables for different importance thresholds κ_{min} and extrapolate the $\kappa_{min} \rightarrow 0$ limit through a polynomial fit of the order 2 – 4. This procedure we will call threshold extrapolation.

In order to perform the IT-NCSM calculation for more than one eigenstate simultaneously, one uses the same steps as explained above with several reference states $|\psi_{ref}^{(i)}\rangle$ simultaneously, where $i = 0, \dots, m$ and m is the number of target states. In this case one has to include a basis state $|\phi_\nu\rangle$ to the importance truncated model space, as soon as $|\kappa_\nu^{(i)}| \geq \kappa_{min}$ holds true for at least one reference state. Thus, the dimension of the importance truncated model space increases with the number of simultaneous target states.

In order to reduce the uncertainties of the extrapolation we will use very small impor-

tance thresholds, with a minimal threshold of $\kappa_{min} = 10^{-5}$. Therefore, even if we use the importance truncation, we still deal with very large model spaces, for example for ^{16}O and $N_{max} = 8$ the dimension of the order 10^9 for NCSM model space decreases to the order of 10^7 for the IT-NCSM model space. Since the resulting eigenvalue problems are still sparse, we will use the Lanczos algorithm to solve them.

Remember that we use a Hamiltonian without irreducible three-body contributions for the importance measure (152), but for the eigenvalue problem (149) we include them. This approximation is reasonable, because the irreducible one- and two-body contributions have a much larger influence to the importance measure than the irreducible three-body contribution of the Hamiltonian. Besides, one can compare the NCSM results with the one of the IT-NCSM to check the used basis truncation.

In conclusion the IT-NCSM facilitates ab initio nuclear structure calculations beyond the domain of the full NCSM, providing the same results [35, 36] where ever the NCSM is applicable. The IT-NCSM extends the range of application to the sd-shell, keeping all the advantages of the NCSM. For instance, there is only a negligible center-of-mass contamination, the calculations provide the eigenstates for a given importance threshold, so one can ascertain other nuclear structure observables by using the threshold-extrapolation technique, and the variational principle holds.

6.2 Hartree-Fock method

In the Hartree-Fock scheme, the many-body state is approximated by a single Slater determinant [23, 38, 39]. In second quantization this Slater determinant for an A -particle system reads

$$|\Phi\rangle = \hat{a}_1^\dagger \hat{a}_2^\dagger \dots \hat{a}_A^\dagger |0\rangle, \quad (154)$$

where $|0\rangle$ is the vacuum state and \hat{a}_k^\dagger are the creation operators of the single-particle states

$$|\alpha_k\rangle = \hat{a}_k^\dagger |0\rangle. \quad (155)$$

The Hartree-Fock single-particle states $|\alpha_k\rangle$ are used as variational degrees of freedom in the minimization of the energy expectation value $E[|\Phi\rangle]$ of the many-body Hamiltonian. In the following we briefly discuss the Hartree-Fock approximation for a Hamiltonian

$\hat{H}^{[1,2,3]} = \hat{T}^{[1]} + \hat{V}^{[2]} + \hat{V}^{[3]}$, with irreducible one-, two- and three-body contributions, in a general basis representation. For a detailed derivation we refer to [40]. The Hartree-Fock single particle states $|\alpha_k\rangle$ are represented in an auxiliary basis $\{|\chi_l\rangle\}$, with the creation operators c_l^\dagger , e.g., the harmonic oscillator basis,

$$|\alpha_k\rangle = \sum_l D_l^{(k)} |\chi_l\rangle \quad \text{or} \quad \hat{a}_k^\dagger = \sum_l D_l^{(k)} \hat{c}_l^\dagger, \quad (156)$$

where the expansion coefficients $D_l^{(k)}$ are used as variational parameters. The idea is to transform the linear many-body eigenvalue problem into a non-linear one-body eigenvalue problem. This is one of the reasons one uses the one-body density matrix operator $\hat{\rho}^{[1]}$ of the Hartree-Fock Slater determinant, with the matrix elements

$$\rho_{ll'}^{[1]} = \langle \chi_l | \hat{\rho}^{[1]} | \chi_{l'} \rangle = \langle \Phi | \hat{c}_{l'}^\dagger \hat{c}_l | \Phi \rangle = \sum_{k, k'} D_l^{(k)} D_{l'}^{(k')*} \langle \Phi | \hat{a}_k^\dagger \hat{a}_k | \Phi \rangle. \quad (157)$$

Due to the fact that the one-body density matrix operator $\hat{\rho}^{[1]}$ is diagonal in the $|\alpha_k\rangle$ -basis representation with the eigenvalue 1 for an occupied state and 0 for an unoccupied state, we obtain

$$\rho_{ll'}^{[1]} = \sum_{k=1}^A D_l^{(k)} D_{l'}^{(k)*}, \quad (158)$$

where we only sum over the k of the occupied states $|\alpha_k\rangle$. The Hamiltonian will be expressed in the auxiliary basis in second quantization

$$\begin{aligned} \hat{H}^{[1,2,3]} &= \sum_{a, a'} t_{aa'}^{[1]} \hat{c}_a^\dagger \hat{c}_{a'} \\ &+ \frac{1}{4} \sum_{a, a'} \sum_{b, b'} V_{ab, a'b'}^{[2]} \hat{c}_a^\dagger \hat{c}_b^\dagger \hat{c}_{b'} \hat{c}_{a'} \\ &+ \frac{1}{36} \sum_{a, a'} \sum_{b, b'} \sum_{c, c'} V_{abc, a'b'c'}^{[3]} \hat{c}_a^\dagger \hat{c}_b^\dagger \hat{c}_c^\dagger \hat{c}_{c'} \hat{c}_{b'} \hat{c}_{a'}, \end{aligned} \quad (159)$$

with the matrix elements

$$t_{aa'}^{[1]} = \langle \chi_a | \hat{T}^{[1]} | \chi_{a'} \rangle, \quad (160)$$

$$V_{ab, a'b'}^{[2]} = a \langle \chi_a \chi_b | \hat{V}^{[2]} | \chi_{a'} \chi_{b'} \rangle_a, \quad (161)$$

$$V_{abc, a'b'c'}^{[3]} = a \langle \chi_a \chi_b \chi_c | \hat{V}^{[3]} | \chi_{a'} \chi_{b'} \chi_{c'} \rangle_a. \quad (162)$$

For the energy expectation value one obtains

$$\begin{aligned}
E[|\Phi\rangle] &= \langle \Phi | \hat{H} | \Phi \rangle \\
&= \sum_{a a'} t_{aa'} \varrho_{aa'}^{[1]} + \frac{1}{4} \sum_{a a'} \sum_{b b'} V_{ab, a'b'}^{[2]} \varrho_{ab, a'b'}^{[2]} \\
&\quad + \frac{1}{36} \sum_{a a'} \sum_{b b'} \sum_{c c'} V_{abc, a'b'c'}^{[3]} \varrho_{abc, a'b'c'}^{[3]}, \tag{163}
\end{aligned}$$

with the two- and three-body density matrix elements $\varrho_{ab, a'b'}^{[2]}$ and $\varrho_{abc, a'b'c'}^{[3]}$.

Owing to the properties of the density operators of a Slater determinant [23, 38, 39, 40], one can reduce the two- and three-body density matrix elements to one-body density matrix elements. From the variational principle one can derive the non-linear one-body eigenvalue problem, using the fact that the one-body density operator of a Slater determinant is Hermitian and idempotent. This non-linear one-body eigenvalue problem is also well known as the Hartree-Fock equation

$$\hat{h}[\varrho^{[1]}] |\alpha_k\rangle = \varepsilon_k |\alpha_k\rangle, \tag{164}$$

where $\hat{h}[\varrho^{[1]}]$ is the density-dependent one-body Hamilton operator given by the matrix elements

$$h_{aa'}[\varrho^{[1]}] = t_{aa'}^{[1]} + \sum_{b b'} V_{ab, a'b'}^{[2]} \varrho_{b, b'}^{[1]} + \frac{1}{2} \sum_{b b'} \sum_{c c'} V_{abc, a'b'c'}^{[3]} \varrho_{b, b'}^{[1]} \varrho_{c, c'}^{[1]}. \tag{165}$$

Representing (164) in the auxiliary basis $\{|\chi_l\rangle\}$, yields

$$\sum_{a'} h_{aa'}[\varrho^{[1]}] D_a^{(k)} = \varepsilon_k D_a^{(k)}. \tag{166}$$

The one-body density matrix elements depend on the Hartree-Fock single-particle states, therefore, we have a non-linear eigenvalue problem for the Hartree-Fock single-particle energies ε_k and the expansion coefficients $D_a^{(k)}$.

Equation (166) is solved in an iterative procedure until full self-consistency is obtained. In practice one starts with a certain guess for the coefficients $D_a^{(k)}$. This coefficients are used to determine the one-body density matrix elements in the one-body Hamiltonian $h_{aa'}[\varrho^{[1]}]$. With a determined one-body Hamiltonian, the Eq. (166) transforms to a linear eigenvalue problem, which can be solved, providing a new set of coefficients $D_a^{(k)}$. This new set of coefficients is used to determine the one-body Hamiltonian again and the

steps described above can be repeated. This procedure will be iterated until the convergence of the coefficients is reached. The coefficients $D_a^{(k)}$ determine the Hartree-Fock single-particle states $|\alpha_k\rangle$. The approximation for the ground state $|\Phi\rangle = |HF\rangle$ is given by a Slater determinant of the A single-particle states $|\alpha_k\rangle$, with the lowest energy. Note that the ground state energy $E[|HF\rangle]$ is not the same as the sum of the single particle energies [23, 38, 39, 40].

Let us summarize the advantages and limitations of the Hartree-Fock approximation. First of all, in the Hartree-Fock scheme the many-body eigenstate is approximated by a single Slater determinant, which is not sufficient to describe the short-range and tensor correlations. Therefore, one has to use an effective interaction, otherwise one obtains unbound ground states for nuclei through the whole nuclear chart [22]. In our case we use the SRG-transformed Hamiltonian $\hat{H}_\alpha^{[2,3]} = \hat{T}_{int}^{[2]} + \hat{V}_{\alpha,NN}^{[2]} + \left(\hat{V}_{\alpha,NN}^{[3]} + \hat{V}_{\alpha,NNN}^{[3]} \right)$, see Chapter 5.

Although we use a Galilei-invariant Hamiltonian, there is the possibility of a center-of-mass excitation, whose contribution to the ground state is expected to be small. However, for the purpose of this thesis, the effect of the center-of-mass contamination on the ground state is irrelevant. A stringent but computationally expensive approach requires an explicit center-of-mass projection, which will not be performed in this thesis.

With the Hartree-Fock scheme we are not limited to light nuclei like for the exact ab initio methods, and are able to investigate ground states of nuclei through the whole nuclear chart (especially closed-shell nuclei). Even if the Hartree-Fock approach does not provide such accurate ground-state energies as the ab initio methods, it is able to illustrate the general systematics, e.g. of the binding energies as function of the mass number. Furthermore, the Hartree-Fock approach provides a variational upper bound for the exact ground-state energy. Finally, the Hartree-Fock solution can serve as a starting point for improved approximations that take the missing correlations into account.

7 Many-body calculation results

In this chapter we present and discuss the results of the many-body calculations with the NSCM and IT-NCSM as well as with the Hartree-Fock approach (see Chapter 6), using the SRG-transformed two- and three-body interaction from χ EFT. To disentangle the effects of the irreducible three-body contributions, we investigate the results of nuclear many-body calculations for irreducible three-body contribution induced during the SRG transformation of the two-body interaction $\hat{V}_{\alpha,NN}^{[3]}$ with and without genuine three-body interaction $\hat{V}_{\alpha,NNN}^{[3]}$ as well as for the pure irreducible two-body interaction $\hat{V}_{\alpha,NN}^{[2]}$. We will use the following notation to identify the various calculations:

- NN-only No genuine NNN interaction and no SRG-induced irreducible three-body contribution ($\hat{H}_{\alpha}^{[2]} = \hat{T}_{int}^{[2]} + \hat{V}_{\alpha,NN}^{[2]}$).
- NN+NNN-induced No genuine NNN interaction, but SRG-induced irreducible three-body contribution ($\hat{H}_{\alpha}^{[2,3]} = \hat{T}_{int}^{[2]} + \hat{V}_{\alpha,NN}^{[2]} + \hat{V}_{\alpha,NN}^{[3]}$).
- NN+NNN-complete Include the genuine NNN interaction as well as the SRG-induced irreducible three-body contribution ($\hat{H}_{\alpha}^{[2,3]} = \hat{T}_{int}^{[2]} + \hat{V}_{\alpha,NN}^{[2]} + \hat{V}_{\alpha,NN}^{[3]} + \hat{V}_{\alpha,NNN}^{[3]}$).

7.1 (IT-)NCSM calculations for ${}^4\text{He}$

We use the NCSM and the IT-NCSM approaches to investigate the interactions defined above, for the ${}^4\text{He}$ nucleus. This nucleus is an ideal candidate for our investigations, because due to the small nucleon number the model spaces are sufficiently small to obtain an energy convergence for the ground-state even with the NCSM, provided that we use a SRG-transformed interaction. For instance, this is relevant to check if the IT-NCSM calculations produce the same results as the NCSM calculations. The following investigations of the ${}^4\text{He}$ ground state will be used to study the sensitivity of the many-body results as a function of the unfixed parameters of the interaction and the many-body calculation. These parameters are the harmonic oscillator frequency, SRG model space as well as the range of the SRG parameter α . The conclusion of this investigations will be used to determine the parameters in the Hartree-Fock calculations (Sec. 7.3).

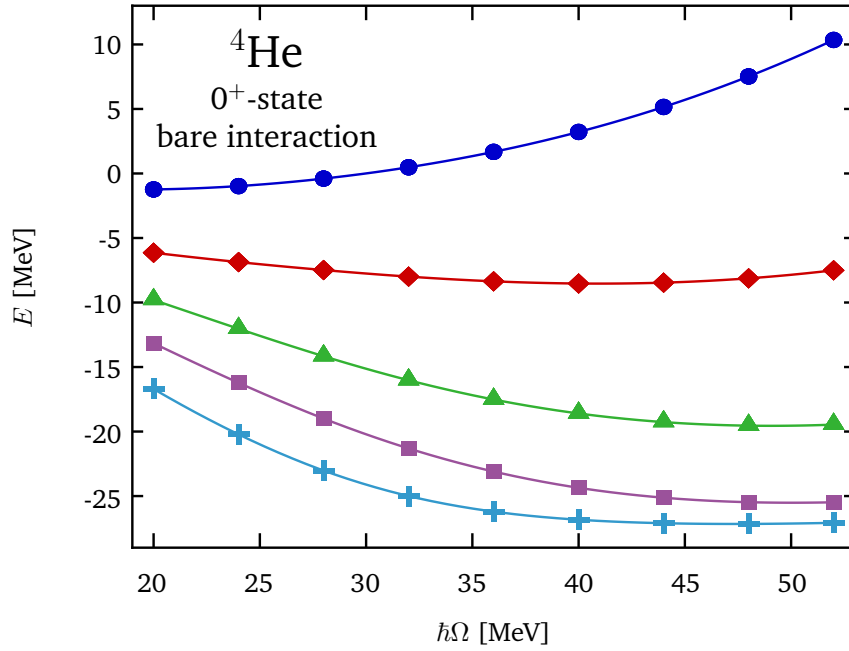


Figure 14: **Frequency dependence of the NN+NNN calculation:** *The figure shows the ${}^4\text{He}$ ground-state energies obtained in NCSM calculations, with the bare NN+NNN interaction, as function of the harmonic oscillator frequency, for different model spaces corresponding to $N_{max} = 2$ (\bullet), $N_{max} = 4$ (\blacklozenge), $N_{max} = 6$ (\blacktriangle), $N_{max} = 8$ (\blacksquare) and $N_{max} = 10$ (\oplus).*

First of all, we discuss the behavior of the ${}^4\text{He}$ ground-state energy for the bare NN+NNN interaction, i.e., without a SRG transformation, as function of the harmonic oscillator frequency, defined by $\hbar\Omega$. In Fig. 14 the corresponding results are shown. With growing NCSM model space, defined by N_{max} , the ground-state energy decreases as expected from the variational principle. Moreover, the energy depends on $\hbar\Omega$. For an exact solution of the eigenvalue problem in an infinite model space the result should be independent of the harmonic oscillator frequency. Generally for the NCSM and IT-NCSM calculations in a finite N_{max} model space there is a minimum in the energy for a certain $\hbar\Omega$. This is seen in Fig. 14, even if the frequency range is sometimes too small. Moreover, the results show that the frequency for the minimal ground-state energy increases with model space and that the frequency dependence flattens out with larger N_{max} . The decrease of the curve for $N_{max} = 10$ shows that the calculations are not yet converged. Therefore, we either have to use a much larger model space or we have to SRG transform the interaction to accelerate the convergence. Because we are limited to three-body matrix elements up to an energy quantum number $E_{3max} = 12$ at the moment (see Sec. 4.6), we can maximally use an ${}^4\text{He}$ many-body model space up to $N_{max} = 12$. This is why we must use SRG-transformed interactions in the following.

Next we analyze whether the model space we use for the SRG transformation is large enough to ensure the convergence of this transformation. As mentioned in Sec. 5.2 we have to check whether the many-body results are invariant for increasing SRG model space. Figure 15 shows a NN+NNN-complete IT-NCSM calculation for the ground-state energy of ${}^4\text{He}$ for two SRG model spaces, which are defined by $E_{max}^{(SRG)}$. In the figures an interaction with $\alpha = 0.08 \text{ fm}^4$ is used. The error bars of the IT-NCSM calculations are caused by the threshold extrapolation (see Sec. 6.1.2). For a harmonic oscillator basis with $\hbar\Omega = 16 \text{ MeV}$ (top left) and $\hbar\Omega = 20 \text{ MeV}$ (top right) there are still significant contributions to the SRG-transformed Hamiltonian from states beyond $E_{max}^{(SRG)} = 28$. These contributions affect the result and lead to a reduction of the ground-state energy. With increasing $\hbar\Omega$ the effect of these high energetic contributions becomes smaller and for $\hbar\Omega = 28 \text{ MeV}$ it approximately vanishes. Moreover, for $E_{max}^{(SRG)} = 32$ and $\hbar\Omega = 16 \text{ MeV}$ the curve converges to an energy several 100 MeV higher than the converged ground-state energies of the other frequencies. This indicates that even an $E_{max}^{(SRG)} = 32$ SRG model space is not sufficient for $\hbar\Omega = 16 \text{ MeV}$ and that larger model spaces are needed to lower the ground-state energy to the same value as for the other frequencies. What we learn from the calculations of Fig. 15 is that the required model space for the SRG transformation depends on the harmonic oscillator frequency and that for small $\hbar\Omega$ larger model

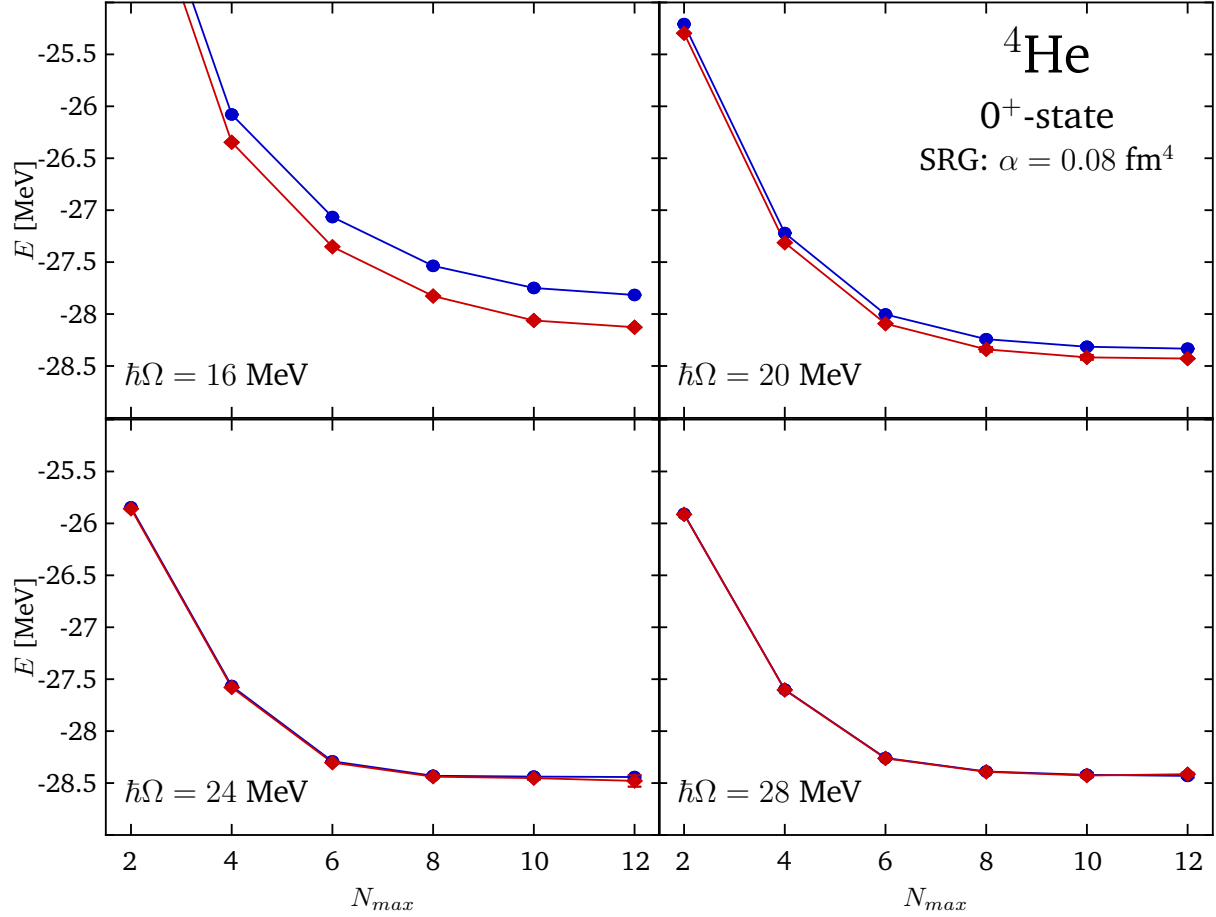


Figure 15: **Ground-state energies for different SRG-model spaces:** The plots show the ${}^4\text{He}$ ground-state energies obtained by the IT-NCSM calculation as function of N_{max} , for a NN+NNN-complete interaction, SRG transformed in an $E_{max}^{(SRG)} = 28$ model space (●) and in an $E_{max}^{(SRG)} = 32$ model space (◆). For the calculations we used a SRG parameter $\alpha = 0.08 \text{ fm}^4$ and the harmonic oscillator frequencies $\hbar\Omega = 16 \text{ MeV}$ (top left), $\hbar\Omega = 20 \text{ MeV}$ (top right), $\hbar\Omega = 24 \text{ MeV}$ (bottom left) and $\hbar\Omega = 28 \text{ MeV}$ (bottom right).

spaces are necessary. We want to point out that for very large $\hbar\Omega$ we expect that the required model space for the SRG transformation increases again, but this topic has to be investigated in the future. Furthermore, there is no guarantee that the influence of $\hbar\Omega$ on the required $E_{max}^{(SRG)}$ is always the same. The relation of these two quantities can depend on the nucleus (see Sec. 7.2) and even on the investigated state or the observable. Therefore, one has to check whether the SRG model space is large enough.

Figure 16 shows the ${}^4\text{He}$ ground-state energy for the NN+NNN-complete IT-NCSM calculation for various α -parameters. The curve for $\alpha = 0.00 \text{ fm}^4$ corresponds to the bare interaction. The energy curves converge in a $N_{max} = 12$ model space for $\alpha \geq 0.02 \text{ fm}^4$, the converged energy of the $\alpha \leq 0.08 \text{ fm}^4$ curves is indicated by the gray dotted line. So even if the ground state energy does not exhibit the fastest convergence for $\hbar\Omega = 28 \text{ MeV}$ with a bare interaction (see Fig. 14), we obtain convergence for the SRG-transformed interaction. The lower plot of Fig. 16 shows the same curves with a closer range about the converged energy. For $\alpha = 0.16 \text{ fm}^4$ and $\alpha = 0.32 \text{ fm}^4$ the converged energies differ from the common converged energy of the other curves (gray dotted line) by about 100 keV. This is due to induced irreducible four-body contributions. With increasing α these obviously repulsive contributions become larger. Note that repulsive contributions lead to a decrease and attractive contributions to an increase of the binding energy. This is a very important observation, because we want to choose α as large as possible to enhance the convergence, as long as the irreducible four-body contribution are negligible. For the ground-state of ${}^4\text{He}$ $\alpha = 0.08 \text{ fm}^4$ is an adequate choice. The calculations of Fig. 16 offer another interesting information, the experimental ground-state energy (black dashed line) is approximately 100 keV higher (less bound) than the converged energy (gray dotted line). This indicates a deficiency in the initial interaction from χEFT . There are various possible reasons for this deviation. For instance we neglect the isospin dependence for the irreducible three-body contributions, but we would not expect that this causes a deviation of 100 keV. What is most likely that the deviation is caused by the missing genuine four-body interaction. Due to the results of the above calculations, we can determine the mentioned parameters for the following calculations. We will use an harmonic oscillator basis with $\hbar\Omega = 28 \text{ MeV}$, a SRG model space corresponding with $E_{max}^{(SRG)} = 28$ and α parameters up to 0.08 fm^4 .

After we have investigated the NN+NNN-complete interaction properties in dependence of the harmonic oscillator frequency, the α parameter as well as the NCSM and SRG model space sizes, we will now examine the influence of the irreducible three-body contributions. Therefore, we first compare the results of the NN-only and NN+NNN-

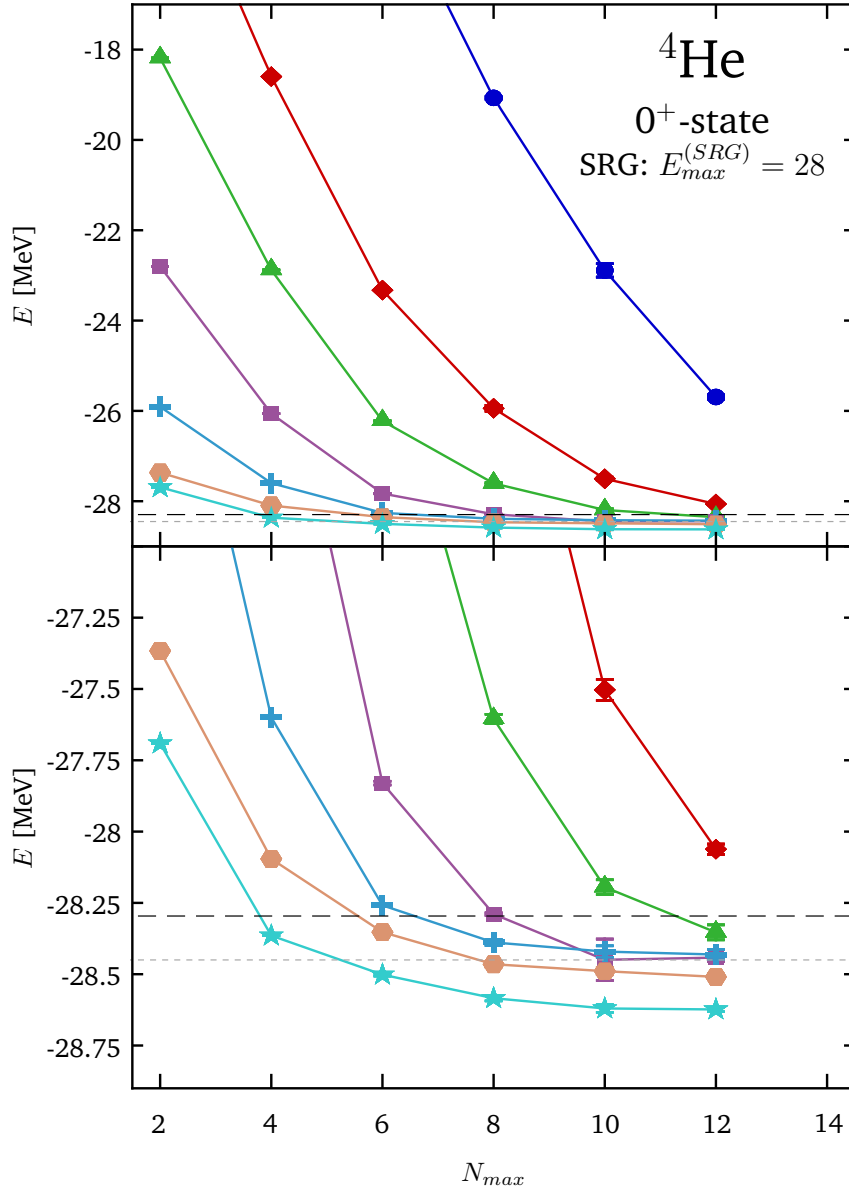


Figure 16: **NN+NNN-complete calculation:** The upper plot shows the ${}^4\text{He}$ ground-state energies obtained by NN+NNN-complete IT-NCSM calculations as function of N_{max} , for the SRG parameter $\alpha = 0.00\text{fm}^4$ (\bullet), $\alpha = 0.01\text{fm}^4$ (\blacklozenge), $\alpha = 0.02\text{fm}^4$ (\blacktriangle), $\alpha = 0.04\text{fm}^4$ (\blacksquare), $\alpha = 0.08\text{fm}^4$ (\blackplus), $\alpha = 0.16\text{fm}^4$ (\blacklozenge) and $\alpha = 0.32\text{fm}^4$ (\blackstar). The dashed black line indicates the experimental value [41] and the gray dotted line corresponds to the converged energy of the curves up to $\alpha = 0.08\text{fm}^4$. In the plot below we see the same curves for a closer range about the converged energy. The interaction is SRG transformed in an $E_{max}^{(SRG)} = 28$ model space and an harmonic oscillator basis with $\hbar\Omega = 28\text{MeV}$ is used.

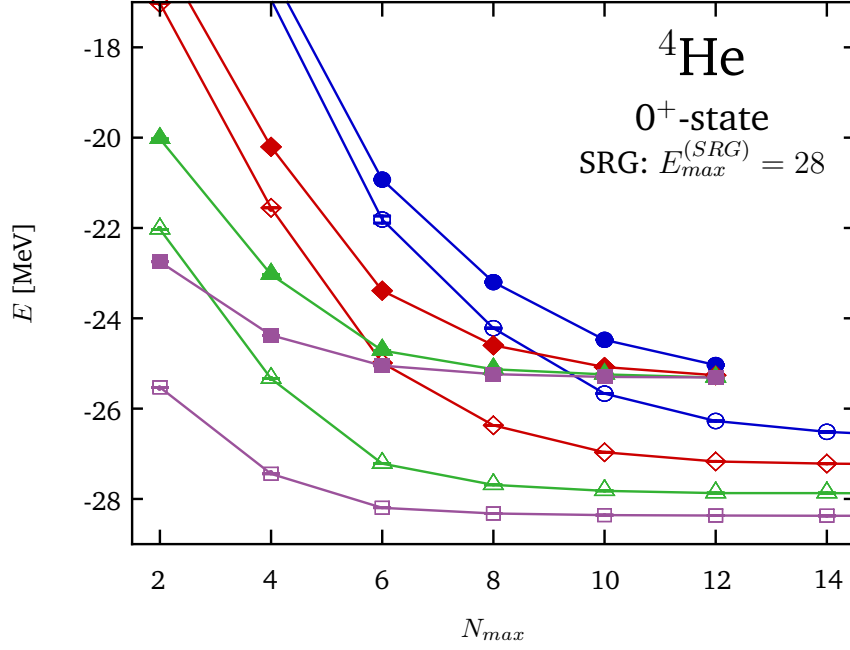


Figure 17: **Comparison of the NN-only with the NN+NNN-induced calculation:** The figure shows the ${}^4\text{He}$ ground-state energies obtained by NN-only (open symbols) and NN+NNN-induced IT-NCSM calculations (solid symbols) as function of N_{max} , for the SRG parameter $\alpha = 0.01 \text{ fm}^4$ (●, ○), $\alpha = 0.02 \text{ fm}^4$ (◆, ◇), $\alpha = 0.04 \text{ fm}^4$ (▲, △) and $\alpha = 0.08 \text{ fm}^4$ (■, □). The interactions are SRG transformed in an $E_{max}^{(SRG)} = 28$ model space and an harmonic oscillator basis with $\hbar\Omega = 28 \text{ MeV}$ is used.

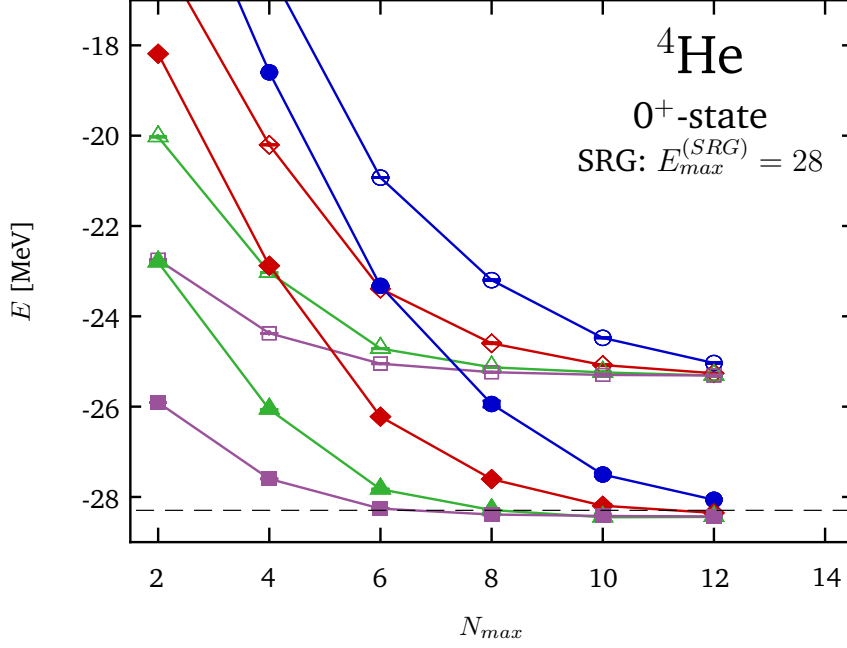


Figure 18: **Comparison of the NN+NNN-complete with the NN+NNN-induced calculation:** The figure shows the ${}^4\text{He}$ ground-state energies obtained by NN+NNN-complete (solid symbols) and NN+NNN-induced (open symbols) IT-NCSM calculations as function of N_{max} , for the SRG parameter $\alpha = 0.01 \text{ fm}^4$ (\bullet, \circ), $\alpha = 0.02 \text{ fm}^4$ (\blacklozenge, \diamond), $\alpha = 0.04 \text{ fm}^4$ ($\blacktriangle, \triangle$) and $\alpha = 0.08 \text{ fm}^4$ (\blacksquare, \square). The interactions are SRG transformed in an $E_{max}^{(SRG)} = 28$ model space and an harmonic oscillator basis with $\hbar\Omega = 28 \text{ MeV}$ is used. The dashed black line indicates the experimental ground state energy [41].

induced IT-NCSM calculations for the ${}^4\text{He}$ ground-state energy, shown in Fig. 17. The NN-only results (open symbols) for the different α parameters do not converge to the same energy. The larger α the lower are the converged energies. This is due to the missing induced contributions, which increase with the α parameter. If one includes the induced three-body interaction (solid symbols) the curves converge to the same energy, which is higher than all the converged energies of the NN-only calculations. The α -independence shows that, it is sufficient to consider only the induced irreducible three-body contribution of the two-body interaction. Note that the induced three-body interaction leads to a shift of the energy curves, but the convergence is not much effected by it. Moreover, the induced three-body contributions are repulsive and with increasing α the repulsiveness enlarges.

Let us consider the role of the genuine three-body interaction. Figure 18 illustrates the NN+NNN-complete (solid symbols) and NN+NNN-induced (open symbols) IT-NCSM

calculation for the ${}^4\text{He}$ ground-state energy. As we already have seen in Figs. 16 and 17 the curves up to $\alpha = 0.08 \text{ fm}^4$ converge to the same energy for the NN+NNN-complete and NN+NNN-induced calculations, respectively. But the converged energy for the NN+NNN-complete interaction is several MeV lower than the one for the NN+NNN-induced interaction. This indicates that the genuine three-body contribution is attractive. Moreover, it seems that the genuine three-body interaction just causes a constant shift of the ground-state energies, without changing the convergence notably.

Finally we compare the results of the NN+NNN-complete and NN-only calculations, illustrated in Fig. 19. The upper plot shows the ${}^4\text{He}$ ground-state energies for the both interactions. Due to the induced and genuine three-body contributions, the curves of the NN-only interaction (open symbols) get shifted. This is shown in the lower plot of Fig. 19, where the NN-only curves (open symbols) are displaced by a constant shift in the way that the NN+NNN-complete and NN-only curves with the same α intersect at $N_{max} = 12$. The two curves with the same α show almost equal convergence behavior. As a consequence the convergence behavior is determined by the irreducible two-body interaction. This is a very interesting property, if this holds true even for other nuclei and states or observables, one could perform the NN-only calculation in a model space with large N_{max} to determine the convergence behavior and ascertain the energy shift, due to the three-body contributions, for a smaller N_{max} , manageable for the irreducible three-body interaction.

7.2 IT-NCSM calculations for ${}^6\text{Li}$

To investigate the influence of the size of the SRG model space with varying harmonic oscillator frequencies, we perform a IT-NCSM calculation with a *NN+NNN-complete* interaction for the ground-state energy of ${}^6\text{Li}$, in analogy to the Helium calculations shown in Fig. 15. We again compare the ${}^6\text{Li}$ ground-state energies of the NN+NNN-complete interaction, SRG transformed in an $E_{max}^{(SRG)} = 28$ and $E_{max}^{(SRG)} = 32$ model space. The results² are summarized in Fig. 20. As in the ${}^4\text{He}$ case the two energy curves differ for $\hbar\Omega = 16 \text{ MeV}$ (top left) and also for $\hbar\Omega = 20 \text{ MeV}$ (top right), which indicates that for these frequencies the effects of the $E_{max}^{(SRG)} \geq 28$ states are not negligible. The two curves corresponding to $E_{max}^{(SRG)} = 28$ (●) and $E_{max}^{(SRG)} = 32$ (◆) for $\hbar\Omega = 24 \text{ MeV}$ (bottom left)

²The actually available three-body matrix elements are limited to an energy quantum number $E_{3max} = 12$ (see Sec. 4.6). Because the unperturbed configuration of ${}^6\text{Li}$ contains two nucleons in the p-shell, the $N_{max} = 10$ model space is the largest NCSM model space we can completely cover, using those matrix elements.

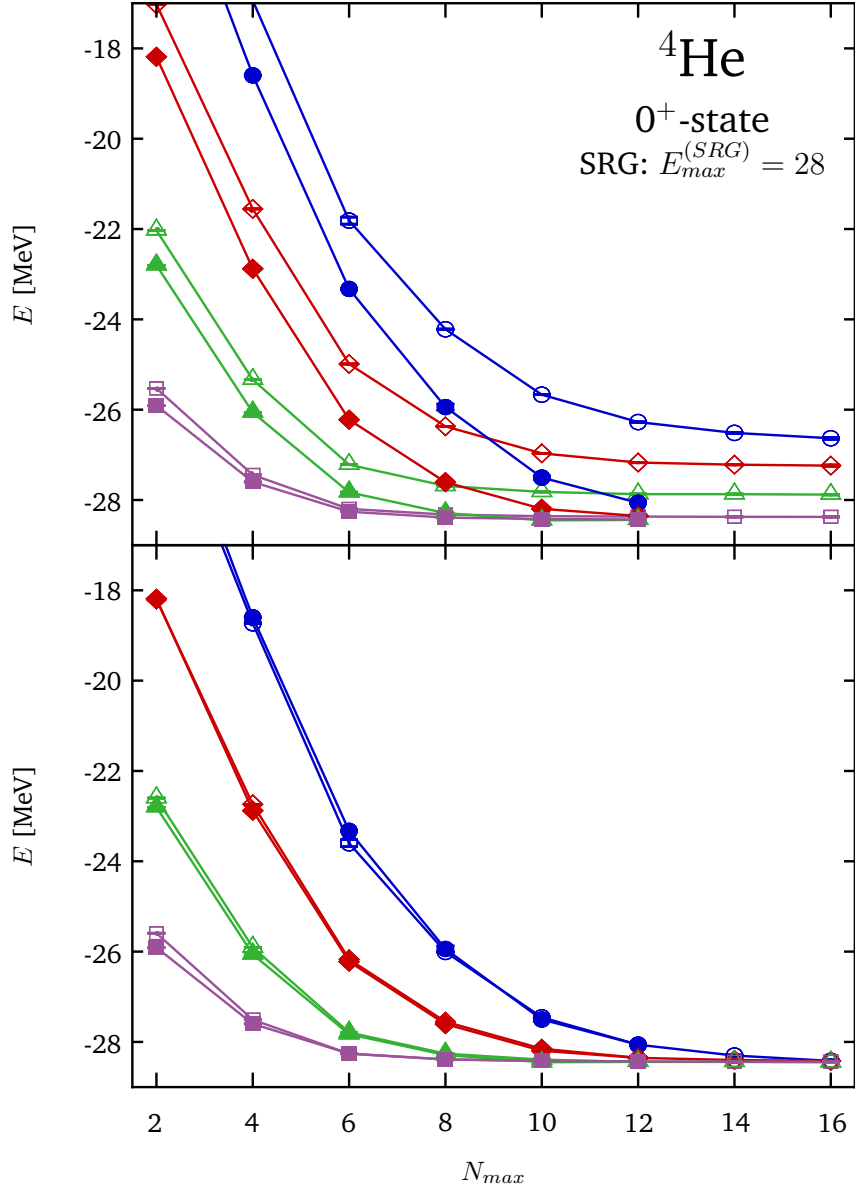


Figure 19: **Comparison of the NN+NNN-complete with the NN-only calculation:** The upper figure shows the ${}^4\text{He}$ ground-state energies obtained by NN+NNN-complete (solid symbols) and NN-only (open symbols) IT-NCSM calculations as function of N_{max} , for the SRG parameter $\alpha = 0.01\text{fm}^4$ (\bullet, \circ), $\alpha = 0.02\text{fm}^4$ (\blacklozenge, \diamond), $\alpha = 0.04\text{fm}^4$ ($\blacktriangle, \triangle$) and $\alpha = 0.08\text{fm}^4$ (\blacksquare, \square). In the figure below the NN-only curves (open symbols) are displaced by a constant shift in the way that the NN+NNN-complete and NN-only curves with the same α intersect at $N_{max} = 12$. This illustration serves to investigate the contribution of the irreducible three-body part to the convergence behavior. The interactions are SRG transformed in an $E_{max}^{(SRG)} = 28$ model space and an harmonic oscillator basis with $\hbar\Omega = 28\text{MeV}$ is used.

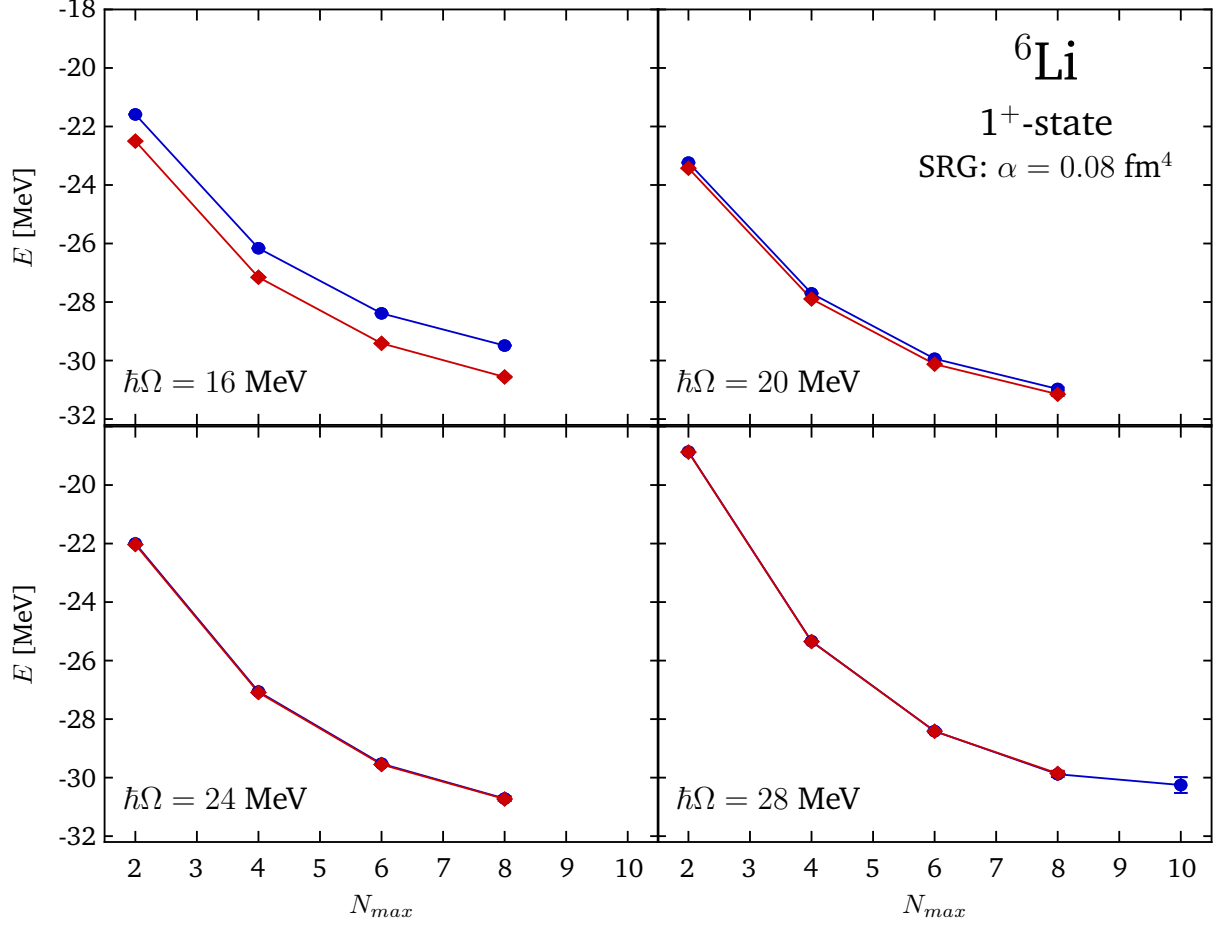


Figure 20: **Ground-state energies for different SRG-model spaces:** The figures show the ${}^6\text{Li}$ ground-state energies obtained by the IT-NCSM calculation as function of N_{max} , for a NN+NNN-complete interaction, SRG transformed in an $E_{max}^{(SRG)} = 28$ model space (\bullet) and in an $E_{max}^{(SRG)} = 32$ model space (\blacklozenge). For the calculations we used the SRG parameter $\alpha = 0.08 \text{ fm}^4$ and the harmonic oscillator frequencies $\hbar\Omega = 16 \text{ MeV}$ (top left), $\hbar\Omega = 20 \text{ MeV}$ (top right), $\hbar\Omega = 24 \text{ MeV}$ (bottom left), and $\hbar\Omega = 28 \text{ MeV}$ (bottom right).

and $\hbar\Omega = 28$ MeV (bottom right) do agree with each other, respectively. This indicates that the $E_{max}^{(SRG)} = 28$ model space is sufficient for the SRG transformation. On closer examination one observes that the curves for $\hbar\Omega = 24$ MeV and for $\hbar\Omega = 28$ MeV show a different convergence behavior. This frequency dependence of the convergence behavior was also illustrated for ${}^4\text{He}$ (Fig. 14). The convergence behavior of the $\hbar\Omega = 24$ MeV curves is improved in comparison to the $\hbar\Omega = 28$ MeV curves and the $\hbar\Omega = 20$ MeV curves converge even faster. It seems as if the frequency, with the fastest convergence, decreases with increasing mass number. Furthermore, it seems that the effect of the high-energy states in the SRG model space is not influenced by the mass number. Of course the available data sets are not sufficient to prove these observations. Therefore, further investigations are required.

7.3 Closed-shell nuclei with the Hartree-Fock method

We will apply the Hartree-Fock method to closed-shell nuclei beyond the p-shell, to investigate the ground-state energies and charge radii. The aim is not to provide precise predictions those observable, but to assess the systematic behavior of our interactions with increasing mass number.

The upper plots in Fig. 21 show the differences of the calculated ground-state energy to the experimental value per nucleon, obtained at the Hartree-Fock level for the NN-only, NN+NNN-induced and NN+NNN-complete Hamiltonians for different α parameters. As mentioned in Sec. 6.2 a calculation with a bare NN and NN+NNN interaction would yield unbound ground states, and the SRG transformation is essential to obtain physical meaningful results. The ground-state energies obtained with SRG-transformed interactions correspond to bound states for all nuclei, indicating that the dominant correlations are indeed introduced very efficiently by the SRG transformation. Let us first concentrate on the ground-state energies for the NN-only calculation (●). For light nuclei the interaction underestimates the binding energies in comparison to experiment. With increasing mass number the ground-state energies drop relative to the experimental values [41]. In contrast the results for the NN+NNN-induced calculation (◆) reproduce the systematics of the ground-state energies very well. The reason is the induced three-body contribution, which is produced during the SRG transformation. As observed in the IT-NCSM calculations (Fig. 17) these induced contributions are repulsive and lead to a decrease of the binding energies. Apparently the importance of the induced three-body contributions for the description of the ground states increases with mass number, this is why the binding energies for the NN-only interaction increase with the mass number

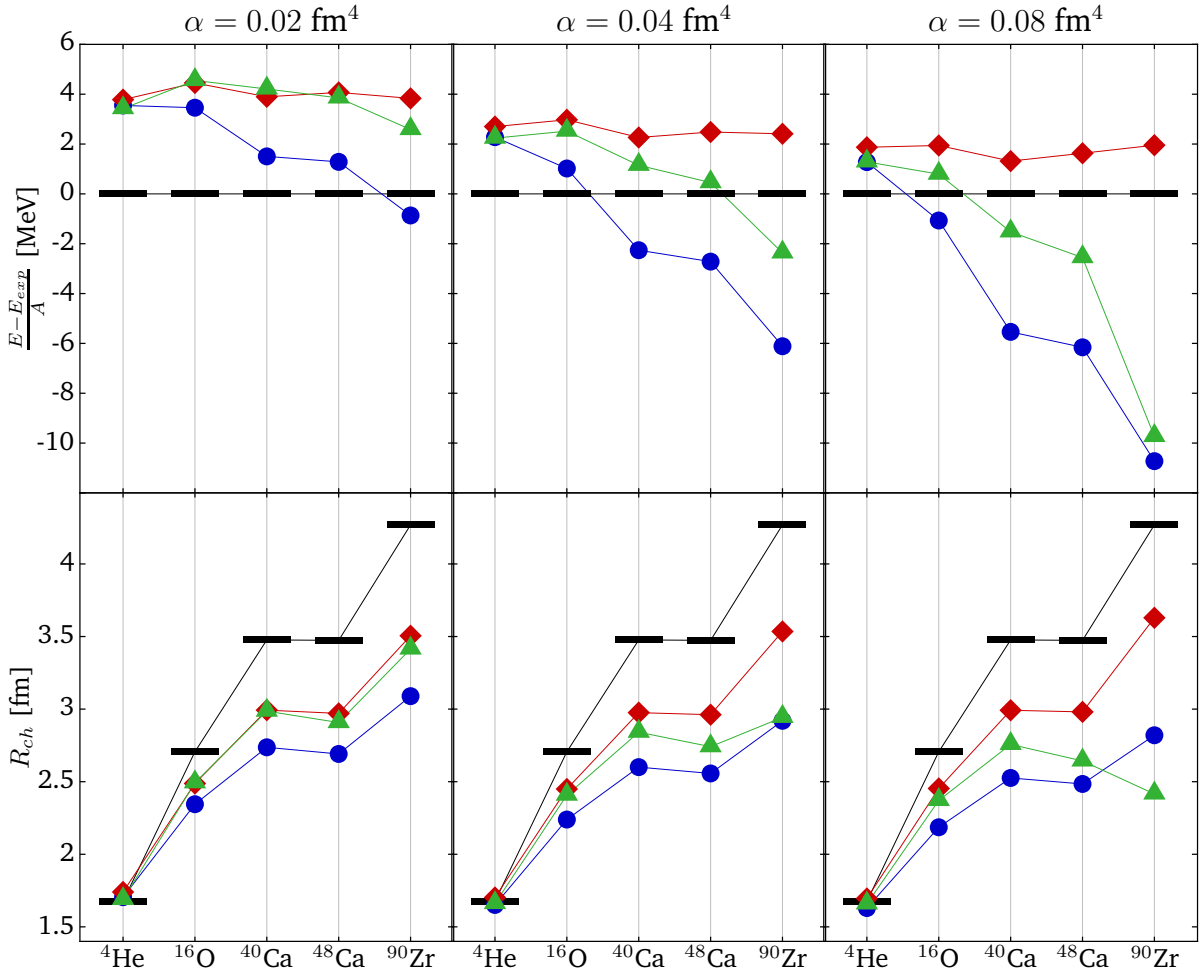


Figure 21: **Investigation of closed-shell nuclei:** Illustrated are the differences of the calculated ground-state energy to the experimental value per nucleon (upper row) and the charge radii (lower row) for a sequence of closed-shell nuclei, obtained by the Hartree-Fock approach. The data sets correspond to the NN-only (●), NN+NNN-induced (◆) and NN+NNN-complete (▲) interactions, which are SRG transformed in an $E_{max}^{(SRG)} = 28$ model space, for $\alpha = 0.02 \text{ fm}^4$ (left column), $\alpha = 0.04 \text{ fm}^4$ (middle column), and $\alpha = 0.08 \text{ fm}^4$ (right column). We use a harmonic oscillator basis with $\hbar\Omega = 28 \text{ MeV}$. For the Hartree-Fock calculation the single-particle states are truncated to an energy quantum number $e_{max} = 14$ and the three-particle states are limited to an energy quantum number $E_{3max} = 12$. The black bars indicate the experimental values [41, 42].

relative to the experimental values. If we increase the SRG parameter α also the induced three-body contributions grow (see Sec. 5.2), therefore, we observe an accelerated drop of the energy differences per nucleon, for increasing α parameter. In conclusion, the information contained in the bare NN interaction is sufficient to describe the general systematics of the ground-state energies, through the nuclear chart. But the Slater determinant used in the Hartree-Fock approach is not able to describe any correlations. That is why we have to apply a SRG transformation to the interaction. To consider the induced irreducible three-body contribution is necessary to describe the general systematics of the ground-state energies. The small α dependence indicates that the induced irreducible m -body contributions with $4 \leq m \leq A$ are insignificant.

We will now include the genuine three-body contributions. The curves for the NN+NNN-complete calculation (\blacktriangle) show a similar trend as the curves of the NN-only calculation but drop less for the light nuclei. With increasing mass number and especially increasing α parameter the drop of the NN+NNN-complete curves is faster than the drop of the NN-only curves. The α dependence indicates that analog to the NN-only calculations the neglected induced irreducible m -body contributions with $4 \leq m \leq A$ are necessary. In addition to this we observe a notable drop in energy from ^{48}Ca to ^{90}Zr for $\alpha = 0.08 \text{ fm}^4$. Unfortunately, the datasets are not sufficient to make a reasonable conclusion, but it seems that the induced higher-order contributions of the genuine NNN interaction become more and more important for increasing mass number and α parameter. Because of analog reasons we would expect that a consideration of the induced four-body contributions of the genuine NNN interaction would again lead to a stabilization of the ground-state energy systematics. The inclusion of four-body contributions would pose an enormous challenge.

An important aspect are the missing correlations in the Hartree-Fock Slater determinant, leading to an underestimated binding energy. The larger the α parameter the less correlations are generated by the interaction. This can also be observed in the upper plots of Fig. 21 by the drop of the ground-state energies with increasing α parameter.

In the three lower plots of Fig. 21 the charge radii of the NN-only, NN+NNN-induced and NN+NNN-complete calculations are shown for different α parameters. The black bars correspond to the experimental charge radii [42]. The charge radii are underestimated for all nuclei but ^4He . Already the NN-only interaction (\bullet) is able to reproduce the pattern of the charge radii and the inclusion of the induced irreducible three-body contribution (\blacklozenge) even enhances the result by increasing the values. With increasing α the charge radii for the NN-only interaction drop, owing to the missing induced three-body

contributions, which become larger with increasing α . For the NN+NNN-induced interaction, in contrast, the charge radii increase with α , what improves the result. Because of the small α dependence of the NN+NNN-induced calculations the consideration of the induced three-body contribution of the two-body interaction is sufficient and the induced m -body contributions with $m \leq 4 \leq A$ can be neglected for the description of the charge-radii at the Hartree-Fock level.

However, the genuine three-body interaction, added in the NN+NNN-complete calculation (▲) reduces the charge radii. For $\alpha = 0.02 \text{ fm}^4$ the effect of the genuine three-body interaction is small and the charge radii approximately correspond to the one of the NN+NNN-induced calculation. But with increasing α the NN+NNN-complete curve drops below the NN+NNN-induced curve. For $\alpha = 0.08 \text{ fm}^4$ the even the pattern cannot be reproduced, due to the massive reduction of the charge radii for the heavy nuclei. Note that for heavy nuclei the radii even decreases with mass number. This observation indicates that the irreducible four-body and higher-order contributions induced by the genuine three-body interaction become very important and the effect of the neglected induced contributions increases with mass number.

In conclusion, the irreducible four-body and higher-order contributions, induced by the genuine three-body interaction, have an important impact on the ground states of heavier nuclei. As long as these contributions are neglected, the NN+NNN-induced calculations produce superior results for the ground-state energies and charge radii. Besides, the induced three-body contribution of the two-body interaction is also crucial for the ground-state charge radii and in particular for the energies.

8 Summary and outlook

In this thesis we apply a SRG-transformed NN+NNN interaction from χ EFT for different nuclear many-body calculations. The two-body part of the initial interaction is obtained at N³LO and the three-body part at N²LO. The corresponding interaction matrix elements are provided in the Jacobi basis. We discussed the SRG transformation of the NN+NNN interaction in the Jacobi basis and investigated the diagonalization properties of the χ EFT interaction through the SRG evolution. For the many-body calculations the interaction matrix elements need to be transformed to an m-scheme representation. Thus, we derive the formulas for the transformation of the interaction matrix elements from the Jacobi basis to m-scheme and implement the transformation in C/C++. We show that a direct transformation to the m-scheme is limited to a model space up to a three-body energy quantum number $E_{3max} = 8$, due to the fast growth of the memory requirement with E_{3max} . In this work we establish a second procedure, where we transform the Jacobi matrix elements to a J -coupled scheme and decouple the matrix elements on-the-fly during the many-body calculations. At the moment the model space of this improved transformation is limited to $E_{3max} = 12$, which is larger than every other m-scheme model space used by a many-body calculation code. For the future we plan to enhance our code by an improved parallelization in order to expand the range of application to a model space corresponding to $E_{3max} = 16$. The enhancement of the model space from $E_{3max} = 8$ to $E_{3max} = 12$ or 16 is crucial to obtain converged results in exact ab initio calculations for nuclei in the p- and sd-shell.

We perform many-body calculations with the NCSM and IT-NCSM for ground-state energies of ⁴He and ⁶Li, using the SRG-transformed interaction from χ EFT. We investigated the influence of the SRG model space and the SRG flow-parameter α to the ground-state energy results and analyzed the effect of the induced and genuine irreducible three-body interactions for ⁴He. In the calculations we observed that the required SRG model space, depends on the harmonic oscillator frequency. In particular for small frequencies in the order of $\hbar\Omega = 16$ MeV the used SRG model space has to be enlarged. In the near future we plan to construct the SRG model space in a more flexible manner, therefore, we will use a maximum energy quantum number $E_{max}^{(SRG)}(J)$ depending on angular momentum. This will enable us to increase $E_{max}^{(SRG)}$ for the relevant angular momenta, while decreasing it for the other angular momenta. In addition we observed that the convergence accelerates with increasing parameter α , but also the induced interaction contributions increase. Thus, one has to find a trade-off between the acceleration of the convergence and the growing induced irreducible four-body contributions which cannot be consid-

ered in the many-body calculations, so far. In this context we aim to study the properties of different SRG generators η_α in order to reduce the induced four-body contributions. Concerning the studies of the irreducible three-body contributions we find that the induced contribution from the genuine two-body interaction is repulsive and leads to an decrease of the ground-state binding energy. The induced irreducible three-body contribution is necessary to obtain the same converged energy for different α parameters, which is not the case for the pure two-body interaction. The genuine three-body interaction is attractive and leads to a ground-state, which is more than 100 keV overbound compared to the experiment. This indicates a deficiency of the initial interaction from χ EFT. The reason could be the absence of the N³LO contribution of the NNN interaction, which has to be compensated by the fit of the LECs c_D and c_E . But more likely is that the discrepancy is caused by the absence of the genuine four-body interaction. In this context one also has to consider the description of the nuclei in the p- and sd-shell. We expect that the discrepancy of the calculated ground-state energies will increase with the mass number. As an outlook we plan to investigate nuclei in the p- and sd-shell and try to determine a different set of LECs to improve their description with the NN+NNN interaction from χ EFT. From the ⁴He ground-state energy calculations we learn that the irreducible three-body contributions do not affect the convergence behavior significantly, but lead to an almost constant shift of the pure two-body results for a range of N_{max} model spaces. We will investigate whether this property also holds for heavier nuclei and other states or observables. In this case one could use the pure two-body interaction in a model space corresponding to N_{max} , which is sufficiently large to obtain the convergence, while the three-body contributions would be considered in a model space with smaller N_{max} . Using such a procedure would enable us to obtain the result for a three-body interaction in a model space, which would not be reachable for a conventional exact ab initio calculation with a three-body interaction.

Finally, we performed Hartree-Fock calculations for a set of closed-shell nuclei, where we investigated the energies and charge radii of the ground states. In conclusion, the repulsive induced three-body contribution from the genuine two-body interaction improves the Hartree-Fock result for both observables. Compared to the experiment the Hartree-Fock ground states are underbound, but the general systematics of the ground-state energies can be reproduced. The charge radii are too small compared to the experiment, but show a similar pattern. The consideration of the genuine three-body interaction leads to a strong overbinding with increasing mass number and α parameter. This seems to be related to induced four-body contributions from the genuine three-body interaction.

As long as we are not able to include four-body interactions, the calculations using a two-body interaction with induced three-body contribution provide better systematics than the calculations with genuine three-body interaction.

In the future we will extend the application of the χ EFT interaction to further nuclei and observables, using also other many-body approaches. In particular the application of many-body perturbation theory will be studied.

A Appendix

A.1 Antisymmetrization in Jacobi basis

In this section we concentrate on the calculation of the coefficients of fractional parentage (CFPs) by diagonalizing the matrix of the antisymmetrizer represented in the Jacobi basis $|\alpha\rangle$. Note that the CFPs are m independent [14], therefore they are identical in the complete and in the intrinsic basis

$$\begin{aligned} c_{\alpha,i} &= \{ \langle n_{cm} l_{cm} | \otimes \langle EiJTM_T | \}^{\mathcal{J}\mathcal{M}\mathcal{J}} \{ |n_{cm} l_{cm}\rangle \otimes |\alpha\rangle \}^{\mathcal{J}\mathcal{M}\mathcal{J}}, \\ &= \langle EiJT|\alpha\rangle. \end{aligned}$$

The major task to compute the CFPs, is to ascertain the matrix elements of the antisymmetrizer in Jacobi basis $\langle \alpha | \hat{\mathcal{A}} | \alpha' \rangle$.

First, we have a look at the Jacobi basis state. As mentioned in Sec. 4.5, $|\alpha\rangle$ is antisymmetric under exchange of the particle 1 and 2. For the formula of the three-body interaction matrix element and especially the T -coefficient (see Sec. 4.5) that does not make a difference, if one has in mind that the $|\alpha\rangle$ state reside in a $1 \leftrightarrow 2$ antisymmetric space. For the implementation of the T -coefficient this has the consequence, that only the T -coefficients are nonzero, which have an even sum of $t_{ab} + s_{ab} + l_{12}$. The antisymmetrizer of particle 1 and 2, has the following definition in three-body space

$$\hat{\mathcal{A}}_{12} = \frac{1}{2!} (\hat{\mathcal{P}}_{123} - \hat{\mathcal{P}}_{213}). \quad (167)$$

If we apply the operator to an antisymmetric state, it will not change the state, since

$$\hat{\mathcal{A}}_{12} \hat{\mathcal{A}} = \hat{\mathcal{A}} \hat{\mathcal{A}}_{12} = \hat{\mathcal{A}}. \quad (168)$$

We will use the special symmetry of the Jacobi state to rewrite the antisymmetrizer in three-body space

$$\hat{\mathcal{A}} = \frac{1}{3!} (\hat{\mathcal{P}}_{123} - \hat{\mathcal{P}}_{213} + \hat{\mathcal{P}}_{231} - \hat{\mathcal{P}}_{132} + \hat{\mathcal{P}}_{312} - \hat{\mathcal{P}}_{321}). \quad (169)$$

Using $\hat{\mathcal{P}}_{ijk} = -\hat{\mathcal{P}}_{jik}$ owing to the antisymmetry of particle 1 and 2 we obtain

$$\begin{aligned} \hat{\mathcal{A}} &= \frac{1}{3} (\hat{\mathcal{P}}_{123} + \hat{\mathcal{P}}_{231} + \hat{\mathcal{P}}_{312}), \\ &= \frac{1}{3} (\hat{\mathbb{1}} + \hat{\mathcal{P}}_{231} + \hat{\mathcal{P}}_{312}). \end{aligned}$$

Expressing the permutation operators by transposition operators yields

$$\hat{\mathcal{A}} = \frac{1}{3}(\hat{\mathbb{1}} + \hat{\tau}_{23}\hat{\tau}_{12} + \hat{\tau}_{12}\hat{\tau}_{23}).$$

Generally the transposition operators do not commute, but in the Jacobi basis $\hat{\tau}_{12} = -1$ and we end with the antisymmetrizer

$$\hat{\mathcal{A}} = \frac{1}{3}(\hat{\mathbb{1}} - 2\hat{\tau}_{23}). \quad (170)$$

Note that (170) holds only in a $1 \leftrightarrow 2$ antisymmetric space. Now we will briefly describe the concept of calculating the matrix elements

$$\begin{aligned} \langle \alpha | \hat{\mathcal{A}} | \alpha' \rangle &= \langle \alpha | \frac{1}{3}(\hat{\mathbb{1}} - 2\hat{\tau}_{23}) | \alpha' \rangle \\ &= \langle [(n_{12}l_{12}, s_{ab})j_{12}, (n_3l_3, s_c)j_3]J, [(t_a t_b)t_{ab}, t_c]T M_T | \frac{1}{3}(\hat{\mathbb{1}} - 2\hat{\tau}_{23}) \\ &\quad \times [(n'_{12}l'_{12}, s'_{ab})j'_{12}, (n'_3l'_3, s'_c)j'_3]J', [(t'_a t'_b)t'_{ab}, t'_c]T' M'_T \rangle. \end{aligned} \quad (171)$$

Since the Jacobi basis is orthonormalized we only have to concentrate on the term with the transposition operator $\hat{\tau}_{23}$. In order to apply $\hat{\tau}_{23}$ to a state we decouple the space,

spin and isospin part, obtaining

$$\begin{aligned}
& \langle [(n_{12}l_{12}, s_{ab})j_{12}, (n_3l_3, s_c)j_3]J, [(t_a t_b)t_{ab}, t_c]TM_T | \hat{\tau}_{23} \rangle \\
& \times | [(n'_{12}l'_{12}, s'_{ab})j'_{12}, (n'_3l'_3, s'_c)j'_3]J', [(t'_a t'_b)t'_{ab}, t'_c]T'M'_T \rangle \\
& = \sum_{LS} \sum_{L'S'} \sum_{M_L M_S} \sum_{M'_L M'_S} \hat{j}_{12} \hat{j}'_{12} \hat{L} \hat{L}' \hat{S} \hat{S}' \hat{j}_3 \hat{j}'_3 \\
& \times \begin{Bmatrix} l_{12} & s_{ab} & j_{12} \\ l_3 & s_c & j_3 \\ L & S & J \end{Bmatrix} \begin{Bmatrix} l'_{12} & s'_{ab} & j'_{12} \\ l'_3 & s'_c & j'_3 \\ L' & S' & J' \end{Bmatrix} c \begin{pmatrix} L & S & J \\ M_L & M_S & M_J \end{pmatrix} c \begin{pmatrix} L' & S' & J' \\ M'_L & M'_S & M'_J \end{pmatrix} \\
& \times \langle (n_{12}l_{12}, n_3l_3)LM_L | \hat{\tau}_{23} | (n'_{12}l'_{12}, n'_3l'_3)L'M'_L \rangle \\
& \times \langle (s_{ab}, s_c)SM_S | \hat{\tau}_{23} | (s'_{ab}, s'_c)S'M'_S \rangle \\
& \times \langle (t_{ab}, t_c)TM_T | \hat{\tau}_{23} | (t'_{ab}, t'_c)T'M'_T \rangle .
\end{aligned} \tag{172}$$

The spin $\langle (s_{ab}, s_c)SM_S | \hat{\tau}_{23} | (s'_{ab}, s'_c)S'M'_S \rangle$ and isospin part $\langle (t_{ab}, t_c)TM_T | \hat{\tau}_{23} | (t'_{ab}, t'_c)T'M'_T \rangle$ have the same form in (172), therefore it is adequate to consider only one of these parts and the space part $\langle (n_{12}l_{12}, n_3l_3)LM_L | \hat{\tau}_{23} | (n'_{12}l'_{12}, n'_3l'_3)L'M'_L \rangle$.

However, we will just present the results, see [43] for a detailed derivation

$$\begin{aligned}
\text{Spin:} \quad & \langle (s_{ab}, s_c) S M_S | \hat{\tau}_{23} | (s'_{ab}, s'_c) S' M'_S \rangle \\
& = \delta_{SS'} \delta_{M_S M'_S} (-1)^{1+s_{ab}+s'_{ab}} \hat{s}_{ab} \hat{s}'_{ab} \begin{Bmatrix} s'_b & s'_a & s_{ab} \\ s'_c & S' & s'_{ab} \end{Bmatrix}.
\end{aligned}$$

$$\begin{aligned}
\text{Isospin:} \quad & \langle (t_{ab}, t_c) T M_T | \hat{\tau}_{23} | (t'_{ab}, t'_c) T' M'_T \rangle \\
& = \delta_{TT'} \delta_{M_T M'_T} (-1)^{1+t_{ab}+t'_{ab}} \hat{t}_{ab} \hat{t}'_{ab} \begin{Bmatrix} t'_b & t'_a & t_{ab} \\ t'_c & T' & t'_{ab} \end{Bmatrix}.
\end{aligned}$$

$$\begin{aligned}
\text{Space:} \quad & \langle (n_{12} l_{12}, n_3 l_3) L M_L | \hat{\tau}_{23} | (n'_{12} l'_{12}, n'_3 l'_3) L' M'_L \rangle \\
& = \delta_{LL'} \delta_{M_L M'_L} \delta_{2n_{12}+l_{12}+2n_3+l_3, 2n'_{12}+l'_{12}+2n'_3+l'_3} \\
& \times \langle \langle 2n_{12} l_{12}, 2n_3 l_3 | 2n'_{12} l'_{12}, 2n'_3 l'_3; L \rangle \rangle_{\frac{1}{3}}.
\end{aligned}$$

With all this formulas we are able to calculate the matrix of the antisymmetrizer in Jacobi representation yielding the block matrix illustrated in Fig. 22. The last task is to diagonalize the block matrix, which can be performed by diagonalizing every single block separately. This operation provides the CFPs defining the antisymmetric Jacobi states

$$|EiJT\rangle = \sum_{\alpha} c_{\alpha,i} |\alpha\rangle, \tag{173}$$

where the states $|\alpha\rangle$ must have the same quantum numbers $E = 2n_{12} + l_{12} + 2n_3 + l_3$, J and T . Have in mind that there are several diagonalization methods leading to different results for the CFPs.

For our implementation of the transformation code (Sec. (4.6)) we need to know the number of antisymmetric Jacobi states for the given quantum numbers E, J, T . This number is equal to the trace of an EJT -Block of the antisymmetrizer.

$$\langle \alpha | \hat{A} | \tilde{\alpha} \rangle = \begin{pmatrix} \boxed{EJT} & & & \\ & \boxed{E'J'T'} & & \\ & & \boxed{E''J''T''} & \\ & & & \boxed{\ddots} \end{pmatrix}$$

Figure 22: **Representation of the antisymmetrizer in Jacobi basis:** The antisymmetrizer only connects Jacobi states with same E, J, T , where $E = n_{12} + l_{12} + n_3 + l_3$ is the energy quantum number of the intrinsic Jacobi state. Thence the matrix of the antisymmetrizer in Jacobi representation, exhibit a EJT -block structure.

A.2 Conversion of two-body to three-body m-scheme matrix elements

In this chapter we want to calculate the three-body m-scheme matrix elements ${}_a \langle \psi^{(3)} | \hat{V}_{NN} | \psi'^{(3)} \rangle_a$ of an irreducible two-body interaction \hat{V}_{NN} by using the two-body m-scheme matrix elements ${}_a \langle \psi^{(2)} | \hat{V}_{NN} | \psi'^{(2)} \rangle_a$ of this interactions, with the k -body m-scheme state

$$|\psi^{(k)}\rangle_a = \frac{1}{\sqrt{k!}} \sum_{\mathcal{P}} (-1)^P \hat{\mathcal{P}} \{ |\alpha_1\rangle \otimes \dots \otimes |\alpha_k\rangle \} = |\alpha_1 \dots \alpha_k\rangle_a, \quad (174)$$

where P is the signature of the permutation operator $\hat{\mathcal{P}}$. In doing so we have to distinguish between three cases depending on the number of different single-particle states $|\alpha_i\rangle$ in the three-body m-scheme states $|\psi'^{(3)}\rangle_a$ and $|\psi^{(3)}\rangle_a$.

First case: Equal three-body states

The three-body matrix elements of the irreducible two-body interaction is given by

$${}_a \langle \psi^{(3)} | \hat{V}_{NN} | \psi^{(3)} \rangle_a = {}_a \langle \psi^{(3)} | \sum_{i < j} \hat{V}_{ij} | \psi^{(3)} \rangle_a = 3 {}_a \langle \psi^{(3)} | \hat{V}_{12} | \psi^{(3)} \rangle_a, \quad (175)$$

where we used the antisymmetry of the m-scheme state. The operator \hat{V}_{ij} acts like the irreducible two-body operator \hat{V}_{NN} in the two-body space of particle i and j and as an identity operator in the other particle spaces. Inserting the antisymmetric three-body

state in (175), yields

$$\begin{aligned}
{}_a\langle\psi^{(3)}|\hat{V}_{NN}|\psi^{(3)}\rangle_a &= 3 \cdot \frac{1}{3!} \left\{ \sum_{\mathcal{P}} (-1)^P \hat{\mathcal{P}} \langle\alpha_1\alpha_2\alpha_3| \right\} \hat{V}_{12} \left\{ \sum_{\mathcal{P}} (-1)^P \hat{\mathcal{P}} |\alpha_1\alpha_2\alpha_3\rangle \right\}, \\
&= \frac{1}{2} \sum_{i<j} (\langle\alpha_i\alpha_j| - \langle\alpha_j\alpha_i|) \hat{V}_{NN} (|\alpha_i\alpha_j\rangle - |\alpha_j\alpha_i\rangle), \\
&= \sum_{i<j} {}_a\langle\alpha_i\alpha_j|\hat{V}_{NN}|\alpha_i\alpha_j\rangle_a. \tag{176}
\end{aligned}$$

From the first to the second line we used the property of the orthonormalized single-particle basis. So we expressed the three-body matrix elements by the two-body matrix elements ${}_a\langle\alpha_i\alpha_j|\hat{V}_{NN}|\alpha_i\alpha_j\rangle_a$ for the first case.

Second case: One different single-particle state

We have a look at the matrix elements of the three-body states $|\psi^{(3)}\rangle = |\alpha_1\alpha_2\alpha_3\rangle$ and $|\psi'^{(3)}\rangle = |\alpha'_1\alpha_2\alpha_3\rangle$

$$\begin{aligned}
{}_a\langle\psi^{(3)}|\hat{V}_{NN}|\psi'^{(3)}\rangle_a &= {}_a\langle\psi^{(3)}|\sum_{i<j} \hat{V}_{ij}|\psi'^{(3)}\rangle_a, \\
&= 3 \cdot \frac{1}{3!} \left\{ \sum_{\mathcal{P}} (-1)^P \hat{\mathcal{P}} \langle\alpha_1\alpha_2\alpha_3| \right\} \hat{V}_{12} \left\{ \sum_{\mathcal{P}} (-1)^P \hat{\mathcal{P}} |\alpha'_1\alpha_2\alpha_3\rangle \right\} \\
&= \frac{1}{2} \sum_{i=2}^3 (\langle\alpha_1\alpha_i| - \langle\alpha_i\alpha_1|) \hat{V}_{NN} (|\alpha'_1\alpha_i\rangle - |\alpha_i\alpha'_1\rangle) \\
&= \sum_{i=2}^2 {}_a\langle\alpha_1\alpha_i|\hat{V}_{NN}|\alpha'_1\alpha_i\rangle_a. \tag{177}
\end{aligned}$$

Note that there is only the sum over i , $|\alpha_1\rangle$ and $|\alpha'_1\rangle$ are the different single-particle states of the both three-body states.

Third case: Two different single-particle states

Using analogous steps as above, the matrix elements of the three-body states $|\psi^{(3)}\rangle = |\alpha_1\alpha_2\alpha_3\rangle$ and $|\psi'^{(3)}\rangle = |\alpha'_1\alpha'_2\alpha_3\rangle$ reads

$${}_a\langle\psi^{(3)}|\hat{V}_{NN}|\psi'^{(3)}\rangle_a = {}_a\langle\alpha_1\alpha_2|\hat{V}_{NN}|\alpha'_1\alpha'_2\rangle_a. \tag{178}$$

There is no fourth case, because the three-body matrix elements of an irreducible two-body interaction, are zero for three different single-particle states in the bra and ket, due to the orthogonality of the single particle basis.

A.3 NN+NNN interactions in four-body basis

We point out why it is necessary to distinguish between the NN and NNN interaction instead of using the three-body matrix elements of a NN+NNN SRG-transformed interaction without a distinction. We use the notation introduced in Sec. 5.2.

For a nucleus with $A = 3$ nucleons, that would be a right choice. But if we investigate a nuclei with more nucleons, e.g. a nucleus with $A = 4$, we have to perform a cluster expansion to construct four-body matrix elements out of the NN+NNN matrix elements. To do this we have to treat the NN and NNN matrix elements in a different way. To get the four-body matrix elements out of the NN matrix elements one has to sum up the permuted two-body matrix elements

$$\langle V_{NN}^{[2]} \rangle^{(4)} = \langle V_{NN}^{[2]} \rangle_{12}^{(2)} + \langle V_{NN}^{[2]} \rangle_{13}^{(2)} + \langle V_{NN}^{[2]} \rangle_{14}^{(2)} + \langle V_{NN}^{[2]} \rangle_{23}^{(2)} + \langle V_{NN}^{[2]} \rangle_{24}^{(2)} + \langle V_{NN}^{[2]} \rangle_{34}^{(2)}, \quad (179)$$

where $\langle V_{NN}^{[2]} \rangle_{ij}^{(2)}$ means the NN interaction operator applied in the two-body space of particle i and j (analog for the three-body matrix elements). The NNN interaction matrix elements in four-body space are given as

$$\langle V_{NNN}^{[3]} \rangle^{(4)} = \langle V_{NNN}^{[3]} \rangle_{123}^{(3)} + \langle V_{NNN}^{[3]} \rangle_{124}^{(3)} + \langle V_{NNN}^{[3]} \rangle_{134}^{(3)} + \langle V_{NNN}^{[3]} \rangle_{234}^{(3)}, \quad (180)$$

yielding the NN+NNN interaction in the four-body space

$$\begin{aligned} \langle V_{NN+NNN}^{[2,3]} \rangle^{(4)} &= \langle V_{NN}^{[2]} \rangle^{(4)} + \langle V_{NNN}^{[3]} \rangle^{(4)} \\ &= \langle V_{NN}^{[2]} \rangle_{12}^{(2)} + \langle V_{NN}^{[2]} \rangle_{13}^{(2)} + \langle V_{NN}^{[2]} \rangle_{14}^{(2)} + \langle V_{NN}^{[2]} \rangle_{23}^{(2)} \\ &\quad + \langle V_{NN}^{[2]} \rangle_{24}^{(2)} + \langle V_{NN}^{[2]} \rangle_{34}^{(2)} \\ &\quad + \langle V_{NNN}^{[3]} \rangle_{123}^{(3)} + \langle V_{NNN}^{[3]} \rangle_{124}^{(3)} + \langle V_{NNN}^{[3]} \rangle_{134}^{(3)} + \langle V_{NNN}^{[3]} \rangle_{234}^{(3)}. \end{aligned} \quad (181)$$

Let us concentrate on the three-body space

$$\langle V_{NN}^{[2]} \rangle^{(3)} = \langle V_{NN}^{[2]} \rangle_{12}^{(2)} + \langle V_{NN}^{[2]} \rangle_{13}^{(2)} + \langle V_{NN}^{[2]} \rangle_{23}^{(2)}, \quad (182)$$

$$\langle V_{NNN}^{[3]} \rangle^{(3)} = \langle V_{NNN}^{[3]} \rangle_{123}^{(3)}. \quad (183)$$

So the NN+NNN interaction in the three-body space is

$$\langle V_{NN+NNN}^{[2,3]} \rangle^{(3)} = \langle V_{NN}^{[2]} \rangle^{(3)} + \langle V_{NNN}^{[3]} \rangle^{(3)} = \langle V_{NN}^{[2]} \rangle_{12}^{(2)} + \langle V_{NN}^{[2]} \rangle_{13}^{(2)} + \langle V_{NN}^{[2]} \rangle_{23}^{(2)} + \langle V_{NNN}^{[3]} \rangle_{123}^{(3)}. \quad (184)$$

If we would use the NN+NNN matrix elements in the same way as the NNN matrix elements to construct the four-body matrix elements we would yield

$$\begin{aligned} \langle V_{NN+NNN}^{[2,3]} \rangle^{(4)} &\stackrel{?}{=} \langle V_{NN+NNN}^{[3]} \rangle_{123}^{(3)} + \langle V_{NN+NNN}^{[3]} \rangle_{124}^{(3)} + \langle V_{NN+NNN}^{[3]} \rangle_{134}^{(3)} + \langle V_{NN+NNN}^{[3]} \rangle_{234}^{(3)}, \\ &= 2 \cdot \left(\langle V_{NN}^{[2]} \rangle_{12}^{(2)} + \langle V_{NN}^{[2]} \rangle_{13}^{(2)} + \langle V_{NN}^{[2]} \rangle_{14}^{(2)} + \langle V_{NN}^{[2]} \rangle_{23}^{(2)} + \langle V_{NN}^{[2]} \rangle_{24}^{(2)} + \langle V_{NN}^{[2]} \rangle_{34}^{(2)} \right) \\ &+ \langle V_{NNN}^{[3]} \rangle_{123}^{(3)} + \langle V_{NNN}^{[3]} \rangle_{124}^{(3)} + \langle V_{NNN}^{[3]} \rangle_{134}^{(3)} + \langle V_{NNN}^{[3]} \rangle_{234}^{(3)}, \\ &\neq \langle V_{NN+NNN}^{[2,3]} \rangle^{(4)}. \end{aligned}$$

As we can see the two-body interaction part of $\langle V_{NN+NNN}^{[2,3]} \rangle^{(4)}$ scales with another factor than the 3-body interaction part. Therefore we have to isolate these parts from each other. To investigate nuclei with $A > 3$.

References

- [1] S. Weinberg: Phys. Lett., B251:288 (1990).
- [2] S. Weinberg: Nucl. Phys., B363:3 (1991).
- [3] A. Nogga: Phys. Rev. C 73, 064002.
- [4] W. Glöckle et al.: Phys. Rep. 274, 107 (1996).
- [5] E. Caurier et al.: Phys Rev. C 66, 024314 (2002)
- [6] R. B. Wiringa: 5th FRIB Workshop on Bulk Nuclear Properties, Michigan 2008, "Recent Developments in Nuclear Quantum Monte Carlo".
- [7] D. R. Entem and R. Machleidt: Phys. Rev. C 68, 041001(R) (2003).
- [8] V. Koch: arXiv:nucl-th/9706075v2 27, Jun 1997 "Aspects of Chiral Symmetry".
- [9] A. Pich: arXiv:hep-ph/9806303v1 8 Jun 1998, "Effektiv Field Theory".
- [10] E. Epelbaum: Progress in Particle and Nuclear Physics 57 (2006) 654-741, "Few-nucleon forces and systems in chiral effective field theory".
- [11] R. Machleidt: arXiv:0909.2881v1 [nucl-th]
"The Missing Three-Nucleon Forces: Where Are They?"
- [12] P. Navrátil: Few Body Syst (2007) 41: 117–140,
"Local three-nucleon interaction from chiral effective field theory"
- [13] D. Gazit, S. Quaglioni and P. Navrátil: Phys. Rev. Lett. 103, 102502 (2009).
- [14] A. Nogga et al.: Phys. Rev. C73, 064002 (2006).
- [15] P. Navrátil et al.: Phys. Rev. Lett. 99, 042501 (2007).
- [16] S. Quaglioni and P. Navrátil: Phys. Lett. B (2007),
doi:10.1016/j.physletb.2007.06.082; arXiv:0704.1336.
- [17] P. Navrátil, G. P. Kamuntavičius and B. R. Barret: Phys. Rev. C61, 044001 (2000).
- [18] P. Navrátil, G. P. Kammuntavičius and B.R. Barret: Phys. Rev. C 61, 044001 (2000).

- [19] D. A. Varshalovich, A. N. Moskalev and V. K. Khersonskii:
“Quantum Theory Of Angular Momentum” (World Scientific).
- [20] G. P. Kamuntavičius et al.: Nucl. Phys. A695, 191 (2001).
- [21] T. A. Brody and M. Moshinsky:
“Tables of Transformation Brackets” (Universidad Nacional Autonoma De Mexico).
- [22] R. Roth et al.: Phys. Rev. C73, 044312 (2006).
- [23] H. Feldmeier: “Einführung in die Theoretische Kernphysik”
lecture notes WS 2007/2008.
- [24] R. Roth, T. Neff and H. Feldmeier: Prog. Part. Nucl. Phys. 65 (2010) 50.
- [25] S. Reinhardt: Diploma Thesis “Comparison and Connection of the Similarity
Renormalization Group and the Unitary Correlation Operator Method”.
- [26] F. Wegner: Ann. Phys. (Leipzig)3 (1994)77.
- [27] B. H. Barlett: “Flow equations for hamiltonians from continuous unitary transfor-
mations” (2003).
- [28] R. Roth, S. Reinhardt and H. Hergert: Phys. Rev. C77, 064003 (2008).
- [29] E. D. Jurgenson et al.: Phys. Rev. C78, 014003 (2008).
- [30] E. D. Jurgenson, P. Navrátil and R. J. Furnstahl: Phys. Rev. 103, 082501 (2009).
- [31] S. C. Pieper and R. B. Wiringa: Ann. Rev. Nucl. Part. Sci. 51 53 (2001).
- [32] R. B. Wiringa and S. C. Pieper: Phys. Rev. Lett. 89, 182501 (2002).
- [33] P. Navrátil, J. P. Vary and B. R. Barret: Phys. Rev. Lett. 84 5728 (2000).
- [34] P. Navrátil, J. P. Vary and B. R. Barret: Phys. Rev. C62, 054311 (2000).
- [35] R. Roth: Phys. Rev. C 79, 064324 (2009).
- [36] R. Roth, P. Navrátil: Phys. Rev. Lett. 99, 092501 (2007).
- [37] R. Roth, Jeffrey R. Gour and P. Piecuch: Phys. Rev. C79, 054325 (2009).
- [38] P. Ring and P. Schuck: “The Nuclear Many-Body Problem”
Springer Verlag, 1st edition, 2000 (2nd printing).

- [39] R. Roth: “Theoretische Kernphysik” lecture notes WS 2006/2007.
- [40] A. Zapp: Diploma Thesis “Kernstruktur mit effektiven Dreiteilchenpotentialen”.
- [41] A. H. Wapstra, G. Audi and C. Thibault: Nucl. Phys. A 729 (2003) 129–336.
- [42] H. de Vries, C. W. de Jager and C. de Vries: At. Data Nucl. Data Tables 36, 495 (1987).
- [43] S. Binder: Master Thesis “Angular Momentum Projection and Three-Body Forces in the No-Core Shell Model”.

Erklärung zur Eigenständigkeit

Hiermit versichere ich, die Master-Thesis ohne Hilfe Dritter nur mit den angegebenen Quellen und Hilfsmitteln angefertigt zu haben. Alle Stellen, die aus diesen Quellen entnommen wurden, sind als solche kenntlich gemacht worden. Diese Arbeit hat in gleicher oder ähnlicher Form noch keiner Prüfungsbehörde vorgelegen.

Darmstadt, den 30. September 2010

Angelo Calci

Danksagung

An erster Stelle möchte ich mich ganz herzlich bei **Herrn Professor Dr. Robert Roth** für die Überlassung dieses spannenden Themas und die freundliche Aufnahme in seine Arbeitsgruppe sowie die hervorragende Betreuung während des gesamten letzten Jahres bedanken.

Darüber hinaus danke ich allen **Mitgliedern der Theorieabteilung des Instituts für Kernphysik** für die freundliche Aufnahme in ihr Team und die vielen anregenden physikalischen und nicht-physikalischen Gespräche.

Ein herzliches Dankeschön geht an **Herrn Dr. Petr Navrátil** für die Bereitstellung seines Fortran Codes und die freundliche Hilfe bei dessen Verständnis. Ohne seine Mithilfe wäre das Gelingen dieser Arbeit nicht möglich gewesen.

Ganz besonders bedanke ich mich bei **Dr. Felix Schmitt** und **Dr. Markus Hild** dafür, dass sie mir bei Linux-Problemen mit Rat und Tat zur Seite standen und sich um die Wartung des “Phantoms” gekümmert haben.

Ein großer Dank gilt **Joachim Langhammer** für die kollegiale Zusammenarbeit und die zahlreichen nützlichen physikalischen Diskussionen.

Desweiteren bedanke ich mich ganz herzlich bei **Sven Binder** für die freundliche Zusammenarbeit und die diversen physikalischen Diskussionen, welche mir bei der Bearbeitung meines Themas sehr weiter geholfen haben sowie für das Korregieren meiner Master-Thesis.

In diesem Zusammenhang möchte ich mich auch bei **Eva Haeger** und **Lotta Heckmann** für das Korrekturlesen meiner Master-Thesis bedanken.